AN EXPERIMENTAL AND ANALYTICAL EXAMINATION OF STRATIFIED THERMAL STORAGE

By

YOUSEF HASAN ZURIGAT

Master of Science in Aeronautical Engineering
Kiev Institute of Civil Aviation Engineers
Kiev, USSR
1976

Master of Science
Oklahoma State University
Stillwater, Oklahoma
1984

Submitted to the Faculty of the Graduate College
of the Oklahoma State University
In Partial Fulfillment of the Requirements
for the Degree of
DOCTOR OF PHILOSOPHY
December, 1988

AN EXPERIMENTAL AND ANALYTICAL EXAMINATION

OF STRATIFIED THERMAL STORAGE

Thesis Approved:

A. J. Ghajar

Thesis Adviser

Kenneth J. Bell

Robert W. Worrell

Donald G. Kilday

Norman N. Durham

Dean of the Graduate College

ACKNOWLEDGMENTS

I would like to express my gratitude to my advisor, Dr. A. J. Ghajar, for his constant guidance and suggestions and I am indebted to him for his inspiration and encouragement. I am also indebted to my committee members, Dr. K. J. Bell, Dr. D. G. Lilley and Dr. P. M. Moretti. Dr. Bell's review and criticism, Dr. Lilley's expertise in computational fluid dynamics, and Dr. Moretti's support and funding efforts have all been extremely beneficial.

In addition, I would like to express my gratitude to my colleagues, who contributed to this work through their graduate studies or other means. Their names appear as authors or co-authors of several publications cited in this thesis. Mr. M. G. Abu-Hamdan has contributed to this work through his M.S. thesis. His input and help were very crucial in the successful completion of this thesis. I also wish to thank my friends Ms. Leah Everhart for her invaluable and timely assistance with the figures, Dr. Yahia Sharaf-Eldeen, Mr. Mousa Abu-Arabi, and Mr. Sankaran Mohan for their encouragement and helpful suggestions. I would like to express my deepest gratitude to my parents, sisters and brothers for their support and encouragement throughout my graduate study at Oklahoma State University. Thanks go to Mrs. Daleene Caldwell, Mrs. Frances Harris, and Mrs. Debbie Garrett for carrying the burden of typing the manuscript and their tolerance of me.

This work was supported by the University Center for Energy Research (UCER) at Oklahoma State University.

TABLE OF CONTENTS

LIST OF TABLES

LIST OF FIGURES

NOMENCLATURE

Roman Letters

C_p specific heat at constant pressure

D physical diffusion coefficient

EXP grid expansion ratio

f friction factor in the baffle perforations, used in Equations (4.2.11) and (4.2.12)

g acceleration of gravity

g_c dimensional constant in British Units, $g_c = 32.174\ Lb_m\text{-}ft/Lb_f\text{-}s^2$

H effective height between tank inlet and outlet

k molecular thermal conductivity

k_t eddy conductivity

ℓ length scale of the resistance term used in Equations (4.2.6) and (4.2.7)

L characteristic length

P pressure

Pe Grid Peclet number, $Pe = uL/D$

Pr Prandtl number, $Pr = \mu C_p/k$

q heat flux

r radius

$\overline{R}$ resistance force vector used in Equation (4.2.2) with components R_x, R_y used in Equations (4.2.6) and (4.2.7)

Re Reynolds number, $Re = \rho V_{max} L/\mu$

Ri Richardson number, $Ri = \Delta\rho g H/\rho_m V^2$

t* dimensionless time, $t^* = Vt/H$

T temperature

t time

u velocity in the x- or r- directions

V average velocity in Equation (3.1.1) and velocity vector in Equation (4.2.2)

v velocity in the y- direction

x,y cartesian or cylindrical (x≡r) coordinates

Greek Letters

α molecular thermal diffusivity in Equation (3.1.1) and donor cell parameter in Equation (5.6.3)

β coefficient of thermal expansion, $\beta = [\rho_o - \rho]/[\rho_o(T - T_o)]$

γ function

Δ designates difference when used as prefix

ϵ diffusivity factor in Equation (3.1.1) or convergence tolerance elsewhere

ζ index for cartesian (ζ=0) or cylindrical (ζ=1) coordinate

θ flow direction angle

μ viscosity

ξ independent variable used in Equation (5.3.1)

ρ density

σ under-relaxation factor

ϕ scalar dependent variable (P or T for example)

ω over-relaxation factor

Subscripts

eff effective

E east

i,j tensor indices (i=j=1,2,3) in Equations (4.2.1) to (4.2.3) and

	indices of computational grid geographical location elsewhere
in	value at the inlet
ℓ	laminar (molecular)
m	mean
N	North
o	initial reference state
S	south
t	turbulent
T	of T-cell
TE	truncation error, used in Table II
u	of u-cell
v	of v-cell
W	west

Superscripts

n	at previous time step
n+1	at current time step
N	at previous iteration
N+1	at the current iteration
T	of the T-cell
P	at the pressure (in section 5.3) and of the P-cell elsewhere
v	of the v-cell
u	of the u-cell
'	fluctuating quantity

Other symbols

—	bar indicating statistical average, e.g., $\overline{u'v'}$

Abbreviations

SOUDS	second order upwind difference scheme
SST	single stratified tank
STS	stratified thermal storage (variable inlet temperature)
TTS	thermocline thermal storage (constant inlet temperature)
WUDS	weighted upwind difference scheme

CHAPTER I

INTRODUCTION

The energy usage in the United States has been estimated to be increasing at an annual rate of 3 to 5 percent (Rapp 1981; Krenz 1984). Considering the present rate of energy consumption of 150×10^{15} Btu/year (Rapp 1981) and the steady increase in population of 2 percent per year (Krenz 1984), very large demands of energy will undoubtedly occur by the turn of this century. This calls for technical innovations to reduce energy needs and use energy more effectively. This is accomplished through (1) further development and widespread use of renewable energy sources (solar, wind, geothermal, nuclear etc.) and (2) development and implementation of energy conservation and management technology.

Thermal storage is an energy management tool that can serve both objectives equally. As shown in Table I, solar energy may become an important contributor to the total energy supply. However, the mismatches between the supply of solar energy and the demand for it are frequently very significant. This places thermal storage as a key technology in successful exploitation of solar energy.

Presently in residential and commercial space cooling applications, electricity is the major source of energy. In these applications, a very high level of energy consumption occurs during a relatively small

TABLE I

ENERGY USE SECTORS FOR POSSIBLE SOLAR AUGMENTATION, 1968 (KRENZ) 1984*

Type of Use	Energy Used (10^{15} Btu/yr)	Percent of National Total Energy Used
1. Space heating, residential	6.68	11.0
2. Domestic hot water, residential	1.74	2.9
3. Space cooling, residential	0.43	0.7
4. Space heating, commercial	4.18	6.9
5. Space cooling, commercial	1.11	1.8
6. Hot water, commercial	0.65	1.1
7. Process steam, industrial	10.13	16.7
Total	24.92	41.1

* While overall national energy usage has increased, it appears that the end-usage distribution has not changed greatly (Krenz 1984).

part of the day (see Figure 1.1). This places an overwhelming economic burden on the utilities which have to provide very high level of plant capacity for peak periods, leading to low average load factors. More expensive fuels are normally used to provide the additional peak capacity. Energy storage can alleviate this problem by shifting part of the cooling operations to off-peak hours. In this manner, the equipment size and electrical capacity may be minimized.

A number of concepts have been developed for hot or cold storage in either sensible or latent forms. Many storage materials were tested and/or used (Guyer and Brownell 1983; Herrick et al. 1977). Water, due to its abundance, low cost, high specific heat and benign character is the most widely used storage medium in low-to-medium temperature sensible thermal storage applications. It is also the working fluid in many energy systems. Therefore, sensible thermal storage in water is

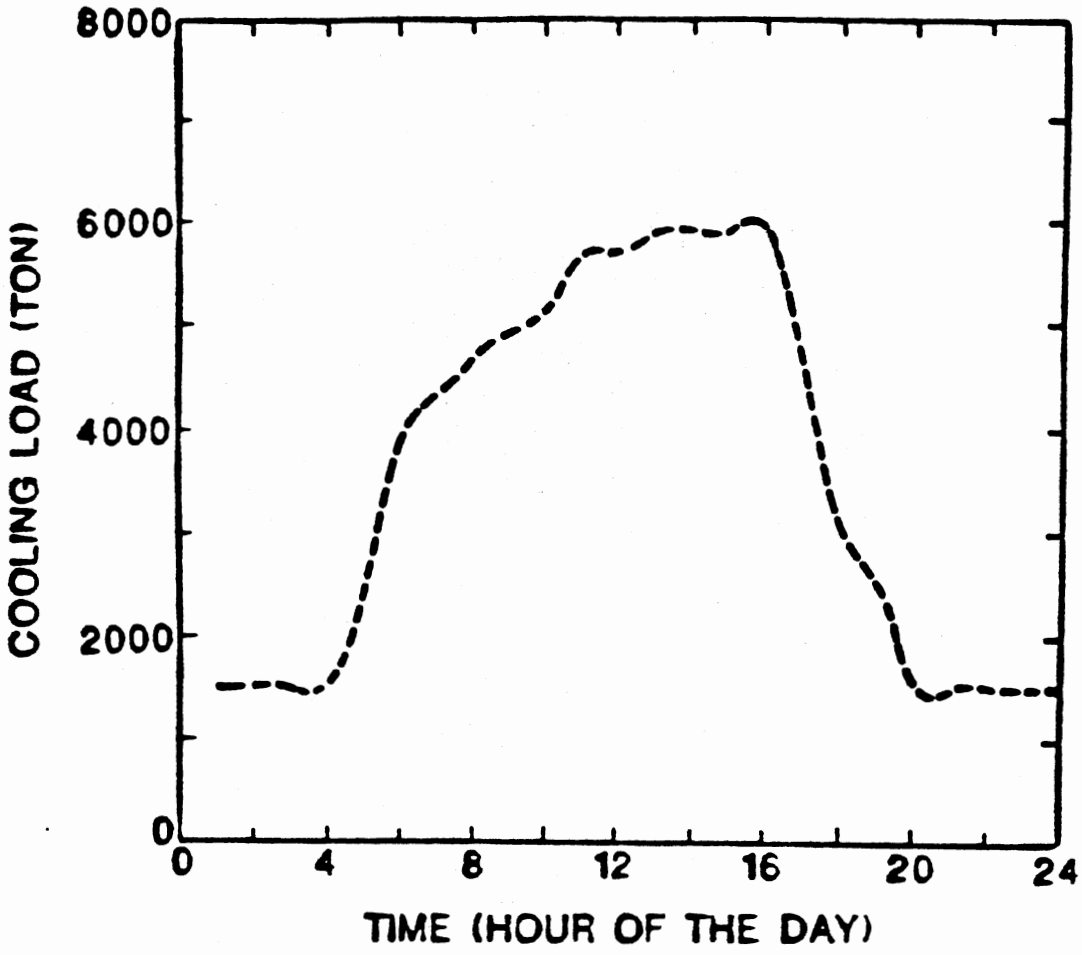

Figure 1.1 Typical Chilled Water Demand Daily Profile of Oklahoma State University Campus (Parker and Moretti 1985)

attractive in both heating and cooling applications.

The capability of storing hot or chilled water from one part of the day or night to another has a number of potential benefits. During the air conditioning season, the goals are:

- to reduce the peak demand for electric power, by shifting electricity consumption to off-peak times of day and night;
- to reduce the size and capital investment in the cooling equipment, by operating the system through more hours of the day and night instead;
- to improve the electric utility load factors by evenly distributing the energy demand over the hours of the day and night;
- to operate the equipment (chillers, cooling towers, etc.) as much as possible when outside temperatures are relatively low and the cycle efficiency is high.

During the heating season, the goals are:

- to integrate the use of solar heating (where appropriate) with the operation of the conventional or back-up heating system, without loss of control or comfort, and without deterioration of electric utility load factors;
- to extend the use of solar heat to a larger part of the day and night;
- to time the operation of heat pumps more effectively, especially when used in conjunction with timed set-back thermostats and to avoid the unnecessary cutting-in of resistance heating.

In the transition seasons, the goal is:

- to carry over natural warmth or cooling from the outside environment between day and night without resorting to electric

or fueled heating and cooling. For example, thermal storage provides the mean for intensive use of the free cooling technique (Parker and Moretti 1985).

Chilled or hot water is stored in tanks which vary in design as dictated by different factors, like thermal performance, architectural, retrofit, and economical constraints. However, all existing designs of thermal storage tank systems share the same objective of maintaining the thermodynamic availability of stored energy so that it can be extracted at nearly the same temperature at which it was stored. The separation of hot and cold water in storage tanks is the key factor in achieving this.

Multiple tanks are one obvious way of achieving the separation, but are not the best choice with regard to simplicity, economic feasibility, and space utilization. Other schemes have been designed and implemented (Tamblyn 1980) e.g., a single tank with diaphragm mounted either horizontally or vertically, labyrinth tanks in which the water is forced to flow through a maze, and the single stratified tank in which use is made of the natural process of stratification that permits the hot water to float on top of the cold water.

The single stratified tank is the most attractive choice in low-to-medium temperature thermal storage applications due to its simplicity and low cost. Moreover, the performance of a single stratified tank is comparable with other types (Wildin and Truman 1985) and has a superior reliability (Seth and Leduc 1983).

The problems of stratified storage of warm or chilled water in a single container are:

- on the one hand, in chilled water systems, the density

differences are very small and the stratifications very weak, leading to low Richardson numbers and a tendency for the chilled water to mix excessively with warmer water in the tank if disturbed by uncontrolled inlet flows;

- on the other hand, water heated by solar panels varies continuously in temperature, and must be inserted into the stratified thermal storage tank at the proper level, which also varies, to avoid excessive mixing.

One or both of these two difficulties apply to most of the promising applications for stratified thermal storage. In addition:

- because of the modest temperature ranges involved, the storage of significant amounts of heat involves relatively large tanks, which must therefore be simple and cheap in construction in order to make good overall economics possible;
- to apply this technology to residential use, the operation of the tanks must be simple, reliable, and low in maintenance; it cannot involve elaborate monitoring, valving, and control systems.

Aside from the aforementioned problems, the integration of thermal storage into a total energy system requires knowledge of the tank performance under different modes of operation and control. Accurate and efficient analytical modeling is a key factor in making overall system simulations possible. While many analytical models exist in the literature, there are no guidelines as to their accuracy, computational efficiency and simplicity.

The present study was undertaken to address some of the problems associated with stratified thermal storage. However, to provide the

proper perspective for the present work, a review of the literature is presented in the next chapter. Research needs, specific objectives and method of approach are also discussed therein.

CHAPTER II

LITERATURE REVIEW, RESEARCH NEEDS, OBJECTIVES AND METHOD OF APPROACH

In this chapter, a review of the work published in the open literature on single stratified thermal storage tanks is presented. Areas of potential further contribution are identified. The present state of the art indicates a lack of comprehensive experimental and analytical studies in certain areas. These are reported at the end of this chapter along with the method of approach adopted in this study.

2.1 Introduction

The single stratified tank (SST) is likely to be the promising thermal storage device in low-to-medium temperature thermal storage applications due to its simplicity, reliability and its potential high performance. Two thermal cases in SST are distinguished: the thermocline thermal storage (TTS) and the stratified thermal storage (STS). In TTS, the temperature of the incoming fluid is fixed or experiences negligible variation, a case normally encountered in chilled water storage. In STS, the temperature is allowed to vary. This case is characteristic of solar thermal energy storage in which the liquid heated in the collectors may have a temperature that varies with each passing cloud.

The performance of a SST is dependent on how well the separation

between hot and cold liquid in the tank is maintained under different static and dynamic flow conditions. The goal is to maintain a high level of thermodynamic availability of stored energy. The mechanisms limiting the approach to high performance are: (1) heat exchange with the ambient surroundings, (2) heat conduction along the wall and the associated buoyancy-driven motions in the fluid body, (3) thermal diffusion from the hot portion of the fluid to the cold portion,and (4) mixing during charge and discharge cycles.

The last mechanism is the major contributor to the loss of thermodynamic availability and remains difficult to evaluate since it is inlet-design-dependent among other factors. The following section outlines the previous works which were undertaken by several investigators to achieve high performance in a SST.

2.2 Present State-of-the-Art

The single stratified tank has been the subject of many investigations, both analytical and experimental. Tests conducted at the Los Alamos Laboratories (Brumleve 1974) confirmed the feasibility of using a natural thermocline (thermocline is defined as the region of steepest temperature gradient in the tank) to achieve separation of hot and cold water inside a single container. The conduction across the thermocline was found to be a minor factor in degradation of the thermocline sharpness as compared to other factors, i.e., mixing during the initial stages of charge and discharge, and heat loss to the surroundings and vertical conduction through the walls which causes both convective currents and large-scale circulation in the tank.

The effect of the conducting wall on the stratified fluid in a

cylinder was examined by Miller (1977). It was found that the degradation of the thermocline was ten times faster in an aluminum tank than in a glass tank. This shows that if the fluid is stored in a container made from a material of a thermal conductivity much greater than that of the fluid, convection currents will be generated at the fluid/wall interface inside the container, causing degradation of the thermocline at a faster rate. This was confirmed by the study of Sherman et al. (1978) in which tests were conducted on a fiberglass tank with no liner and with copper, aluminum, steel and stainless steel liners. These tests showed that vertical conduction down the tank walls can reduce thermal stratification to a significant extent.

The effect of several geometric and dynamic parameters on thermal stratification, i.e., inlet port location and geometry, mass flow rate, tank height-to-diameter ratio, and inlet and outlet water temperature difference were studied by Lavan and Thompson (1977). Stratification was found to improve with increasing height-to-diameter ratio, with increasing inlet to outlet temperature difference, and with increasing inlet and outlet port diameters, and to decrease with increasing flow rates. Best results were obtained when the inlet and outlet ports were near the end walls and when the flow was directed towards these walls. A height-to-diameter ratio of 4 was recommended by Cole and Bellinger (1982) to provide the best stratification without excessive thermal loss. A ratio of 10 was recommended by Abdoly and Rapp (1982). However, this value would result in a high surface area-to-volume ratio and subsequently increase the heat loss and/or the insulation cost and tank cost.

Internal baffling of the tank to enhance thermal stratification was

tested by Davis and Bartera (1975). However, this approach was not fully explored by the investigators to provide conclusive results. The tests conducted were not comprehensive since they treated only a special case wherein the thermocline was already above the level of collector return water when the pump was turned on.

The position and sharpness of the thermocline were found to be a function of the Richardson and Peclet numbers, and a critical value of Richardson number of 0.244 was found to be the limit below which stratification does not occur (Sliwinski et al. 1978). It was suggested by Wildin and Truman (1985) that a value of Richardson number greater than or equal to unity is sufficient for maintaining good stratification.

The extent to which mixing occurs naturally in a stratified tank as well as the design improvements that can be made to minimize it were examined by Baines et al. (1982). Based on their experiments, it was determined that there are two factors which limit the approach to ideal stratification: the critical layer thickness which defines the volume of fluid that must be introduced before mixing across the thermocline ceases, and the thermocline thickness. Both factors were found to be controlled by the design of the inlet system. Several inlet designs were used by several investigators to enhance thermal stratification in storage tanks (Wildin and Truman 1985; Cole and Bellinger 1982); see Figure 2.1. However, these designs perform well only when the tank inlet temperature remains constant. In this case the designs that introduce the flow with minimum velocity in a gravity current form (inlet flow is maintained horizontal and introduced at the uppermost or lowermost section of the tank) were found to be the best for this type of tank (see Figure 2.1a).

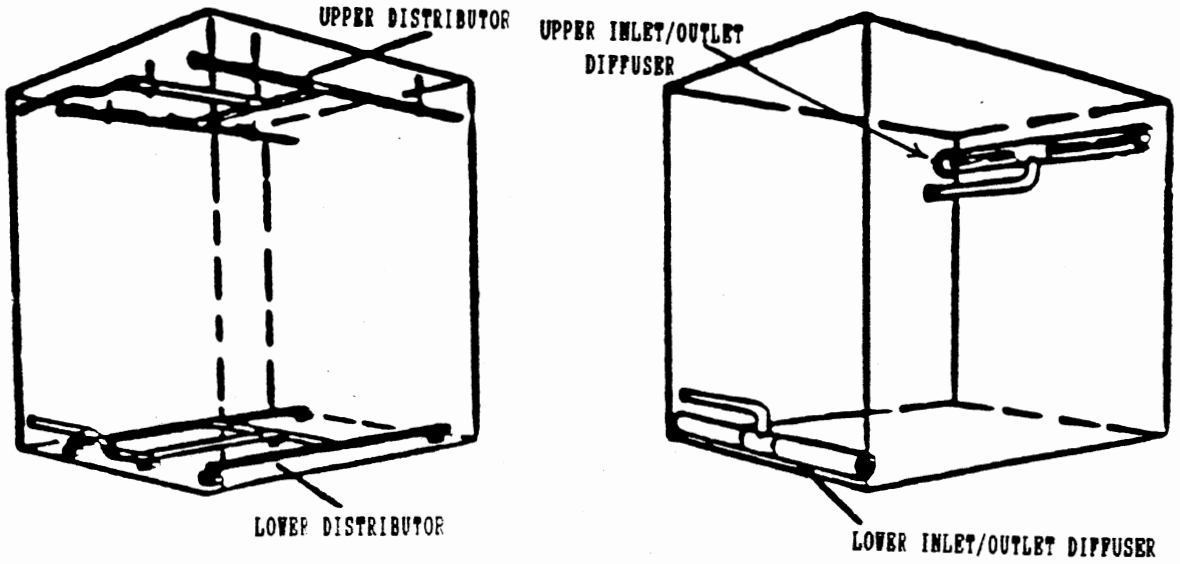

a: Wildin and Truman (1985)

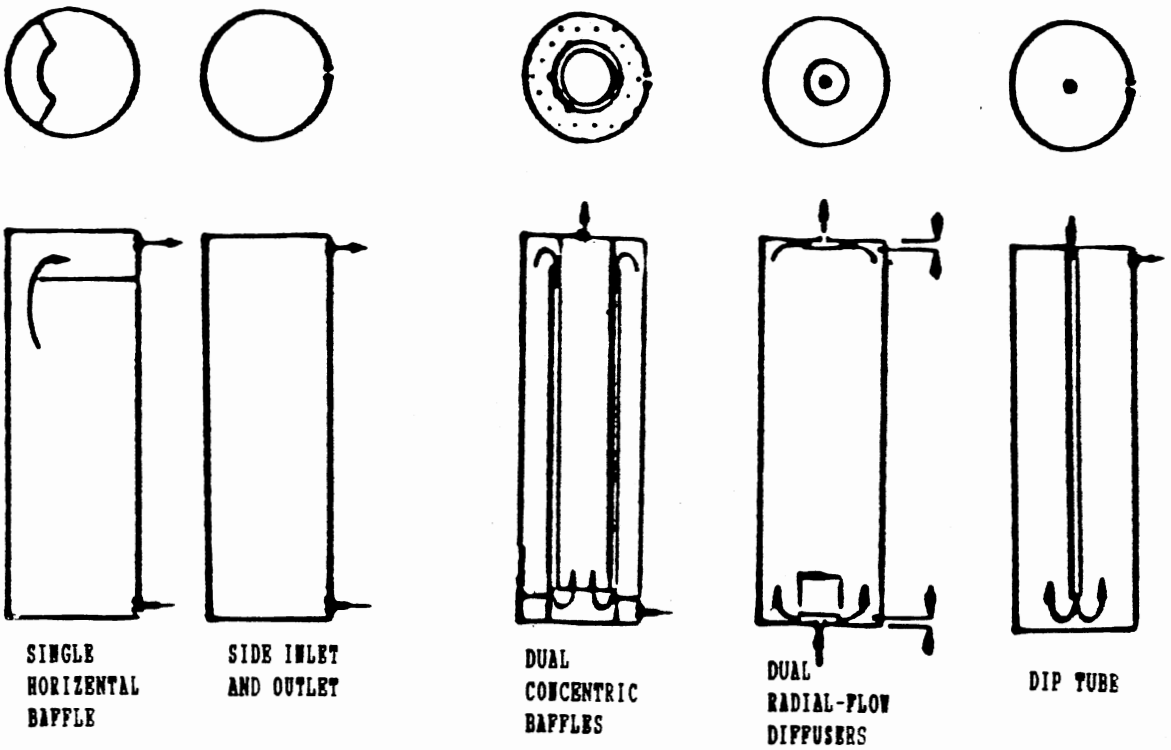

b: Cole and Bellinger (1982)

Figure 2.1 Stratified Thermal Storage Tank Inlet Diffusers

Notable design attempts of inlets for the variable temperature case (inlet distributors) are those which consist of a rigid or flexible porous manifold (RPM or FPM, respectively) that removes the momentum of the incoming fluid and inhibits mixing while allowing buoyancy forces to position the fluid at the appropriate level in the tank (Gari et al. 1979; Loehrke et al. 1979), see Figure 2.2. As can be seen in Figure 2.3, the performance of these distributors is superior to the conventional inlet diffusers. Note also that the FPM performance is much better than the RPM. However, as reported by Loehrke et al. (1979), the RPM is potentially more reliable since it is fixed and self-purging of the entrapped air which can seriously degrade the performance of the FPM. Nevertheless, the theory and experiments of Gari et al. (1979) and Loehrke et al. (1979) did not result in satisfactory design guidelines for this type of distributors.

Analytical studies were aimed at modeling the flow in thermocline and stratified thermal storage tanks to investigate several flow parameters and tank configurations. The one-dimensional nature of the flow in a thermocline tank was recognized from early studies (Close 1967; Brumleve 1974) and by the radial measurements of the temperature distribution in the tank (Gross 1982). Therefore most of the modeling efforts were one-dimensional. Examples of these include the fully stratified storage tank models of Close (1967), Duffie and Beckman (1974) and its modified version by Sharp (1978) and the one-dimensional models with mixing effects; Cole and Bellinger (1982), Wildin and Truman (1985) and Oppel et al. (1986). The last three models are for thermocline type thermal storage tank (constant inlet temperature). Han and Wu (1978) developed a model based on the viscous entrainment concept

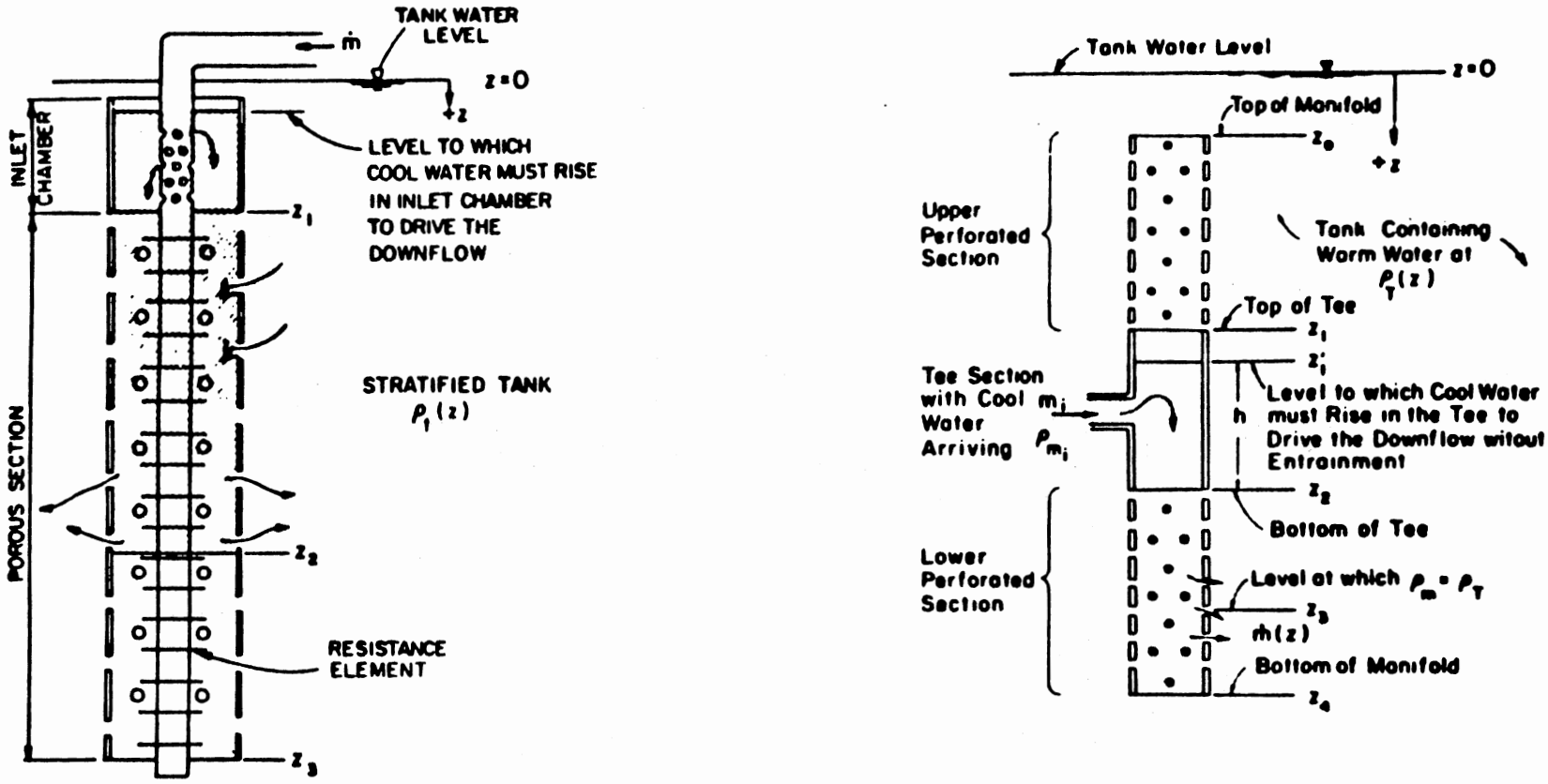

Figure 2.2 Stratified Thermal Storage Tank Inlet Distributors (Gari et al. 1979 and Loehrke et al. 1979)

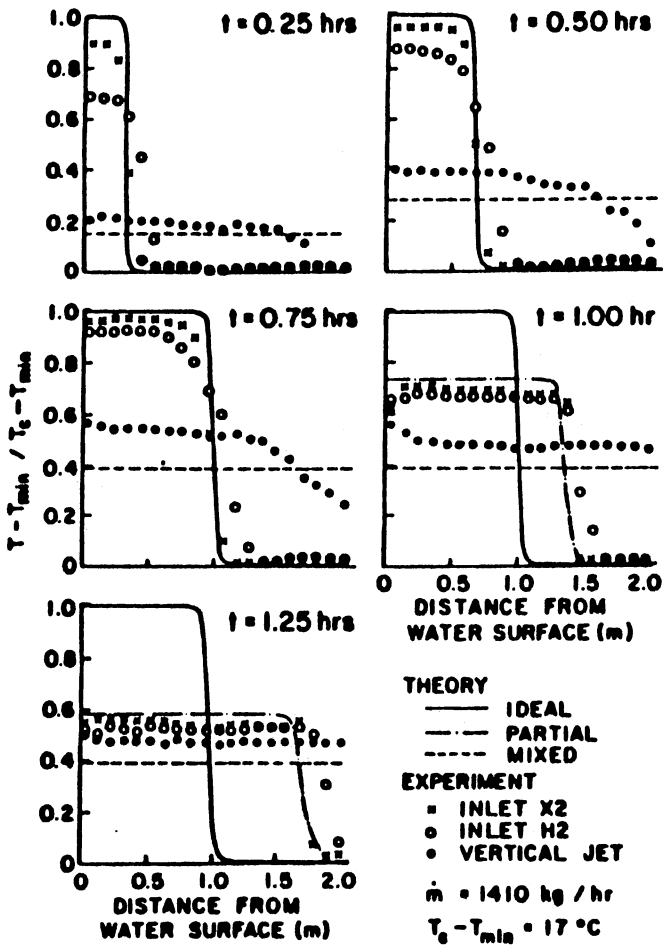

Tank temperature profiles during partial charge and recycle experiments, conventional inlets.

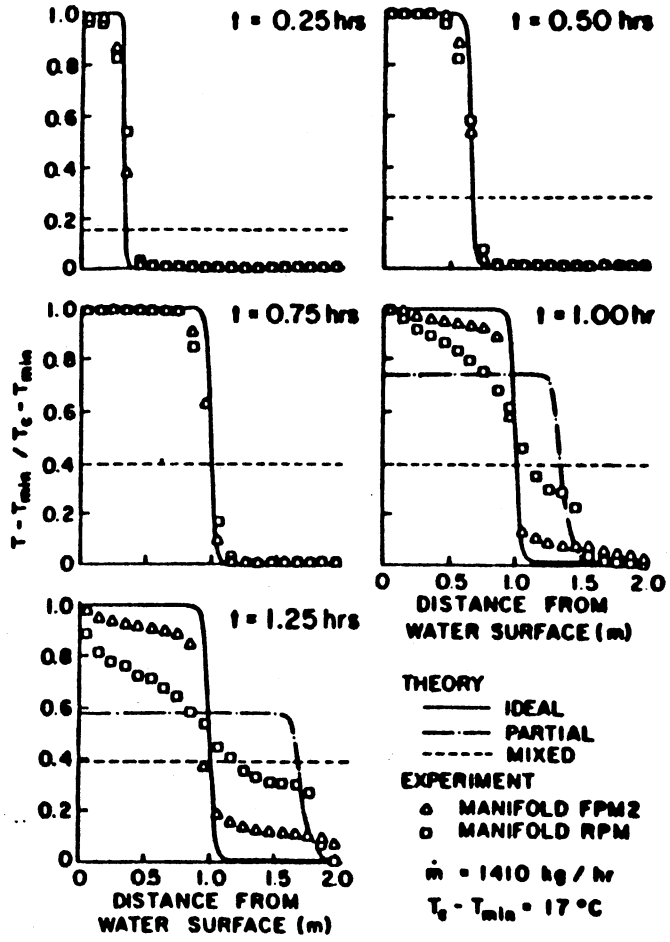

Tank temperature profiles during partial charge and recycle experiments, distribution manifolds.

Figure 2.3 Comparison of Inlet Manifold Performance with Conventional Inlet Diffusers (Gari et al. 1979)

which allows for variable inlet temperature. The predictions of this model, as reported by the originators, had a better agreement with the experiments compared to that of fully stratified model.

More complex models have appeared in the literature. The two-dimensional model of Cabelli (1977) has incorporated two flow circuits and two geometric configurations of horizontal and vertical entry into the tank. Comparison of the predicted temperature profiles with the results from a one-dimensional model (Cabelli 1977) showed a discrepancy of less than 12 percent. Nevertheless, the values of Reynolds number used in the study were limited by the mesh size to magnitudes smaller than those expected in practical situations. It should be noted that the equations solved were those for laminar flow in which case the turbulent effects were not taken into account. Therefore, it is not surprising to see results comparable with those from a one-dimensional model.

The limitation on Reynolds number values used by Cabelli (1977) was due to instabilities inherent in the central difference representation of the convective terms as Reynolds number increases beyond a certain limit. This discrepancy was treated later by Guo and Wu (1985) who developed a two-dimensional model applicable for high Reynolds and Grashof numbers. They used the power-law scheme (Patankar 1980) which is stable for large values of Reynolds numbers. However, this scheme is known to produce numerical diffusion which compromises the accuracy, especially when the flow is not aligned with the numerical grid. The numerical simulation of Guo and Wu (1985) identifed Richardson number as the important parameter for characterization of the physical conditions of flow pattern and temperature stratification inside the storage

tank. At Ri << 1, the forced convection becomes important, and leads to a complete mixing case. While these results agree qualitatively with the results from previous experimental studies (for example, Sliwinski et al. (1978)), no direct comparison with experimental data regarding the velocity and temperature fields was furnished. Moreover, laminar flow was assumed in the simulations. In the two-dimensional model of Chan et al. (1983) the governing equations for laminar flow in a stratified tank were solved using a technique based on the marker and cell method (Welch et al. 1966). Different inflow and outflow configurations were simulated. However, their results showed the flow direction into and from the storage tank has a negligible effect on the thermal storage efficiency. This is in disagreement with the experimental evidence, for example, Lavan and Thompson (1977) and Baines et al. (1982).

A three-dimensional model of a stratified tank has been developed by Sha and Lin (1978). The governing equations of mass, momentum and energy in cylindrical coordinates were solved based on the marker and cell technique (Welch et al. 1966). A zero-equation turbulent model was used to account for turbulent effects. In this model both inlet temperature and inlet velocity were allowed to vary. Also the model provided for perforated and nonperforated baffling by including extra resistance terms in the governing equations. It seems at the first look that the model includes all the desirable features. However, no direct quantitative comparison with experiments was done since several modifications in the code were needed (as pointed out by Sha and Lin 1978). In their final report (Sha et al. 1980), however, no such comparison was made.

2.3 Areas of Research Needs

The lack of comparison between the analytical predictions from the two- and three-dimensional models with the experiments is due in part to the lack of detailed experimental data. In fact, most of the published data consist of temperature measurements from a single one-dimensional array of thermocouples spanning the height of the tank, for example Davis and Bartera (1975), Lavan and Thompson (1977), Sliwinski et al. (1987), Kuhn et al. (1980) and Abduly (1981). It should be noted that, while the flow in a stratified tank far from the inlet region is one-dimensional, two- and possibly three-dimensional effects are present in the inlet region. These effects control the subsequent development of the temperature field downstream. The radial isotherm assumption in regions at or close to the inlet is not quite justified (see Figure 2.4). Therefore, temperature measurements at more than one point at different elevations in the tank are needed for both constant and variable inlet temperature cases, that is, TTS and STS cases respectively. This should serve two purposes:

1. to obtain more accurate representation of the temperature at each elevation so that more accurate one-dimensional models can be developed.
2. to expand the data base that is useful for design improvements and with which two- and three-dimensional models can be verified. The development of two- or three-dimensional models is crucial for design assessments. A few models have been developed but their accuracy has not been tested.

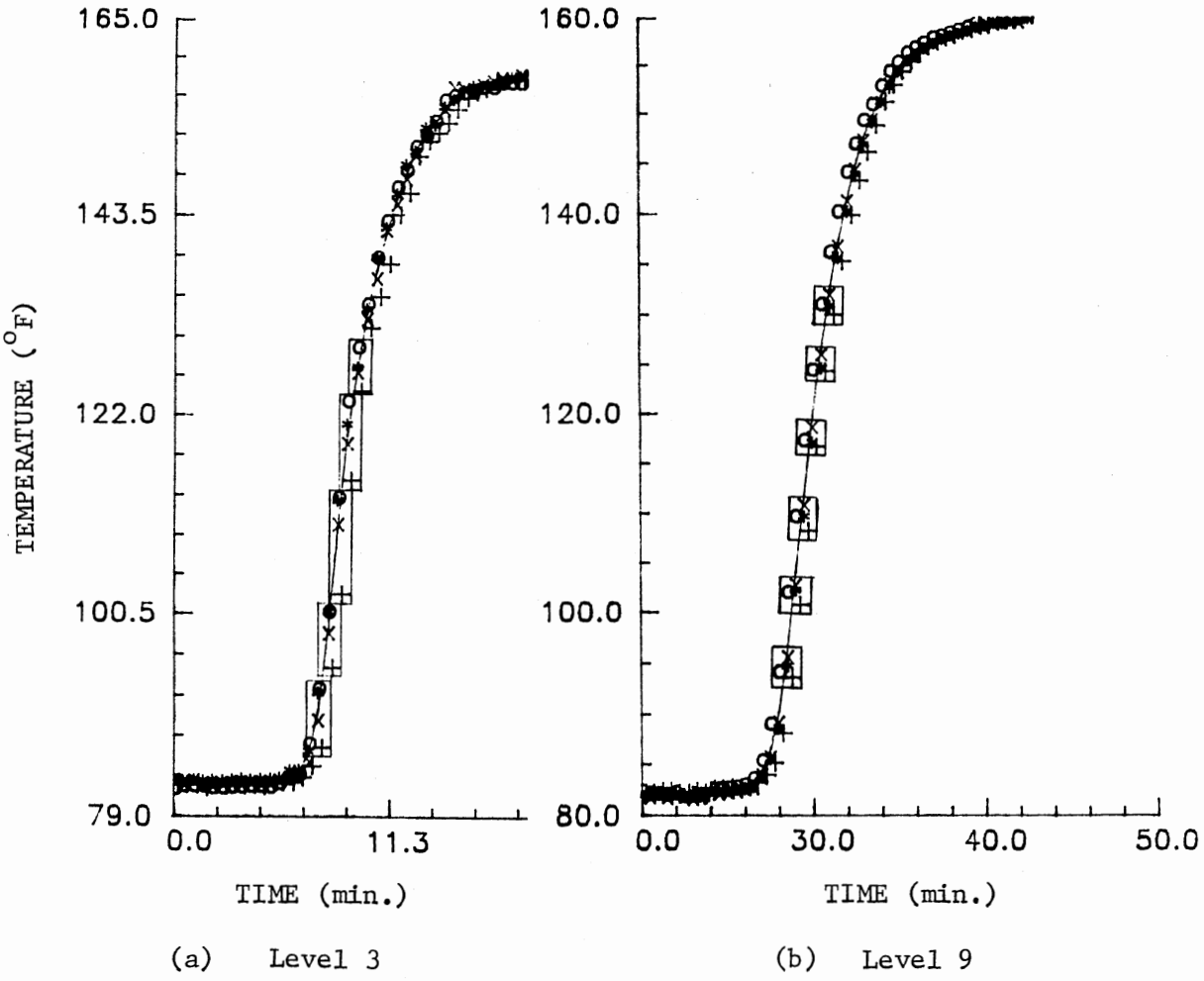

(a) Level 3 (b) Level 9

Run # 60 (Zurigat and Liche 1987)

Figure 2.4 Transient Temperature Profiles at Different Levels in the Storage Tank as Measured by Individual Thermocouples at Each Level (see Figure 3.1)

Aside from the lack of comprehensive experimental data, the modeling efforts have their own inadequacies:

1. On the one hand, many of the one-dimensional models available in the literature ignore the mixing effects due to the introduction of the fluid into the tank, for example, Close (1967), Duffie and Beckman (1974), Cabelli (1977) and Sharp (1978). Other models, while accounting for mixing, do not allow for variable inlet temperature, for example, Cole and Bellinger, (1982), Wildin and Truman (1985) and Oppel et al. (1986). The model of Han and Wu (1978) accounts for mixing and allows for variable inlet temperature. However, its accuracy needs to be established by verification with experiments.

   The one-dimensional models serve mainly as a tool in overall system energy management simulations. Information on their relative accuracy, computational efficiency and implementation simplicity is lacking. A comparative study of these models is needed to make energy system management simulations practical.

2. On the other hand, the two- and three-dimensional models developed in the literature have not been of much use in design assessments. This is particularly due to the numerical inaccuracies introduced by the numerical techniques used, for example the upstream first order differencing of convective terms and the resulting numerical diffusion (Leonard 1981). There is a need for a numerical model that is based on the recent advances in methods for reducing numerical diffusion (Huang et al. 1985).

2.4 Scope, Objectives and Method of Approach

The literature review presented in this chapter revealed several areas of need of research. These were discussed in the previous section. A comprehensive experimental and analytical study directed toward achieving better stratified tank performance is lacking.

This study was undertaken to investigate the design improvements of single stratified tank needed to achieve high performance under wide range of flow conditions. The main objectives of this study are:

1. develop the analytical and empirical tools that aid in identifying the means for promoting stratification in a single stratified tank.

2. develop design and performance data which will assist in the widespread use of thermal storage technology and make the ensuing benefits available to both utilities and consumers.

3. develop technical data to support and/or aid in making simulations of overall energy systems involving thermal storage practical.

The method of approach adopted in this study included the following steps:

1. Experimentation with a fresh-saline water system to isolate parasitic effects, i.e., heat loss to the ambient and conduction along the wall and the associated buoyancy-driven motions, and

to assist in developing a one-dimensional analytical model incorporating inlet mixing characterization (Zurigat et al. 1988a).

2. Experimentation with a hot-cold water system to investigate the performance of SST under actual conditions. Upgrading the one-dimensional analytical model developed in Step 1 above to include heat loss to the ambient (Ghajar et al. 1987) and developing mixing correlations for different inlet designs (Zurigat et al. 1988b).

3. Development of a microcomputer-based data acquisition system and data reduction software to increase the capacity, speed and reliability of data collection and analysis (Rao et al. 1988).

4. Conducting a comparative study of one-dimensional SST models available in the literature by validation with our experimental data (Zurigat et al. 1987) and with those of other investigators (Maloney 1987).

5. Experimentation with stratification in SST under variable inlet temperature conditions. This includes model tests with inlet distributor for different flow conditions (see Chapter IV and Abu-Hamdan (1988)).

6. Development of a two-dimensional analytical model of SST for parametric and design assessments based on the governing

conservation equations of mass, momentum, and energy. A state-of-the-art numerical scheme was employed to ensure accurate and reliable predictions (see Chapters IV and V).

CHAPTER III

EXPERIMENTAL AND ANALYTICAL TREATMENT OF SST UNDER CONSTANT INLET TEMPERATURE CONDITIONS

In this chapter, the study of single stratified tank (SST) under constant inlet temperature conditions (thermocline thermal storage) is outlined. The results obtained are discussed and important conclusions related to thermocline thermal storage performance and design are drawn herein.

3.1 Introduction

The interest in sensible thermal storage in liquids has been motivated by the fact that it is attractive and practical in low-to-medium temperature thermal storage applications, that is, residential and commercial space heating and cooling and hot water applications. In these applications the single stratified tank (SST) is the best choice for its potential high performance, simplicity and low cost. As mentioned earlier two thermal conditions are normally encountered in SST, the constant (thermocline) and variable (stratified) inlet temperature conditions. In the early phase of this study the thermocline thermal storage was investigated, both experimentally and analytically. The flow in thermocline thermal storage was modeled by the one-dimensional turbulent energy equation:

$$\frac{\partial T}{\partial t} + V\frac{\partial T}{\partial x} = \alpha\varepsilon_{eff}\frac{\partial^2 T}{\partial x^2} \qquad (3.1.1)$$

where ε_{eff} is an effective diffusivity factor (mixing index) given by:

$$\varepsilon_{eff} = (\alpha + \varepsilon_H)/\alpha \qquad (3.1.2)$$

For laminar flow $\varepsilon_H = 0$ and ε_{eff} becomes unity indicating a no-mixing case. For turbulent flow ε_{eff} is much greater than unity. In the latter case the magnitude of ε_{eff} is indicative of the extent of mixing in thermocline thermal storage tank.

The magnitude of ε_{eff} cannot be determined theoretically. Therefore, experiments were conducted to quantify the dependency of ε_{eff} on various geometric and flow conditions. Laboratory model tests with both fresh-saline water (Zurigat et al. 1988a) and hot-cold water (Zurigat et al. 1988b) systems were conducted. The details of these experiments and the accompanying modeling efforts are described in several publications cited herein. An overview of the results obtained throughout this phase of the investigation is presented in the next section.

3.2 Discussions of the Results

The experiments with a fresh-saline water system revealed some interesting features of the flow in a stratified tank, that is, the interaction between buoyancy and momentum and the effect of inlet design on stratification. Mixing was found to decrease significantly in situations where the inlet fluid exhibits high buoyancy. In these cases, the inlet configurations had little effect on the development of

the thermocline in the storage tank, as long as they were diffusive. The reverse is true when buoyancy is insignificant. For example, the thermocline widens and different inlets perform differently.

These results lead to the following conclusions:

- The dimensionless parameters of importance in thermocline thermal storage are the Reynolds and Richardson numbers.
- In chilled water storage applications where buoyancy forces are negligible in the temperature range of interest (40 to 55°F), the inlet design plays a major role in achieving thin thermocline and a more efficient thermal storage tank thereafter.
- In hot water solar energy storage applications, the inlet design in thermocline (constant inlet temperature) thermal storage tank, although important, is not a controlling factor in achieving high efficiencies by virtue of high temperature differences (high Richardson numbers). However, the achievement of high Richardson numbers is possible only if the solar collection strategy, as proposed by Cole and Bellinger (1982), is based on displacing one tank volume per collection day. Clearly, any recycling of the heated and stored fluid would tend to decrease the Richardson number to a significant degree leading to a case similar to that of chilled water.

Based on the foregoing discussion, it may be advantageous to look for conditions under which a high degree of stratification can be maintained under all through-flow conditions regardless of whether it is chilled or hot water storage. The solution lies in choosing a combination of flow parameters and inlet design configurations. To

achieve this, the approach employed in this study was two-fold: (1) developing the means for quantifying the mixing processes in the tank (mixing index) and (2) characterizing the inlet configurations by using the developed mixing index. The introduction of the effective diffusivity factor in combination with laboratory model tests proved to be successful in determining the range of conditions that enhance stratification. This was expressed in terms of Richardson number alone. Based on the experiments with fresh-saline water system a value of Richardson number of 5.0 was found to be the limit below which the diffuser design and layout starts to be a determining factor in thermocline thermal storage tank performance. The study (Zurigat et al. 1988a) showed that the perforated diffuser gives the best performance as opposed to other configurations tested. Using this diffuser, a plug-type flow was approached and consequently the mixing index was found to be minimum.

It should be noted that while the experiments with fresh-saline water system helped in establishing the main parameters governing the flow in a stratified tank, they were based on one point measurements which can not resolve the sequence of events at or close to the inlet region. Therefore a well-instrumented hot-cold water system was developed (Zurigat et al. 1988b and Rao et al. 1988). Based on these measurements, it was observed that two- and three- dimensional effects at and close to the inlet region were clearly present. With this system, a better temperature representation at different elevations in the tank (see Figure 3.1) was achieved. In this manner, a more accurate one-dimensional model was developed (Ghajar et al. 1987 and Zurigat et al. 1988b). This model was shown (Zurigat et al. 1987 and Maloney 1987)

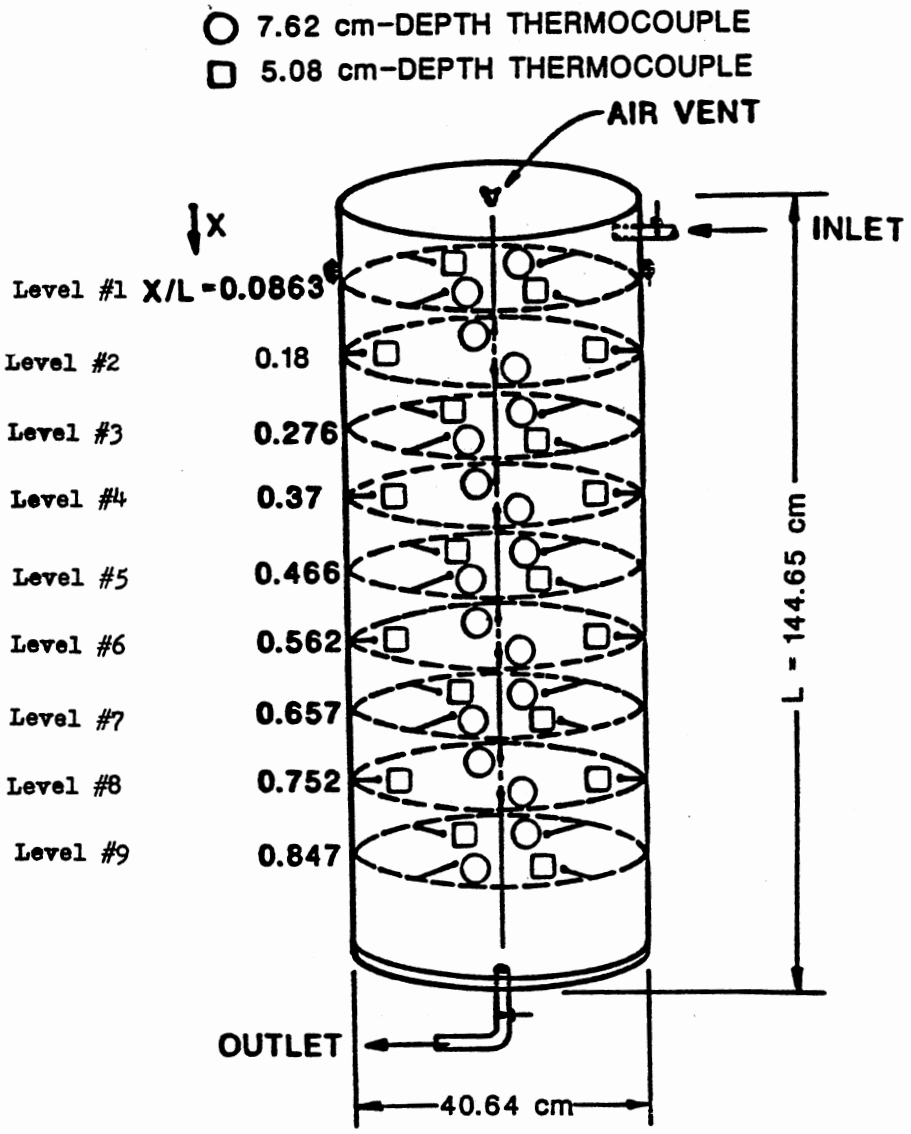

Figure 3.1 Test Tank Thermocouples Configuration (Zurigat and Liche 1987)

to be one of the most accurate one-dimensional models in the literature and certainly the most definitive, since it included inlet mixing correlations. The results of the study with hot-cold water system (Zurigat and Liche 1987 and Zurigat et al. 1988b) for three different inlet geometries indicated that for Richardson numbers greater than 3.6 no significant difference in the performance of the storage tank for the inlets tested was observed. This is slightly less than the value of 5.0 obtained from the previous study (Zurigat et al. 1988a). It is worth noting the important implications of these results to thermocline thermal storage tanks design. That is, these numbers put more stringent conditions on thermal storage devices installed in the basements of buildings for either chilled water storage or heat rejection storage by virtue of the small height-to-width ratios of these devices.

In view of the complexity of flow processes in the storage tank it should be noted that it is difficult to develop a generic one-dimensional model which will predict the temperature profile throughout the tank. The role of the inlet design in development of such a model is important since the physical processes are so complex and particular to each individual inlet design. In this case, the best one could do is to correlate the data from experiments for one inlet design and thereby characterize the performance of that design with respect to geometric and flow parameters. The alternative is to develop two- or three-dimensional models which are more capable of accounting for different flow processes under a wider range of conditions. Further work in this direction was undertaken. This is the subject of the next chapter.

CHAPTER IV

EXPERIMENTAL AND ANALYTICAL TREATMENT OF SST UNDER VARIABLE INLET TEMPERATURE CONDITIONS

This study was undertaken to investigate the design improvements of single stratified tanks for better performance. The significance and potential benefits of stratified thermal storage were discussed in Chapter I. The literature review presented in Chapter II established the need for this work. A comprehensive experimental and analytical approach was adopted to fill some of the gaps in the literature.

The studies presented in the previous chapter (see Chapter III) were restricted to thermocline thermal storage (constant inlet temperature). In practice, however, the inlet temperature may vary. Further investigation was carried out to deal with this problem using both experimental and analytical approaches. These are presented in the following sections.

4.1 Experimental Approach

4.1.1 Physical Model

As stated earlier, in the variable inlet temperature case, the incoming stream has to be distributed to the corresponding levels in the tank, with minimum mixing with the unlike temperature levels. While it is technically feasible to control the flow inlet location using a series of valves with temperature sensing controls (see Figure 4.1), the

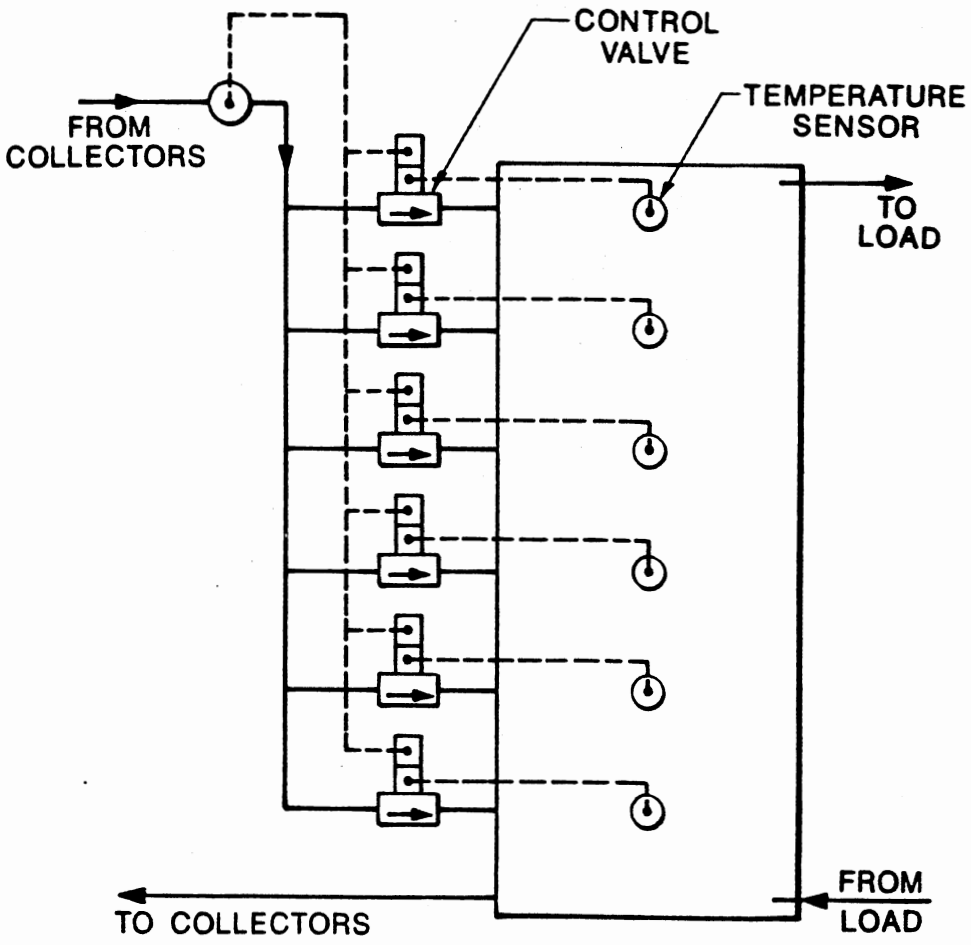

Figure 4.1 Fully Stratified Storage Tank with Temperature Sensor-Control Valve Assembly

high cost and low reliability of such a system make it impractical. A simple passive technique is more desirable.

It is known from buoyant-flow theory that when a buoyant jet is discharged vertically into a stably stratified ambient fluid, a buoyancy force opposite to the initial momentum flux is ultimately encountered. When the initial momentum is totally destroyed, the jet ceases to continue and begins to spread horizontally at the level of neutral buoyancy (Chen and Rodi 1979).

Considering these facts, simple inlet distributors may be designed. Figure 4.2 shows a simple inlet distributor which consists of a distribution manifold and a cylindrical deflection baffle. The incoming stream is discharged into the tank horizontally where the initial momentum is greatly reduced and is then deflected by the baffle. A plume-like flow will then commence in either the upward or the downward direction. The deflected plume attaches itself to the tank wall (Pera and Gebhart 1975) and spreads horizontally at the neutral buoyancy level. Entrainment of the tank fluid by the plume is reduced by the presence of the wall; to reduce it further, the deflection baffle may have perforated extensions (see Figure 4.2)

4.1.2 Experimental Setup and Procedures

Experiments with the hot-cold water system (see Figure 4.3) were conducted to quantify the performance of stratified tank under variable inlet temperature conditions and to provide the needed input for the analytical model described in the next section. The system (for details see Abu-Hamdan 1988) consists of a hot water supply tank (100 gallon), an insulated steel test tank (16 in. diameter and 60 in. high, 0.1 in.

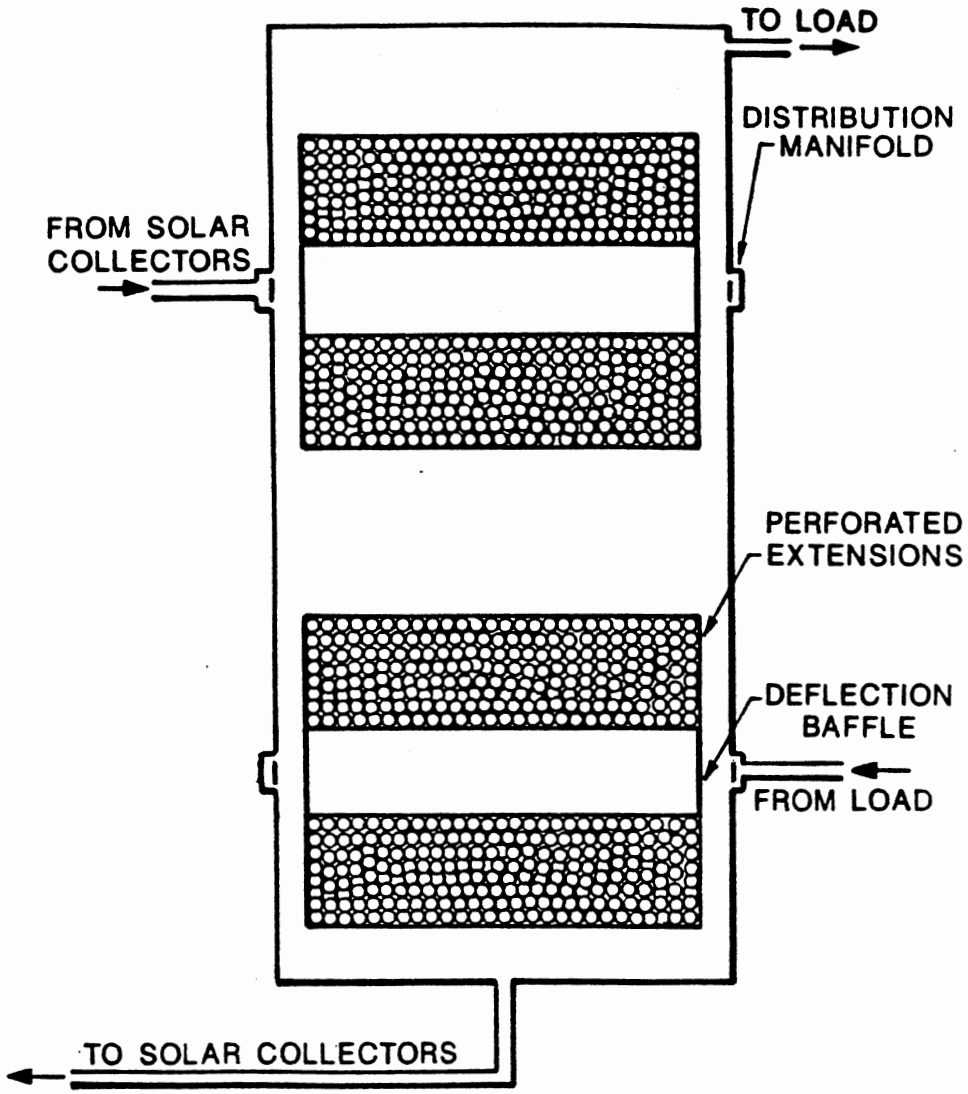

Figure 4.2 Schematic of Stratified Thermal Storage Tank - Baffle Arrangement

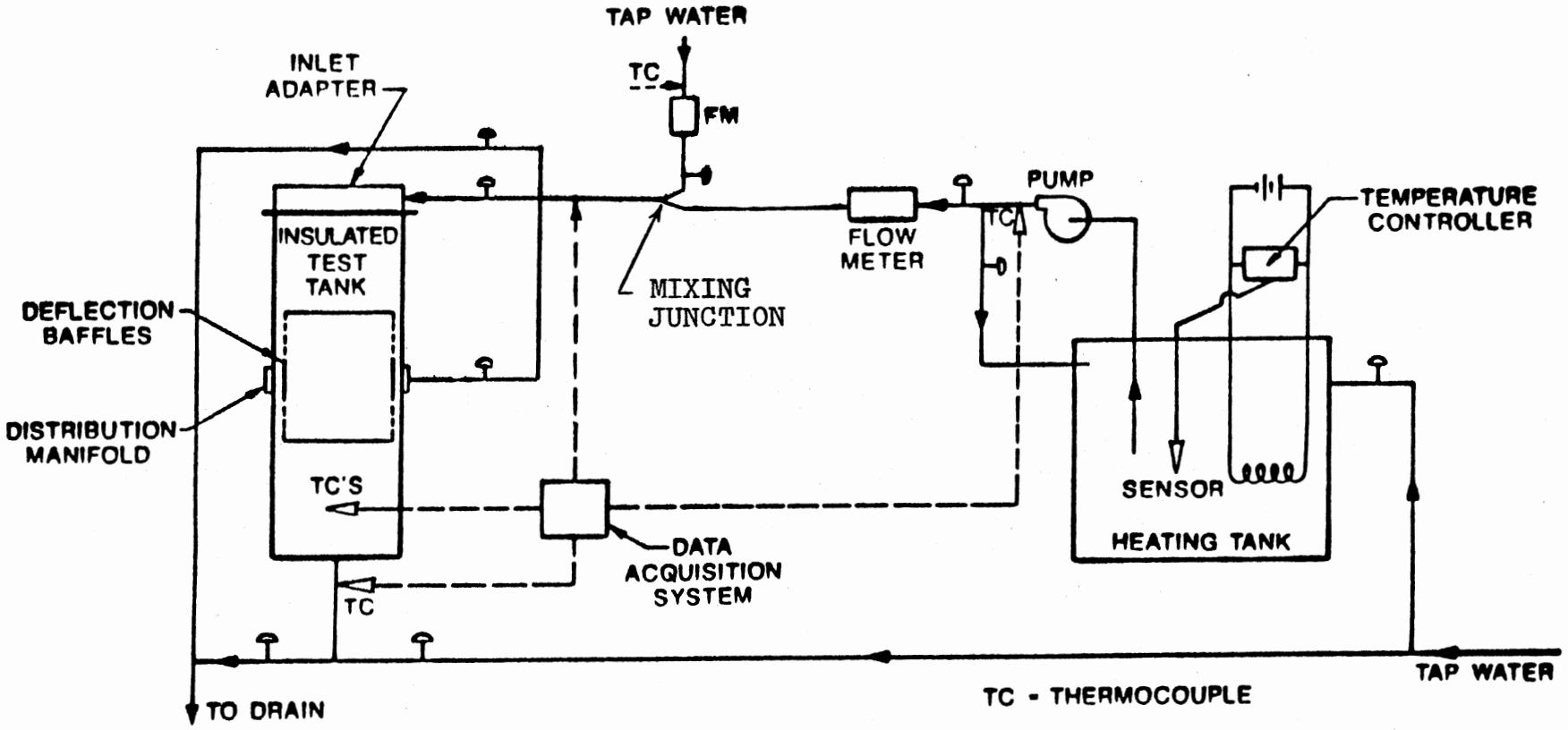

Figure 4.3 Hot-Cold Water System Experimental Setup Schematic

thick wall wrapped with 3 in. of fiberglass insulation of 3.7 R-value), a metered flow system, temperature-sensor arrays, and the data acquisition system. A mixing valve is used to furnish the desired inlet temperature variation which ranges between the two temperature extremes ($T_o \leq T_{in}(t) \leq T_{max}$).

The hot water supply tank is equipped with five electric resistance heaters of 5500 Watts each. This allows for obtaining supply water temperatures of up to 200°F in approximately one hour. The test tank is equipped with an inlet adapter to facilitate the installation of conventional inlet configurations. The baffle is mounted symmetrically around the mid-height of the tank.

Transient temperature profiles inside the test tank were measured using 36 T-type thermocouples mounted at 9 levels with 4 thermocouples in each level. Four additional thermocouples were used to monitor the tap water temperature at the inlet of the mixing valve, the exit temperature from the mixing valve (test tank inlet temperature), the exit temperature from the test tank, and the hot water supply tank temperature. Ambient surrounding temperature was measured using a mercury thermometer.

The data acquisition system used consists of a 40-channel data logger interfaced with a TI computer. The data acquisition system and the data reduction software written in C-language are reported by Rao et al. (1988).

The tests covered a wide range of conditions, i.e., flow rates and temperature variations. Duplicate tests were conducted with conventional inlets to measure the improvement in performance. These tests were restricted to the charge mode of operation since this mode of

operation is doubly important for both solar collectors and storage tanks.

4.2 Analytical Approach

4.2.1 The General Governing Equations

The flow in a stratified tank is governed by the well-known conservation equations of mass, momentum and energy. It is assumed that the flow is turbulent (Schlichting, 1979) and the viscous dissipation is negligible (Mach number is small). The governing equations written in Cartesian tensor notation are:

$$\text{Continuity} \quad \frac{\partial \rho}{\partial t} + \frac{\partial \rho \bar{u}_i}{\partial x_i} = 0 \tag{4.2.1}$$

$$\text{Momentum} \quad \frac{D\rho\bar{V}}{Dt} = -\nabla\bar{P} + \nabla^2\mu\bar{V} - \frac{\partial}{\partial x_j}(\rho\overline{u_i' u_j'}) + g_i\rho - \bar{R}_i \tag{4.2.2}$$

$$\text{Energy} \quad C_p \frac{D\rho\bar{T}}{Dt} = -\frac{\partial}{\partial x_i}(q_i) \tag{4.2.3}$$

$$\text{where} \quad q_i = -K\frac{\partial \bar{T}}{\partial x_i} + C\rho\overline{u_i' T_i'}$$

In addition, an equation of state is provided of the form:

$$\rho = \rho\,(\bar{T}) \tag{4.2.4}$$

The terms $\rho\overline{u_i' u_j'}$ and $\rho\overline{u_i' T_i'}$ are the turbulent stress tensor and the turbulent heat flux respectively which are modeled by an appropriate turbulence model. The term $\bar{R}_i$ in the momentum equation is the resistance force vector (Chang, 1981) which arises, for example, due to

the presence of baffles.

4.2.2 The Mathematical Model

Considering the geometry of the physical model under testing, the flow in the stratified tank can be modeled as two-dimensional and axisymmetric. It is possible to invoke the Boussinesq approximation (Crapper and Baines, 1977) wherein the density is assumed constant except in the bouyancy term of the momentum equations. Further by invoking the Boussinesq assumption which relates the apparent turbulent shearing stress to the rate of mean strain through an apparent scalar turbulent or "eddy" viscosity, the governing equations (Equations 4.2.1 through 4.2.3) written in primitive variables and in conservative form in both cartesian ($\zeta = 0$) and cylindrical coordinates ($\zeta = 1$, $x \equiv r$) reduce to (statistical averaging bar is dropped out for convenience):

Continuity

$$\frac{\partial u}{\partial x} + \frac{\partial v}{\partial y} + \zeta \frac{u}{x} = 0 \tag{4.2.5}$$

u-Momentum

$$\frac{\partial u}{\partial t} + \frac{\partial uu}{\partial x} + \frac{\partial uv}{\partial y} + \zeta \frac{u^2}{x} = - \frac{g_c \partial P}{\rho_o \partial x} + \frac{\partial}{\partial x} \left(\frac{\mu_{eff}}{\rho_o} \frac{\partial u}{\partial x}\right)$$

$$+ \frac{\partial}{\partial y} \left(\frac{\mu_{eff}}{\rho_o} \frac{\partial u}{\partial y}\right) + \zeta \left[\frac{\mu_{eff}}{x\rho_o} \left(\frac{\partial u}{\partial x} - \frac{u}{x}\right)\right] - \frac{R_x}{\rho_o \ell_x} \tag{4.2.6}$$

v-Momentum

$$\frac{\partial v}{\partial t} + \frac{\partial uv}{\partial x} + \frac{\partial vv}{\partial y} + \zeta \frac{uv}{x} = - \frac{g_c \partial P}{\rho_o \partial y} + g_y \beta(T - T_o)$$

$$+ \frac{\partial}{\partial x}\left(\frac{\mu_{eff}}{\rho_o} \frac{\partial v}{\partial x}\right) + \frac{\partial}{\partial y} \left(\frac{\mu_{eff}}{\rho_o} \frac{\partial v}{\partial y}\right) + \zeta \frac{\mu_{eff}}{x\rho_o} \frac{\partial v}{\partial x} - \frac{R_y}{\rho_o \ell_y} \qquad (4.2.7)$$

Energy

$$\frac{\partial T}{\partial t} + \frac{\partial uT}{\partial x} + \frac{\partial vT}{\partial y} + \frac{\zeta}{x} uT = \frac{\partial}{\partial x}\left(\frac{K_{eff}}{\rho_o C_p} \frac{\partial T}{\partial x}\right)$$

$$+ \frac{\partial}{\partial y} \left(\frac{K_{eff}}{\rho_o C_p} \frac{\partial T}{\partial y}\right) + \zeta \frac{K_{eff}}{x\rho_o C_p} \frac{\partial T}{\partial x} \qquad (4.2.8)$$

The effective viscosity and conductivity appearing in the above equations are defined as the sum of the laminar and turbulent contributions, that is,

$$\mu_{eff} = \mu_\ell + \mu_t \qquad (4.2.9)$$

$$K_{eff} = K_\ell + K_t \qquad (4.2.10)$$

where μ_t and K_t are the turbulent contributions obtained from the turbulence model discussed in the next section.

The resistance terms, R_x, R_y are defined by Sha et al. (1980) as:

$$R_x = \frac{1}{2} f\rho|u|u \qquad (4.2.11)$$

$$R_y = \frac{1}{2} f\rho|v|v \qquad (4.2.12)$$

where the friction factor, f, is to be calculated based on the diameter and thickness of the perforations. The ℓ_x and ℓ_y appearing in the resistance terms are the appropriate length scales associated with R_x and R_y respectively. They may be taken as the grid sizes in the x- and y-directions.

4.3 Turbulence Model

The commonly-used description of turbulent motion in terms of time-averaged quantities rather than instantaneous gave rise to the familiar closure problem. This in turn has led to the development of turbulence models which describe the relevant correlations, that is, the turbulent shear stress and heat flux quantities.

The turbulence models are classified in several ways. The most widely used classification is that based on the number of differential equations solved in addition to the mean flow equations. Thus, the zero-, one-, and two- equation models are frequently referenced. In these models, the well known Boussinesq assumption is used. A fourth class of models which do not use this assumption solve for the Reynolds stresses from differential equations. These models are labeled the Reynolds Stress Equation Models.

The main concepts of turbulence modeling are described in the monograph by Launder and Spalding (1972) and the calculation methods for various classes of turbulent flows are presented by Bradshaw et al. (1981). The two-equation turbulent models are the most widely used class of models in present engineering calculations. In these models, two partial differential equations are used to describe the development of turbulent kinetic energy and its rate of dissipation. The most

recent reviews of two-equation turbulence models and other turbulent models have been reported by Nallasamy (1985), Markatos (1986) and Ferziger (1987).

The two-equation turbulence models constitute a significant improvement over the zero-equation turbulence models since, in the former, the length scale in turbulent flows is expressed in terms of flow parameters, i.e, the upstream "history" of the flow, while in the latter, it is assumed that turbulence is in local equilibrium, with turbulent energy locally produced and dissipated at the same rate. In certain situations, (Nallasamy 1985), the two-equation turbulence models are not suitable due to the assumption of isotropic eddy viscosity employed in these models. The Reynolds stress models overcome this problem by providing a transport equation for individual stresses.

Despite the obvious advantage in using the multi-equation turbulence models, it should be noted that their performance varies with the flow configuration studied. Adjustment of the "universal" constants in these models is frequently needed when applying these models to situations for which these constants were not optimized. In addition, the increased computational complexity results in increased computer time which is a limiting factor in many cases.

Based on the foregoing discussion, a zero-equation model was used in this study. It is believed that this model in conjunction with the use of an accurate discretization scheme, discussed in the next section, is superior to using a two-equation model with the conventional upwind scheme used in the previous investigations.

The proposed turbulence model is the simple eddy viscosity model (Sha et al. 1980) given by:

$$\mu_t = 0.007\ C_\mu\ \rho U_{max} \ell \tag{4.3.1}$$

where

$$C_\mu = \begin{cases} 0.1 & \text{for } Re_{max} > 2000 \\ 0.1\ (0.001\ Re_{max}^{-1}) & \text{for } 1000 \leq Re_{max} \leq 2000 \\ 0 & \text{for } Re_{max} < 1000 \end{cases} \tag{4.3.2}$$

$$U_{max} = \max\ (u,v)$$

$$Re_{max} = \max\ (Re_y,\ Re_x) \tag{4.3.3}$$

$$\ell = \max\ (\Delta x,\ \Delta y)$$

and

$$K_t = \frac{C_p \mu_t}{Pr_t} \tag{4.3.4}$$

where the turbulent Prandtl number, Pr_t, is evaluated by:

$$Pr_t = 0.8\ [1 - \exp\ (-6x10^{-5}\ Re_{max}\ Pr^{1/3})]^{-1} \tag{4.3.5}$$

The Reynolds number, Re is based on the maximum fluid velocity and the characteristic length; ℓ.

4.4 Solution Technique

Numerical computations of flow in a stratified thermal storage tank can, in principle, produce results comparable with the experiments due to their capability of accounting for the nonlinearities inhibiting closed form solution and their flexibility in incorporating turbulence models. However, these computations are seriously affected by numerical diffusion, instability, and computational cost. Therefore, the choice

of the numerical procedure and the discretization scheme is critical to the success and validity of the results.

The computer codes most widely used at present, i.e, TEACH-T, TEACH-L and SOLA employ discretization schemes based on conventional 'upwind' or 'donor cell' differencing of convective terms. This gives rise to a discretization error (numerical diffusion) which limits the present codes to diagnostic purposes only, by virtue of the qualitative nature of the results. Numerical diffusion (truncation and crossflow) is shown (Huh et al. 1986) to be significant compared to the physical diffusion (see Table II). Therefore, it should be reduced to enable computer codes to be used as design tools. It should be noted that several computer codes (Busnaina (1979); Busnaina (1983); Lilley and Rhode (1982)) were developed at Oklahoma State University based on the conventional upwind differencing of convective terms. While these codes are quite useful in many instances, the pressing need for more accurate predictions requires new prediction tools employing more advanced numerical techniques.

The upwind scheme gained popularity among computational fluid practitioners because it is superior to the central difference scheme when the local grid Peclet number is large (Spalding 1972). However, it was soon recognized that the stability furnished by the upwind scheme was bought at the expense of accuracy. As a result, thermal hydraulic computer predictions generally describe more diffusion and mixing than are seen in experimental results. In practical situations where a large number of computational cells must be used, numerical diffusion (truncation and crossflow) is often found to dominate the effects of turbulent diffusion. Hence any improvements in turbulence modeling,

TABLE II

RATIOS OF TRUNCATION ERROR DIFFUSION COEFFICIENT TO CROSSFLOW DIFFUSION AND PHYSICAL DIFFUSION FOR SEVERAL VALUES OF PECLET NUMBERS (Huh et al. 1986)*

$Pe = u\Delta x/D_e$	$D_{TE}/u\Delta x$	D_{TE}/D
0.1	0.49	0.05
0.2	0.48	0.1
0.5	0.47	0.23
1.0	0.44	0.44
2.0	0.41	0.82
5.0	0.36	1.79
10.0	0.32	3.17
100.0	0.21	20.67
1000.0	0.14	143.74
10^8	0.05	4.38×10^7

* $D_{TE} = D_e - D$ where D_e is the effective (i.e., numerical plus physical) diffusion coefficient which is reflected in the numerical solution.

which is the target of physical modeling efforts, will be overshadowed without the removal of numerical diffusion.

The increasing demand for accuracy in numerical computations has lead to the development of several new schemes (see Table III). A number of comparative studies of these schemes has been conducted (see Table IV) by application to flow situations with well-established analytical or numerical solutions or with experimental data (see Table V). These studies suggest that the Second Order Upwind, the Skew Upwind

and the Quadratic Upwind Interpolation Difference Schemes offer better accuracy than the other schemes. Therefore one of these three schemes was adopted in this study; namely, the Second Order Upwind Difference Scheme (SOUDS). The conventional Weighted Upwind Difference Scheme (WUDS) was also implemented.

The choice between explicit and implicit formulations is rather difficult to justify. It was argued by Issa (1983) that the explicit scheme is prohibitively expensive for steady state solutions while for transient solutions it may offer some advantage. However, the simplicity of implementation and the accuracy of the explicit scheme are two factors to be weighed against computational inefficiency which is normally overcome by the implicit formulation. In this study, the explicit formulation was adopted.

TABLE III

PARTIAL LIST OF DISCRETIZATION SCHEMES DEVISED BY VARIOUS INVESTIGATORS

No.	Numerical Scheme	Contributor
1.	Central Difference	
2.	Upstream (Upwind) Difference	
3.	Hybrid (Central & Upwind)	Spalding (1972)
4.	Weighted Upwind Difference	Hirt et al. (1975)
5.	Skew Upwind Difference	Raithby (1976)
6.	Skew Upwind Weighted Difference	Raithby (1976)
7.	Quadratic Upwind Interpolation	Leonard (1979)
8.	Locally Analytic Differencing	Wong and Raithby (1979)
9.	Power-Law Difference	Patankar (1980)
10.	Selective Grid Refinement Approach	McGuirk et al. (1982)
11.	Donor Cell Corrective Scheme	Huh et al. (1986)
12.	Second Order Upwind Differencing	Shyy (1985)
13.	Modified Central Difference Scheme with Controlled Numerical Diffusion	Runchal (1986)

The model equations were discretized on a staggered regular rectangular grid with non-uniform spacing with finer spacing situated in the region close to the wall where the baffle is located. While there are no universal rules about what maximum (or minimum) ratio the adjacent grid intervals should maintain, it is generally established that the grid spacing should be directly linked to the way the dependent variable changes in the calculation domain (Patankar, 1980). The discretization of the mathematical model described earlier is given in the next chapter along with the solution algorithm used.

TABLE IV

COMPARATIVE STUDIES OF PERFORMANCE OF VARIOUS DESCRETIZATION SCHEMES FROM TABLE III AS APPLIED TO VARIOUS FLUID FLOW PROBLEMS FROM TABLE V.

Contributor	Discretization Schemes (Table III) (Numbers in Parentheses Refer to Problems from Table V)	Remarks
Runchal (1972)	1, 2, 3, (1)	3 is the best from convergence and accuracy points of view
Raithby (1976)	1, 2, 4, 5, 6, (1)	5 & 6 reduce the error greatly, no stability problems.
	2, 5, 6, (2)	Results with 5&6 are angle dependent but generally better than 2. Overshoot and undershoot may occur with 5&6. Number of iterations for 5 & 6 is larger.
	2, 5, (3)	5 gave much better predictions.
Smith and Hutton (1982)	1, 2, 3, 4, 5, 6, 7, 8, 9, (11)	No single scheme emerged as the best.
McGuirk et al. (1982)	10, (19)	Grid-independent solution can be obtained using this method

TABLE IV (Continued)

Claus et al. (1984)	5, 5*, 7, (2)	Solution is angle dependent. For θ up to 15°, 7 is superior. For θ > 15°, 5 & 5* are superior.
	3, 5*, 7, (4)	7 is superior to 3 and 5*. It responds to grid refinement. 3 and 5* are highly inaccurate.
	3, 5*, 7, (20)	At θ = 40°, 5* & 7 are more accurate than 3. At θ = 25°, 5* is better than 7. 7 displays unphysical oscillations. It is also slower to converge. At θ = 0, all schemes are good.
5* is a bounded version of 5.		
Syed and Chiappetta (1985)	3, 5*, 7, (6)	5* & 7 perform equally well and they are superior to 3. 7 is less sensitive to grid refinement.
	3, 5*, 7, (7)	7 is unstable with fine mesh (uncompatible with TEACH solver).
	3, 5*, 7, (12)	5* is the best.
	3, 5*, 7, (13)	In the initial region with coarse grid the results do not agree with data regardless of the scheme used. With fine grid 7 was excluded. 3 & 5* are comparable.

TABLE IV (Continued)

	3, 5*, 7, (14)	7 is more accurate than 3 an 5*
	3, 5*, 7, (15)	5* reduces numerical diffusion considerably but there is a disagreement with experiments
Huang et al. (1985)	5, 7, 8, 9, (1)	5, 7 & 8 are much better than 9 with 7 being the worst among the best.
	5, 7, 8, 9, (2)	9 gives maximum false diffusion for θ = 45°, 5 gives exact solution. 7 & 8 are superior to 9 but they suffer from over- and under-shoots. For other flow angles 5 gives rise to more serios over-shoots than 7 and 8.
	5, 7, 8, 9, (4)	7 performs exceptionally well. 5 performs poorly, 8 fails to converge.
	5, 7, 8, 9, (16)	At Pe=5, 7 is superior. At low Raleigh number, differences between the schemes were minor.
	5, 7, 8, 9, (17)	5 & 7 solutions in regions of steep velocity gradients are much close to the true behavior. However, 5 produces oscillations in velocity.

TABLE IV (Continued)

	5, 7, 8, 9, (18)	All schemes but 5 gave excellent agreement. 5 and 9 fail to conserve total pressure.
Runchal et al. (1987)	3, 13, (1, 2, 5, 6, 7, 8, 9, 10, 11)	13 is much better in all the cases except in 5 where the hydrodynamic results were better than 3 but the temperature results were less accurate than 3.
Sharif and Busnaina (1987)	4, 5, 7, 13, (2)	4 produces maximum numerical diffusion. For all Peclet numbers 5, 7, and 13 have less numerical diffusion and have a comparable accuracy. At $\theta=45°$, 5 is the best. 7 and 13 produce over-shoots with maximum occuring at $\theta=26.6°$.
	4, 5, 7, 13, (13)	For $\theta=26.6°$, 5 introduces the least numerical diffusion but exhibits significant oscillation for $\|Pe\|=\infty$. 4 has the most numerical diffusion. 13 introduces moderate numerical diffusion and oscillation. For $\theta=45°$, 7 introduces significant oscillations.

TABLE V

FLUID FLOW PROBLEMS TESTED BY DIFFERENT FINITE DIFFERENCE DISCRETIZATION SCHEMES

No.	Test Problem	Available Solution
1.	Fluid in a Steady State of Solid Body Rotation	Closed Form
2.	Transport of a Step Change in Scalar in a Two-Dimensional Uniform Velocity Field at an Angle	Closed Form
3.	Interaction of Two Parallel Two-Dimensional Slot Jets	Experimental
4.	Square Cavity with a Moving Wall	Numerical (very fine grid)
5.	Square Cavity with a Moving Heated Wall	Numerical (very fine grid)
6.	Laminar Flow over a Backward Facing Step	Experimental
7.	Turbulent Flow over a Backward Facing Step	Experimental
8.	Uniform Constant Velocity Flow in Straight Pipe with Exponential Temperature Distribution	Closed Form
9.	Same as 8 above with Spatially Varying Heat Source	Closed Form
10.	Recirculating Flow with Temperature Source in a Prescribed Recirculating Velocity Field in a Square Cavity	Closed Form
11.	Step-Like Discontinuity in a Recirculating Flow	Numerical (very fine grid)
12.	Swirling Flow Downstream of a Sudden Expansion (Laminar)	None (Reference is made to turbulent experiments)

TABLE V. (Continued)

No.	Test Problem	Available Solution
13.	Coannular Nonswirling Turbulent Flow	Experimental
14.	Coannular Swirling Turbulent Flow	Experimental
15.	Cross Flow Multiple Jets in Duct (Three-Dimensional)	Experimental
16.	Laminar Buoyancy-Driven Cavity Flow	Numerical (Best available)
17.	Laminar Impinging Jet	None
18.	Irrotational Corner Flow	Closed Form
19.	Flow Downstream of a Confined Axisymmetric Baffle	Experimental
20.	Laminar Flow with Various Inlet Flow Angles	None

CHAPTER V

FINITE-DIFFERENCE FORMULATION OF THE MATHEMATICAL MODEL

In this chapter, the finite-difference analog of the mathematical model presented in the previous chapter is discussed. Both the conventional Weighted Upwind Difference Scheme (WUDS) and the more advanced scheme, i.e., the Second Order Upwind Difference Scheme (SOUDS) are formulated. The grid system, boundary conditions and the solution procedures are also presented.

5.1 The Grid System

The two-dimensional plane or axisymmetric flow domain is divided into rectangular cell divisions, with nonuniform spacing (see Figure 5.1). The location of the field variables P, u, v and T are shown for an arbitrary i,j-cell. It is seen that P and T are cell centered while the u- and v- velocities are located on the faces of the cell. This staggered arrangement eliminates the need for boundary conditions on pressure and allows for setting the boundary conditions on velocities with ease. A layer of fictitious cells is added on all sides of the computational domain to facilitate the application of momentum and thermal boundary conditions.

As pointed out by Sharif and Busnaina (1987) the staggered arrangement described above gives rise to three different control

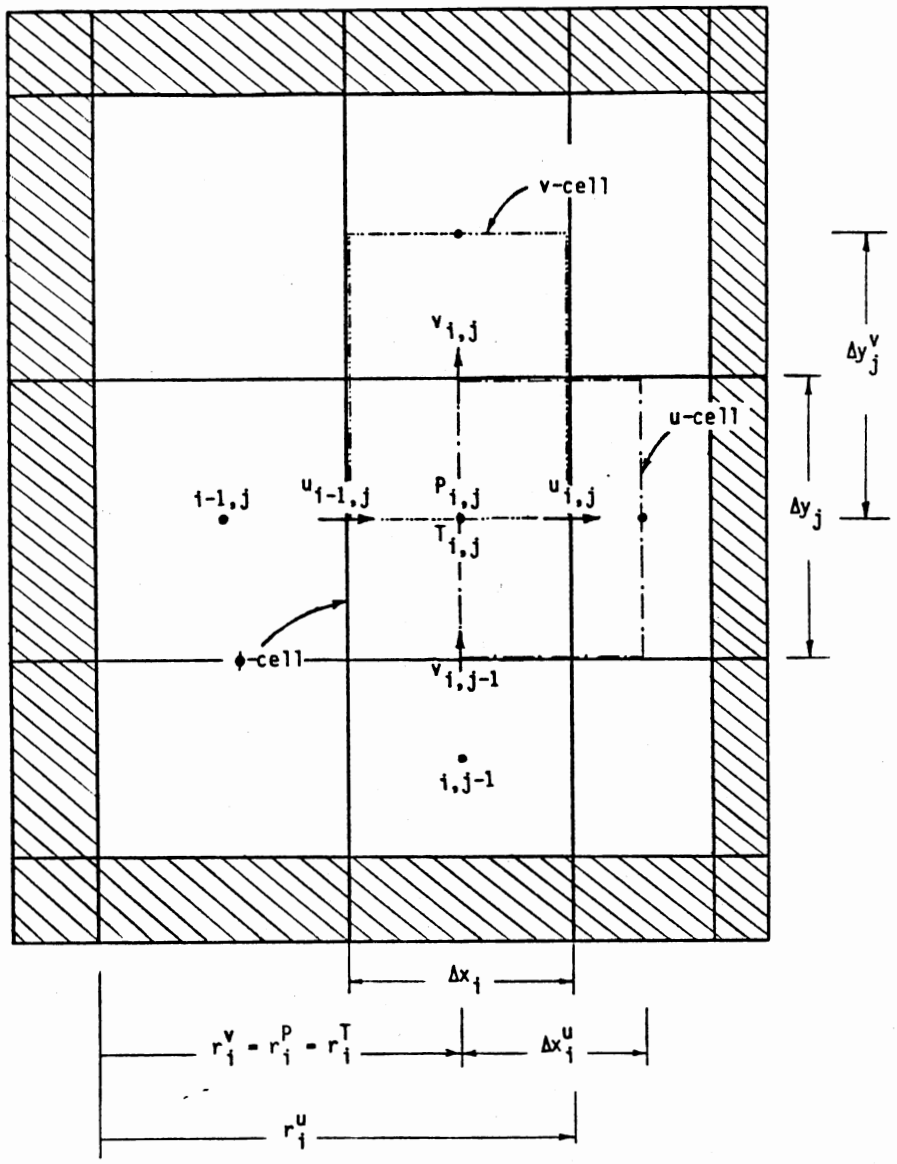

Figure 5.1 Grid Layout Showing Location of the Nodal Variables u, v, P, and T, ij Notation, and the ϕ- (T, P), u-, and v- Cells

volumes, the u-cell, the v-cell and the ϕ-cell for solving the x- (or r-) momentum, the y-momentum and the scalar transport equations, respectively (see Figure 5.1). With this convention the following grid dimensions are defined:

$$\Delta xh_i = \Delta x_i/2 \tag{5.1.1}$$

$$\Delta yh_j = \Delta y_j/2 \tag{5.1.2}$$

$$\Delta x_i^u = \Delta xh_i + \Delta xh_{i+1} \tag{5.1.3}$$

$$\Delta y_j^v = \Delta yh_j + \Delta yh_{j+1} \tag{5.1.4}$$

where Δx_i and Δy_j are the ϕ-cell dimensions. In addition, in the axisymmetric cylindrical coordinates the following dimensions are defined:

the radius to the center of the u-cell

$$r_i^u = \sum_{n=2}^{i} \Delta x_n \tag{5.1.5}$$

and the radius to the centers of the v-, P- and T-cells

$$r_i^v = r_i^P = r_i^T = r_i^u - \Delta xh_i \tag{5.1.6}$$

The non-uniform grid is generated using the procedure described by Lilley (1986) wherein an expanding or contracting grid is generated by the choice of an expansion ratio, EXP. That is, for values of EXP > 1.0 an expanding grid will result and for EXP < 1.0 a contracting grid is obtained. A uniform grid is obtained by the choice of a value of unity for EXP.

5.2 Finite-Difference Formulation

The discretization of partial differential conservation equations requires separate treatments for individual terms. For example, the time derivatives are discretized using forward one-sided difference while the approximation of diffusion terms makes exclusive use of the second-order central differencing. The approximation of the advection terms, however, requires special treatment which, as pointed out in the previous chapter, has been the topic of numerous studies. The formulation devised by Sharif and Busnaina (1987) for discretizing the conservation equations in cartesian coordinates is adopted and extended to axisymmetric cylindrical coordinates:

5.2.1 Continuity Equation (Equation 4.2.5)

$$[(u_{i,j}^{n+1} - u_{i-1,j}^{n+1})/\Delta x_i] + [(v_{i,j}^{n+1} - v_{i,j-1}^{n+1})/\Delta y_j] +$$

$$[\zeta(u_{i,j}^{n+1} + u_{i-1,j}^{n+1})/2r_i^P] = D_{i,j}^{n+1} \qquad (5.2.1)$$

where the superscript n+1 indicates the values at the new time step. The velocity divergence, $D_{i,j}^{n+1}$, should equal zero for perfect satisfaction of continuity. However, this is difficult to achieve numerically and some vanishingly small mass residue in a given computational cell is allowed within a preset tolerance. It will be seen in a later section that the satisfaction of continuity in this manner serves in solving the pressure-velocity coupling problem.

5.2.2 u-Momentum Equation (Equation 4.2.6)

$$\left(\frac{\partial u}{\partial t}\right)_{i,j} = (u^{n+1}_{i,j} - u^{n}_{i,j})/\Delta t \qquad (5.2.2.)$$

where the superscript n indicates the value at previous time step.

$$\left(\frac{\partial uu}{\partial x}\right)_{i,j} = \text{DUUDX} = (u_{E,u}\,\tilde{u}_E - u_{W,u}\,\tilde{u}_W)/\Delta x^u_i \qquad (5.2.3)$$

$$\left(\frac{\partial vu}{\partial x}\right)_{i,j} = \text{DVUDX} = (v_{N,u}\,\tilde{u}_N - v_{S,u}\,\tilde{u}_S)/\Delta y_j \qquad (5.2.4)$$

$$\left(\frac{\zeta uu}{x}\right)_{i,j} = \text{FUU} = \zeta(u_{E,u}\,\tilde{u}_E \Delta x h_i + u_{W,u}\tilde{u}_W \Delta x h_{i+1})/(r^u_i \Delta x^u_i \qquad (5.2.5)$$

$$\left(\frac{\partial P}{\partial x}\right)_{i,j} = \text{DPDX} = (P^n_{i+1,j} - P^n_{i,j})/\Delta x^u_i \qquad (5.2.6)$$

$$\left(\frac{\partial^2 u}{\partial x^2}\right)_{i,j} = \text{VISXU} = [(u^n_{i+1,j}-u^n_{i,j})/\Delta x_{i+1}-(u^n_{i,j}-u^n_{i-1,j})/\Delta x_i]/\Delta x^u_i \qquad (5.2.7)$$

$$\left(\frac{\partial^2 u}{\partial y^2}\right)_{i,j} = \text{VISYU} = [(u^n_{i,j+1}-u^n_{i,j})/\Delta y^v_j-(u^n_{i,j}-u^n_{i,j-1})/\Delta y^v_{j-1}]/\Delta y_j \qquad (5.2.8)$$

$$\frac{\zeta}{x}\left(\frac{\partial u}{\partial x} - \frac{u}{x}\right)_{i,j} = \text{VISCU} = \zeta[(u^n_{i+1,j} - u^n_{i-1,j})/2\Delta x^u_i - u_{i,j}/r^u_i]/r^u_i \qquad (5.2.9)$$

The superscript tilda (~) is used throughout this chapter to designate the velocity terms that are derived in Appendix A for WUDS and SOUDS methods. The subscripted velocities in Equations (5.2.3) to (5.2.5) are defined and derived in Appendix A.

The finite-difference analog of the resistance term in Equation (4.2.6) is derived as follows:

Linearize $Rx^{n+1}_{i,j}$ as (Sha et al. 1980):

$$Rx_{i,j}^{n+1} = Ax_{i,j}^{n} + Bx_{i,j}^{n}\, u_{i,j}^{n+1} \tag{5.2.10}$$

where the coefficients $Ax_{i,j}^{n}$ and $Bx_{i,j}^{n}$ for non-perforated baffles are defined as:

$$Ax_{i,j}^{n} = 0 \tag{5.2.11}$$

$$Bx_{i,j}^{n} = 10^{30} \tag{5.2.12}$$

and for perforated baffles (from Equation 4.2.11) are:

$$Ax_{i,j}^{n} = -\frac{1}{2} f\rho_{i,j}^{u} |u_{i,j}^{n}| u_{i,j}^{n} \tag{5.2.13}$$

$$Bx_{i,j}^{n} = f\rho_{i,j}^{u} |u_{i,j}^{n}| \tag{5.2.14}$$

where the friction factor, f, is a function of the baffle thickness to hole diameter ratio, and the porosity of the baffle (Engineering Sciences Data Item No. 72010, U.K., 1972). In the absence of baffles both $Ax_{i,j}^{n}$ and $Bx_{i,j}^{n}$ are set to zero. The density, $\rho^{u}{}_{i,j}$, is evaluated by:

$$\rho_{i,j}^{u} = (\Delta xh_{i+1}\rho_{i,j}^{n} + \Delta xh_{i}\rho_{i+1,j}^{n})/\Delta x_{i}^{u} \tag{5.2.15}$$

Substitution of Equations (5.2.2) to (5.2.10) in Equation (4.2.6) and rearranging explicitly gives the velocity at the new time step:

$$u_{i,j}^{n+1} = \{u_{i,j}^{n} + \Delta t[-g_c DPDX/\rho_o + \mu_{eff}(VISXU + VISYU + VISCU)/\rho_o \quad .$$

$$- DUUDX - DVUDX - FUU - Ax^{*}_{i,j}]\}/Bx^{*}_{i,j} \qquad (5.2.16)$$

where

$$Ax^{*}_{i,j} = Ax^{n}_{i,j}/\rho_o \Delta x^{u}_{i} \qquad (5.2.17)$$

$$Bx^{*}_{i,j} = 1.0 + \Delta t\ Bx^{n}_{i,j}/\rho_o\ \Delta x^{u}_{i} \qquad (5.2.18)$$

Notice that in the presence of non-perforated baffles $Bx^{n}_{i,j}$ evaluated by Equation (5.2.12) is large enough to force the calculated velocity to vanish by virtue of Equation (5.2.18). When no baffles are present $Bx^{*}_{i,j}$ becomes unity and $Ax^{n}_{i,j}$ is set to zero as in Equation (5.2.11). When baffles are present the calculated velocity is reduced according to the resistance encountered. It should be noted that the vertical baffle at i,j-location is placed such that it coincides with the right face of the ϕ-cell.

5.2.3 v-Momentum Equation (Equation 4.2.7)

$$(\frac{\partial v}{\partial t})_{i,j} = (v_{i,j}^{n+1} - v_{i,j}^{n})/\Delta t \qquad (5.2.19)$$

$$(\frac{\partial uv}{\partial x})_{i,j} = DUVDX = (u_{E,v}\tilde{v}_E - u_{W,v}\tilde{v}_W)/\Delta x_i \qquad (5.2.20)$$

$$(\frac{\partial vv}{\partial y})_{i,j} = DVVDY = (v_{N,v}\tilde{v}_N - v_{S,v}\tilde{v}_S)/\Delta y_j^{v} \qquad (5.2.21)$$

$$(\zeta\frac{uv}{x})_{i,j} = FUV = \zeta(u_{E,v}\tilde{v}_E + u_{W,v}\tilde{v}_W)/2r_i^{v} \qquad (5.2.22)$$

$$\left(\frac{\partial P}{\partial y}\right)_{i,j} = (P_{i,j+1} - P_{i,j})/\Delta y^{v}_{j} \tag{5.2.23}$$

$$\left(\frac{\partial^2 v}{\partial x^2}\right)_{i,j} = VISXV = [(v^{n}_{i+1,j}-v^{n}_{i,j})/\Delta x^{u}_{i}-(v^{n}_{i,j}-v^{n}_{i-1,j})/\Delta x^{u}_{i-1}]/\Delta x_{i} \tag{5.2.24}$$

$$\left(\frac{\partial^2 v}{\partial y^2}\right)_{i,j} = VISYV = [(v^{n}_{i,j+1}-v^{n}_{i,j})/\Delta y_{j+1}-(v^{n}_{i,j}-v^{n}_{i,j-1})/\Delta y_{j}]/\Delta y^{v}_{j} \tag{5.2.25}$$

$$\left(\frac{\zeta}{x}\frac{\partial v}{\partial x}\right)_{i,j} = VISCV = \zeta[(v_{E,v} - v_{W,v})/\Delta x_{i}]/r^{v}_{i} \tag{5.2.26}$$

Again the subscripted velocities and/or those with tilda in Equations (5.2.20) to (5.2.22) and in Equation (5.2.26) are defined and derived in Appendix A.

The finite-difference analog of the resistance term in Equation (4.2.7) is derived in a similar manner as in Equations (5.2.10) to (5.2.14) with subscript x replaced by y and u-velocity replaced by v-velocity. Also the density, $\rho^{u}_{i,j}$, is replaced by $\rho^{v}_{i,j}$ which is evaluated as:

$$\rho^{v}_{i,j} = (\Delta yh_{j+1}\rho^{n}_{i,j} + \Delta yh_{j}\rho^{n}_{i,j+1})/\Delta y^{v}_{j} \tag{5.2.27}$$

This being done, substitution of Equations (5.2.19) to (5.2.27) and those analogous to Equations (5.2.10) to (5.2.14) in Equation (4.2.7) gives:

$$v^{n+1}_{i,j} = \{v^{n}_{i,j} + \Delta t[-g_c DPDY/\rho_o + \mu_{eff}(VISXV + VISYV + VISCV)/\rho_o - DUVDX - DVVDY - FUV - g_y(\rho_o - \rho^{v}_{i,j})/\rho_o - Ay^{*}_{i,j}]\}/By^{*}_{i,j} \tag{5.2.28}$$

where $$Ay^{*}_{i,j} = Ay^{n}_{i,j}/\rho_o \Delta y^{v}_{j} \tag{5.2.28a}$$

$$By^{*}_{i,j} = 1.0 + \Delta t By^{n}_{i,j}/\rho_o \Delta y^{v}_{j} \tag{5.2.28b}$$

It should be pointed out that the horizontal baffle at i,j-location is situated such that it coincides with the northern face of the ϕ-cell.

5.2.4 Energy Equation (Equation 4.2.8)

$$(\frac{\partial T}{\partial t})_{i,j} = (T^{n+1}_{i,j} - T^{n}_{i,j})/\Delta t \tag{5.2.29}$$

$$(\frac{\partial uT}{\partial x})_{i,j} = DUTDX = (u_{E,T}\bar{T}_E - u_{W,T}\bar{T}_W)/\Delta x_i \tag{5.2.30}$$

$$(\frac{\partial vT}{\partial y})_{i,j} = DVTDY = (v_{N,T}\bar{T}_N - v_{S,T}\bar{T}_S)/\Delta y_j \tag{5.2.31}$$

$$(\zeta\frac{uT}{x})_{i,j} = UTC = \zeta(u_{E,T}\bar{T}_E + u_{W,T}\bar{T}_W)/2r^{T}_{i} \tag{5.2.32}$$

$$(\frac{\partial^2 T}{\partial x^2})_{i,j} = DIFTX = [(T^{n}_{i+1,j} - T^{n}_{i,j})/\Delta x^{u}_{i} - (T^{n}_{i,j} - T^{n}_{i-1,j})/\Delta x^{u}_{i-1}]/\Delta x_i \tag{5.2.33}$$

$$(\frac{\partial^2 T}{\partial y^2})_{i,j} = DIFTY = [(T^{n}_{i,j+1} - T^{n}_{i,j})/\Delta y^{v}_{j} - (T^{n}_{i,j} - T^{n}_{i,j-1})/\Delta y^{v}_{j-1}]/\Delta y_j \tag{5.2.34}$$

$$\left(\frac{\zeta}{x}\frac{\partial T}{\partial x}\right)_{i,j} = DIFTC = \zeta[(T^n_{i+1,j}\Delta xh_i + T^n_{i,j}\Delta xh_{i+1})/\Delta x^u_i$$

$$- (T^n_{i,j}\Delta xh_{i-1} + T^n_{i-1,j}\Delta xh_i)/\Delta x^u_{i-1}]/(\Delta x_i r^T_i) \tag{5.2.35}$$

The subscripted velocities and the temperatures with superscript tilda in Equations (5.2.30) to (5.2.32) are defined and derived in Appendix A. Substitution of Equations (5.2.29) to (5.2.35) in Equation (4.2.8) and rearranging gives:

$$T^{n+1}_{i,j} = T^n_{i,j} + \Delta t K_{eff}(DIFTX + DIFTY + DIFTC - DUTDX$$

$$- DVTDY - UTC)/\rho_o C_p \tag{5.2.36}$$

Equations (5.2.16), (5.2.28) and (5.2.36) along with Equations (5.2.1) constitute the complete finite-difference analog of the conservation equations (Equations (4.2.5) to (4.2.8)). Examining these equations two observations are in order:

1. The presence of temperature-dependent source term; the bouyancy term, in Equation (4.2.7) results in coupling between velocity and temperature, i.e., momentum-to-energy coupling. On the other hand, velocities appearing in the advection terms in the energy equation (Equation 4.2.8) result in the converse energy-to-momentum coupling. This bidirectional coupling generally requires iterative solution. This will be discussed in a later section.

2. The absence of separate equation for pressure poses a problem in calculating the flow field variables. The pressure appears in both the u- and v-momentum equations. This velocity-pressure coupling requires special treatment since the accuracy of the computed pressure field determines that of the computed velocity field which, in turn, determines the satisfaction of continuity requirements. Thus for a given initial guess of the pressure field or for that calculated from a previous time step, the calculated velocity field will not, in general, satisfy the continuity equation, Equation (5.2.1). An iterative adjustment of the pressure at each computational cell and the velocities thereafter is normally employed; this is the topic of the next section.

5.3 Pressure-Velocity Adjustment Equations

The pressure adjustment is done such that the residue $D_{i,j}^{n+1}$ in Equation (5.2.1) is minimized. The Newton-Raphson scheme, which is iterative in character, is used to find the necessary pressure adjustment increment. The increment in the independent variable ξ that satisfies the function γ is determined from (Carnahan et al. 1969):

$$\frac{\partial \gamma}{\partial \xi} \Delta\xi = -\omega\gamma \tag{5.3.1}$$

where ω is an over-relaxation factor used to speed up the convergence. Applying this to our case and rearranging gives the correction increment in pressure.

$$\Delta P^N_{i,j} = - \omega D^N_{i,j} / \frac{\partial D^N_{i,j}}{\partial P^N_{i,j}} \tag{5.3.2}$$

where the superscript N indicates the N-th iteration in the same time step.

The new pressure is then determined by:

$$P^{N+1}_{i,j} = P^N_{i,j} + \Delta P^N_{i,j} \tag{5.3.3}$$

where $P^N_{i,j}$ is the pressure from previous iteration in the same time step. The pressure increment results in a velocity increment which is obtained by writing the momentum equations, i.e., Equations (5.2.16) and (5.2.28) for the four velocities of the ϕ-cell with the new pressure, $P^{N+1}_{i,j}$ and subtracting a similar expression with $P^N_{i,j}$. Thus, from Equation (5.2.16) we have:

$$u^{P^N}_{i,j} = \{u^N_{i,j} + \Delta t[(P^N_{i,j} - P^N_{i+1,j})g_c/\rho_o \Delta x^u_i + OT]\}/Bx^*_{i,j} \tag{5.3.4}$$

$$u^{P^{N+1}}_{i,j} = \{u^N_{i,j} + \Delta t[(P^{N+1}_{i,j} - P^N_{i+1,j})g_c/\rho_o \Delta x^u_i + OT]\}/Bx^*_{i,j} \tag{5.3.5}$$

where OT designates other terms appearing in Equations (5.2.16) and (5.2.28). Subtracting Equation (5.3.4) from (5.3.5) gives:

$$\Delta u^{N+1}_{i,j} = u^{P^{N+1}}_{i,j} - u^{P^N}_{i,j} = \frac{\Delta t(P^{N+1}_{i,j} - P^N_{i,j})g_c}{Bx^*_{i,j}\ \rho_o\ \Delta x^u_i} \tag{5.3.6}$$

or by Equation (5.3.3) we have:

$$\Delta u^{N+1}_{i,j} = \frac{\Delta t \ \Delta P^{N}_{i,j} g_c}{Bx^{*}_{i,j} \ \rho_o \ \Delta x^{u}_{i}} \tag{5.3.7}$$

The new velocity $u^{N+1}_{i,j}$ is then calculated from:

$$u^{N+1}_{i,j} = u^{N}_{i,j} + \Delta u^{N+1}_{i,j} = u^{N}_{i,j} + \frac{\Delta t \ \Delta P^{N}_{i,j} g_c}{Bx^{*}_{i,j} \ \rho_o \ \Delta x^{u}_{i}} \tag{5.3.8}$$

In a similar fashion we have for the velocity at the left face of the ϕ-cell, $u^{N+1}_{i-1,j}$:

$$u^{P^N}_{i-1,j} = \{u^{N}_{i-1,j} + \Delta t[(P^{N}_{i-1,j} - P^{N}_{i,j}) g_c / \rho_o \Delta x^{u}_{i-1} + OT]\} / Bx^{*}_{i-1,j} \tag{5.3.9}$$

$$u^{P^{N+1}}_{i-1,j} = \{u^{N}_{i-1,j} + \Delta t[(P^{N}_{i-1,j} - P^{N+1}_{i,j}) g_c / \rho_o \Delta x^{u}_{i-1} + OT]\} / Bx^{*}_{i-1,j} \tag{5.3.10}$$

Subtracting (5.3.9) from (5.3.10) gives:

$$\Delta u^{N+1}_{i-1,j} = u^{P^{N+1}}_{i-1,j} - u^{P^{N}}_{i-1,j} = \frac{\Delta t (P^{N}_{i,j} - P^{N+1}_{i,j}) g_c}{Bx^{*}_{i-1,j} \ \rho_o \Delta x^{u}_{i-1}} \tag{5.3.11}$$

or by Equation (5.3.3) we have:

$$\Delta u^{N+1}_{i-1,j} = \frac{-\Delta t\ \Delta P^{N}_{i,j} g_c}{\overset{*}{Bx}_{i-1,j}\ \rho_o \Delta x^{u}_{i-1}} \tag{5.3.12}$$

and the new velocity is thus:

$$u^{N+1}_{i-1,j} = u^{N}_{i-1,j} + \Delta u^{N+1}_{i-1,j} = u^{N}_{i-1,j} - \frac{\Delta t\ \Delta P^{N}_{i,j} g_c}{\overset{*}{Bx}_{i-1,j}\ \rho_o \Delta x^{u}_{i-1}} \tag{5.3.13}$$

The v-velocities $v^{N+1}_{i,j}$ and $v^{N+1}_{i,j-1}$ are derived similarly, the result being:

$$v^{N+1}_{i,j} = v^{N}_{i,j} + \frac{\Delta t\ \Delta P^{N}_{i,j} g_c}{\overset{*}{By}_{i,j}\ \rho_o\ \Delta y^{v}_{j}} \tag{5.3.14}$$

$$v^{N+1}_{i,j-1} = v^{N}_{i,j-1} - \frac{\Delta t\ \Delta P^{N}_{i,j} g_c}{\overset{*}{By}_{i,j-1}\ \rho_o\ \Delta y^{v}_{j-1}} \tag{5.3.15}$$

The pressure increment $\Delta P^{N}_{i,j}$ is calculated from Equation (5.3.2) where the partial derivative is derived as follows:

Rewrite the discretized momentum equations, i.e., Equations (5.2.16) and (5.2.28) for the velocities on the ϕ-cell faces:

$$u^{P^N}_{i,j} = \{u^N_{i,j} + \Delta t[(P^N_{i,j} - P^N_{i+1,j})g_c/\rho_o \Delta x^u_i + OT]\}/Bx^*_{i,j} \qquad (5.3.16)$$

$$u^{P^N}_{i-1,j} = \{u^N_{i-1,j} + \Delta t[(P^N_{i-1,j} - P^N_{i,j})g_c/\rho_o \Delta x^u_{i-1} + OT]\}/Bx^*_{i-1,j} \qquad (5.3.17)$$

$$v^{P^N}_{i,j} = \{v^N_{i,j} + \Delta t[(P^N_{i,j} - P^N_{i,j+1})g_c/\rho_o \Delta y^v_j + OT]\}/By^*_{i,j} \qquad (5.3.18)$$

$$v^{P^N}_{i,j-1} = \{v^N_{i,j-1} + \Delta t[(P^N_{i,j-1} - P^N_{i,j})g_c/\rho_o \Delta y^v_{j-1} + OT]\}/By^*_{i,j-1} \qquad (5.3.19)$$

Substituting Equations (5.3.16) to (5.3.19) in the continuity equation, Equation (5.2.1), and taking the partial derivative with respect to $P^N_{i,j}$ gives after some rearrangement:

$$\frac{\partial D^N_{i,j}}{\partial P^N_{i,j}} = \frac{\Delta t g_c}{\rho_o}\Bigg[\frac{1}{\Delta x_i}\left(\frac{1}{\Delta x^u_i\, Bx^*_{i,j}} + \frac{1}{\Delta x^u_{i-1} Bx^*_{i-1,j}}\right) +$$

$$\frac{1}{\Delta y_i}\left(\frac{1}{\Delta y^v_j\, By^*_{i,j}} + \frac{1}{\Delta y^v_{j-1} By^*_{i,j-1}}\right) +$$

$$\frac{\zeta}{2r^P_i}\left(\frac{1}{\Delta x^u_i\, Bx^*_{i,j}} - \frac{1}{\Delta x^u_{i-1,j} Bx^*_{i-1,j}}\right)\Bigg] \qquad (5.3.20)$$

Note that if baffles are not present and uniform grid spacing ($\Delta x_i = \Delta x$; $\Delta y_j = \Delta y$) is used, Equation (5.3.20) becomes:

$$\frac{\partial D^N_{i,j}}{\partial P^N_{i,j}} = \frac{2\Delta t g_c}{\rho_o}\left[\frac{1}{\Delta x^2} + \frac{1}{\Delta y^2}\right] \tag{5.3.21}$$

Substitution of Equation (5.3.20) in Equation (5.3.2) results in the general pressure adjustment increment equation:

$$\Delta P^N_{i,j} = \frac{-\omega\rho_o D^N_{i,j}}{\Delta t g_c}\left[\frac{1}{\Delta x_i}\left(\frac{1}{\Delta x^u_i \overset{*}{Bx}_{i,j}} + \frac{1}{\Delta x^u_{i-1}\overset{*}{Bx}_{i-1,j}}\right) + \right.$$

$$\frac{1}{\Delta y_j}\left(\frac{1}{\Delta y^v_j \overset{*}{By}_{i,j}} + \frac{1}{\Delta y^v_{j-1}\overset{*}{By}_{i,j-1}}\right) +$$

$$\left.\frac{\zeta}{2r^p_i}\left(\frac{1}{\Delta x^u_i \overset{*}{Bx}_{i,j}} - \frac{1}{\Delta x^u_{i-1,j}\overset{*}{Bx}_{i-1,j}}\right)\right] \tag{5.3.22}$$

5.4 Pressure-Velocity Adjustment Iteration Procedure

As stated earlier, the velocities calculated from Equations (5.2.16) and (5.2.28) do not, in general, satisfy the continuity requirements. The pressure and velocities are adjusted iteratively in the following order:

1. Velocities calculated from Equations (5.2.16) and (5.2.28) are

used to calculate the residual $D^N_{i,j}$ from the continuity equation, Equation (5.2.1).

2. The pressure adjustment increment is calculated from Equation (5.3.22).

3. The pressure is adjusted using Equation (5.3.3).

4. The velocities are adjusted using Equations (5.3.8), (5.3.11), (5.3.14) and (5.3.15).

These steps are repeated for each computational cell in the flow domain keeping track of the maximum value of $D^N_{i,j}$ occurring during each sweep. The process of sweeping the computational domain in the above manner continues until the absolute value of the residual $D^N_{i,j}$ becomes vanishingly small, i.e., $D^N_{i,j} < \varepsilon$ where ε is a prescribed tolerance, say, $\varepsilon = 10^{-6}$. The general and special boundary conditions discussed in the next section are applied at the beginning of each iteration of the above procedure.

5.5 The Boundary Conditions

As stated earlier in this Chapter, the computational domain is surrounded by an extra layer of cells from all four sides to enable the imposition of boundary conditions. While these conditions are particular to each particular problem, general boundary conditions, frequently encountered in fluid flow and heat transfer computations, were employed to enable the user to solve variety of problems with

ease. Four types of general boundary conditions were incorporated in the computer code. These are listed below and demonstrated in Figure 5.2 for left side wall of the computational domain:

1. Rigid free-slip wall - the normal velocity at the wall is set to zero and the tangential velocity, should have zero normal gradient:

$$\left.\begin{aligned} u_{1,j} &= 0 \\ v_{1,j} &= v_{2,j} \end{aligned}\right\}, \quad \text{for all } j \tag{5.5.1}$$

This condition generally applies to cells adjacent to lines of symmetry. However, it was suggested by Lilley (1988) that: "when total time requirements necessitate a coarse grid, it is not possible to resolve thin boundary layers along confining walls and free-slip boundary conditions for tangential velocities are more appropriate."

2. Rigid no-slip wall - both the normal and tangential velocities should vanish at the wall. This is expressed as:

$$\left.\begin{aligned} u_{1,j} &= 0 \\ v_{1,j} &= -\, v_{2,j} \end{aligned}\right\}, \quad \text{for all } j \tag{5.5.2}$$

The above two conditions are imposed after each pass through the mesh

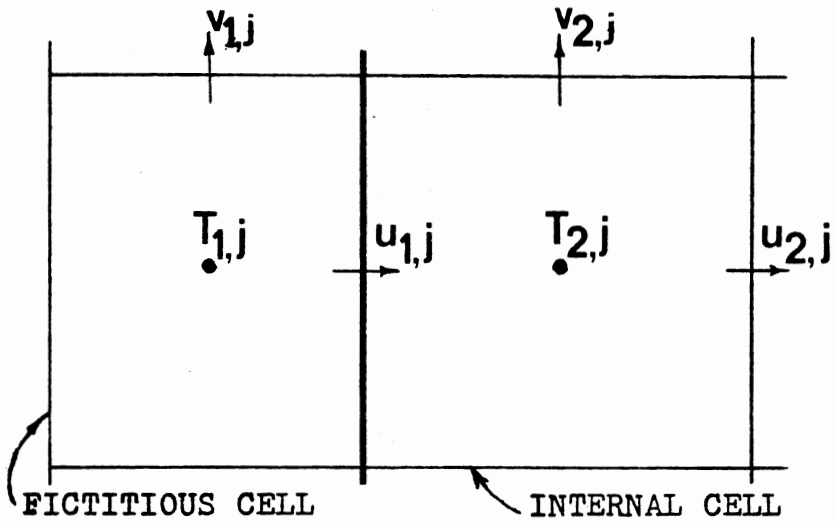

Figure 5.2 Variables Position at the Wall

and during the pressure-velocity correction procedure after each iteration.

3. Continuative or outflow wall - the normal velocity is prescribed such that the fluid is permitted to flow out of the outlet with a minimum of upstream influence. This is done as:

$$\left.\begin{aligned} u_{1,j} &= u_{2,j} \\ v_{1,j} &= v_{2,j} \end{aligned}\right\}, \quad \text{for all } j \tag{5.5.3}$$

This condition is imposed only after each time step and not after each pressure-velocity adjustment iteration.

4. Insulated wall - the insulated wall is prescribed by setting the temperature gradient across the wall to zero.

$$T_{1,j} = T_{2,j} \quad , \quad \text{for all } j \tag{5.5.4}$$

The prescription of these boundary conditions is done by specifying user-input parameters. However, these boundary conditions can be overriden by the imposition of special boundary conditions which are prescribed for the particular problem considered.

5.6 Stability and Accuracy

The stability of explicit finite-difference schemes for solving transient flow and heat transfer problems is controlled by the choice of

spatial intervals which are often dictated by the required accuracy in resolving thin boundary layers.

Once the choice of the grid size is made, two restrictions on time step are generally imposed (Lilley 1988).

1. In any one time step, Δt, material cannot move through more than one computational cell. This restriction is expressed by the inequality:

$$\Delta t < \min \left\{ \frac{\Delta x_i}{|u_{i,j}|}, \frac{\Delta y_j}{|v_{i,j}|} \right\}, \quad \text{over all } i,j \tag{5.6.1}$$

Usually, Δt is chosen equal to 0.25 to 0.33 of that calculated from Equation (5.6.1).

2. When a nonzero value of diffusivity is used, momentum or heat must not diffuse more than approximately one cell in any one time step. This is expressed by:

$$\lambda \Delta t < \frac{1}{2} \min \left(\frac{1}{\Delta x_i^2} + \frac{1}{\Delta y_j^2} \right), \quad \text{over all } i,j \tag{5.6.2}$$

where λ stands for the diffusivity of either momentum or heat.

These restrictions apply to both the WUDS and the SOUDS numerical schemes. To ensure the stability of WUDS, however, an additional restriction on the choice of the donor-cell parameter, α, (see Appendix A) is imposed. This is given by:

$$1 \geq \alpha > \max \left\{ \frac{|u_{i,j}| \Delta t}{\Delta x_i}, \frac{|v_{i,j}| \Delta t}{\Delta y_j} \right\}, \quad \text{over all } i,j \tag{5.6.3}$$

α is normally chosen slightly larger (1.2 to 1.5 times) than that calculated by Equation (5.6.3).

5.7 Summary of Solution Procedure and Computer Program Flow Chart

The solution procedure of the discretized mathematical model presented in the preceeding sections can be summarized as follows:

1. Data Input: this includes the choice of coordinate system, method of solution, physical dimensions of the flow field, selection of general boundary conditions, location of baffles, and other control indices explained in the computer code as needed.

2. Grid Generation: this step is accomplished by calling the grid generation subroutine which calculates all the grid geometric dimensions described in Section 5.1.

3. Specification of Initial Conditions: this includes initialization of the flow field variables before the start of calculations.

4. Specification of Special Boundary Conditions: this step allows pertinent boundary conditions to be specified. This includes inflow and outflow conditions and inlet temperature profiles. Applying this step after the imposition of the general boundary conditions results in overriding the general boundary

conditions where appropriate.

5. Solution of the Momentum Equations: the u- and v- velocities are calculated based on Equations (5.2.16) and (5.2.28). These velocities are considered the best estimates at the new time step and generally will not satisfy the continuity requirements by virtue of the pressure-velocity coupling described earlier. The next step is, therefore, executed.

6. Pressure-Velocity Adjustment: this step is carried out as described in Section 5.4. The velocities so calculated satisfy the velocity divergence within the preset, as needed, tolerance.

7. Solution of the Energy Equation: the converged velocities from the previous step are used in calculating the temperature field from the energy equation, Equation (5.2.36).

Steps 4 to 7 complete one calculation cycle over one time step. However, the bidirectional coupling between momentum and energy through the buoyancy term in the former and through the u- and v- velocities in the latter requires iterative solution within the same time step. This means that the temperature-dependent buoyancy term in the v-momentum equation is evaluated again after obtaining the temperature field from step 7 above. This is done by underrelaxation of density (Patankar 1980) via:

$$\rho = \sigma\rho_{new} + (1 - \sigma)\rho_{old} \qquad (5.7.1)$$

where the new density, ρ_{new}, is calculated as a function of the temperature computed in step 7 and ρ_{old} from the temperature at the beginning of the time step. The underrelaxation factor, σ, assumes values between zero and unity. A value of 0.5 results in the average density.

It should be noted that with the buoyancy calculated based on Equation (5.7.1), only the v-momentum equation needs to be solved again with fewer terms reevaluated. In this manner, steps 5, 6 and 7 are re-executed until the change in temperature calculated in step 7 at any point in the flow field is below a preset tolerance as needed.

The above outlined solution steps are summarized in Figure 5.3. The next chapter discusses the validation of the computer code developed based on the formulations and procedures discussed in this chapter. The application of the code to a single stratified tank is also presented therein.

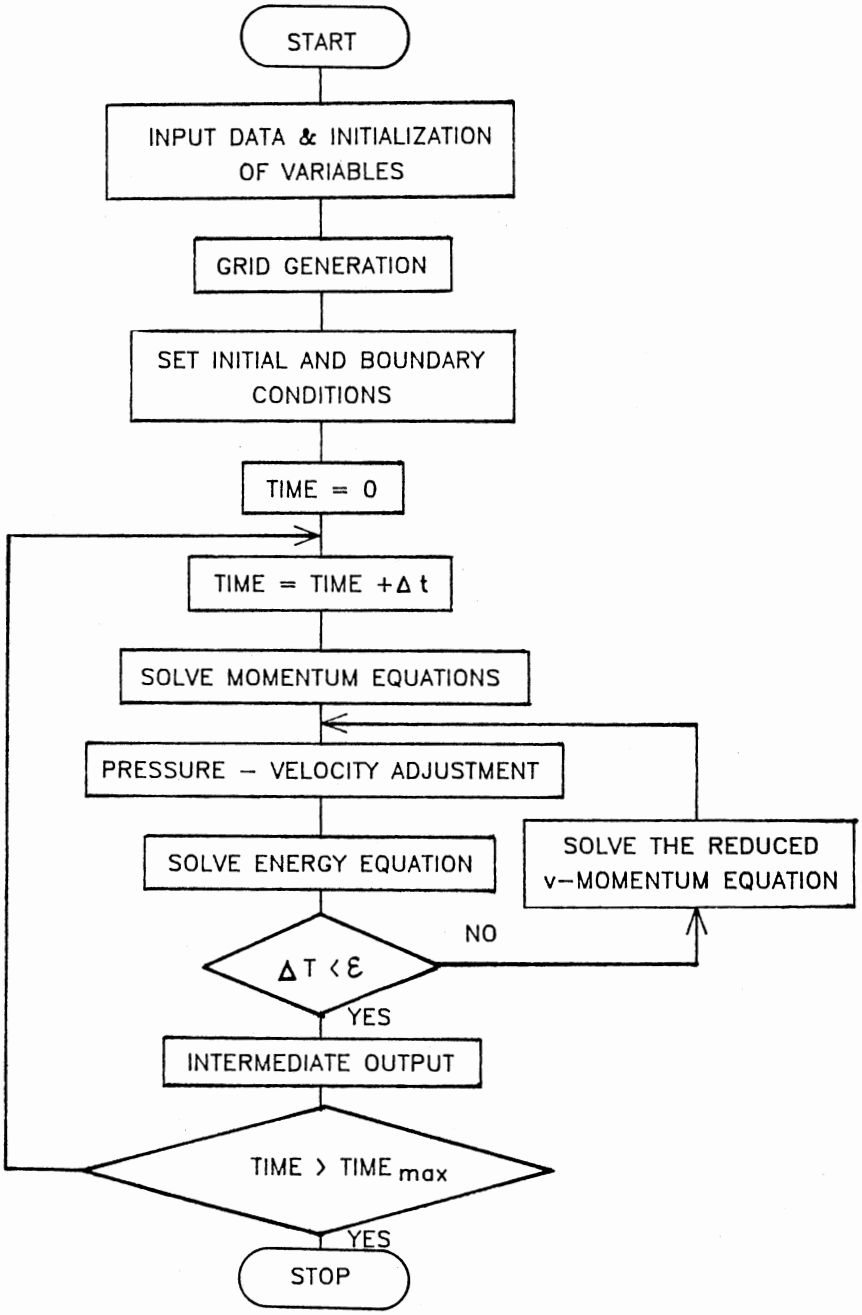

Figure 5.3 Computer Program Flow Chart

CHAPTER VI

RESULTS AND DISCUSSION

In this chapter the computer code developed based on the formulation and procedures described in the previous chapter is validated by comparison with known analytic solutions and/or experimental data. Application of the model to a single stratified tank under constant and variable inlet temperature conditions and comparison with the experimental data is presented. Both laminar and turbulent flow conditions are treated and comparison between the two methods of solution, WUDS and SOUDS, is conducted.

6.1 Code Validation and Preliminary Analysis

An important step in developing a computer code is to validate its performance by application to known analytic or numerical solutions. This allows, in addition to verifying the functional status of the code, for investigating the sensitivity of the results to various input parameters introduced in the numerical procedures employed. Results for laminar forced convection are presented first.

6.1.1 Uniform Flow With a Step Change in Temperature

Consider the plug flow situation with a step change in temperature with known analytic solution (Cabelli 1977). The flow is considered to

be one-dimensional and therefore only a few terms in the governing equations are of importance. However, this problem has been widely used as a test problem to investigate the numerical diffusion resulting from the application of different numerical schemes. In this case, however, the crossflow diffusion is absent leaving only the truncation error diffusion added to the physical diffusion.

As stated in Section 5.4, the stability and accuracy of the WUDS requires a certain amount of upstream differencing to maintain both stability and a low level of numerical diffusion (donor cell parameter, α, in inequality (5.4.3)). Figure 6.1 shows the transient response to a step change in temperature for different values of α. It is seen that oscillations are persistent even at $\alpha = 0.35$ (4 times larger than the one obtained from inequality (5.4.3)). For $\alpha = 0.7$, no oscillations are present. It is clear that the rule expressed by inequality (5.4.3) is not generally applicable and one has to choose a value of α that produces oscillation-free solutions.

When solving the same problem using SOUDS, the solution, while being stable, exhibits wiggles known as over- and under-shoots (see Figure 6.2). To suppress these wiggles a remedy suggested by Sharif and Busnaina (1987) known as "bounding" produces a wiggles-free solution as shown in Figure 6.2. This being adopted, the solutions using WUDS and SOUDS (see Figure 6.3) show that the SOUDS introduces less numerical diffusion as compared with WUDS.

6.1.2 Uniform Flow at 45° to the Grid Lines With a Step Change in Temperature

Consider the flow situation shown in Figure 6.4. Two streams at

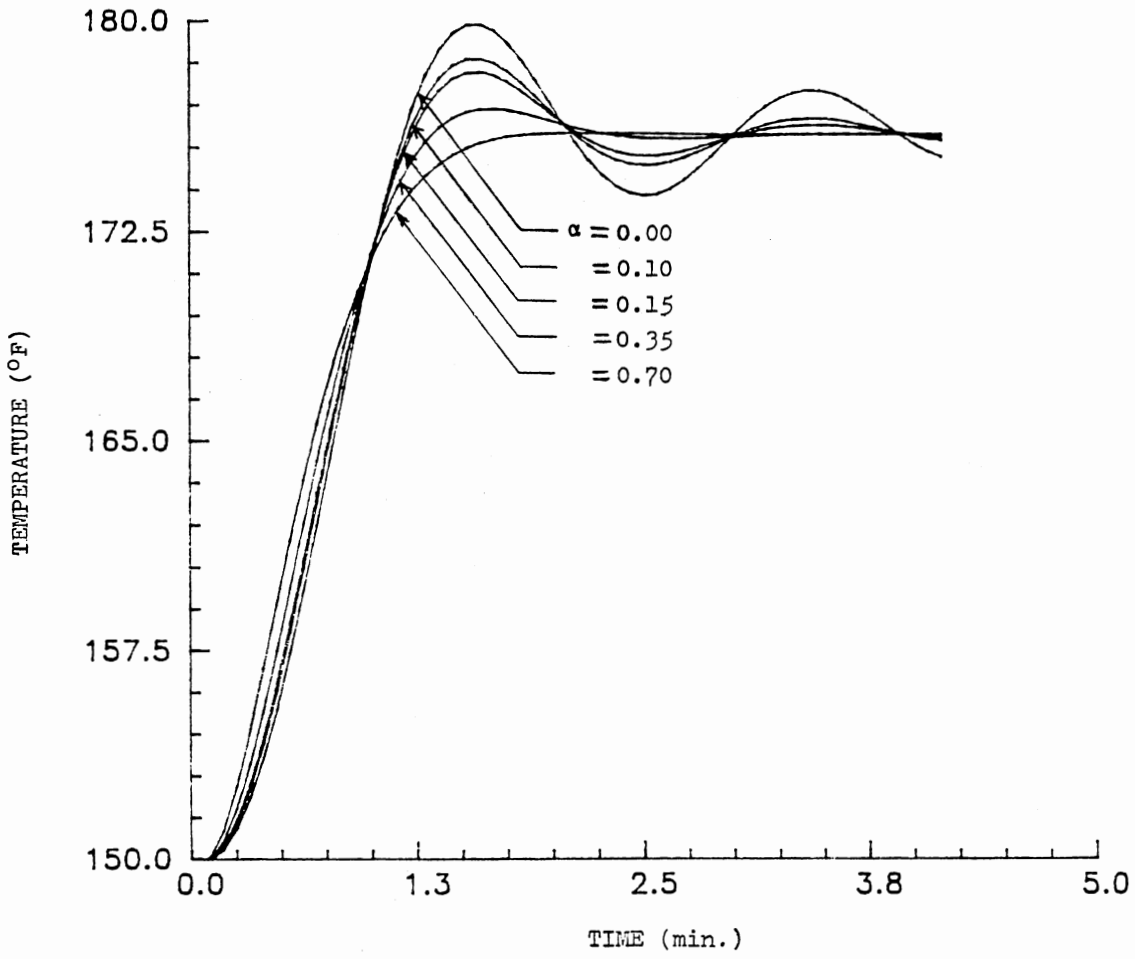

Figure 6.1 Transient Response to a Step Change in Temperature Using WUDS With Different Values of Upstream Differencing Parameter α

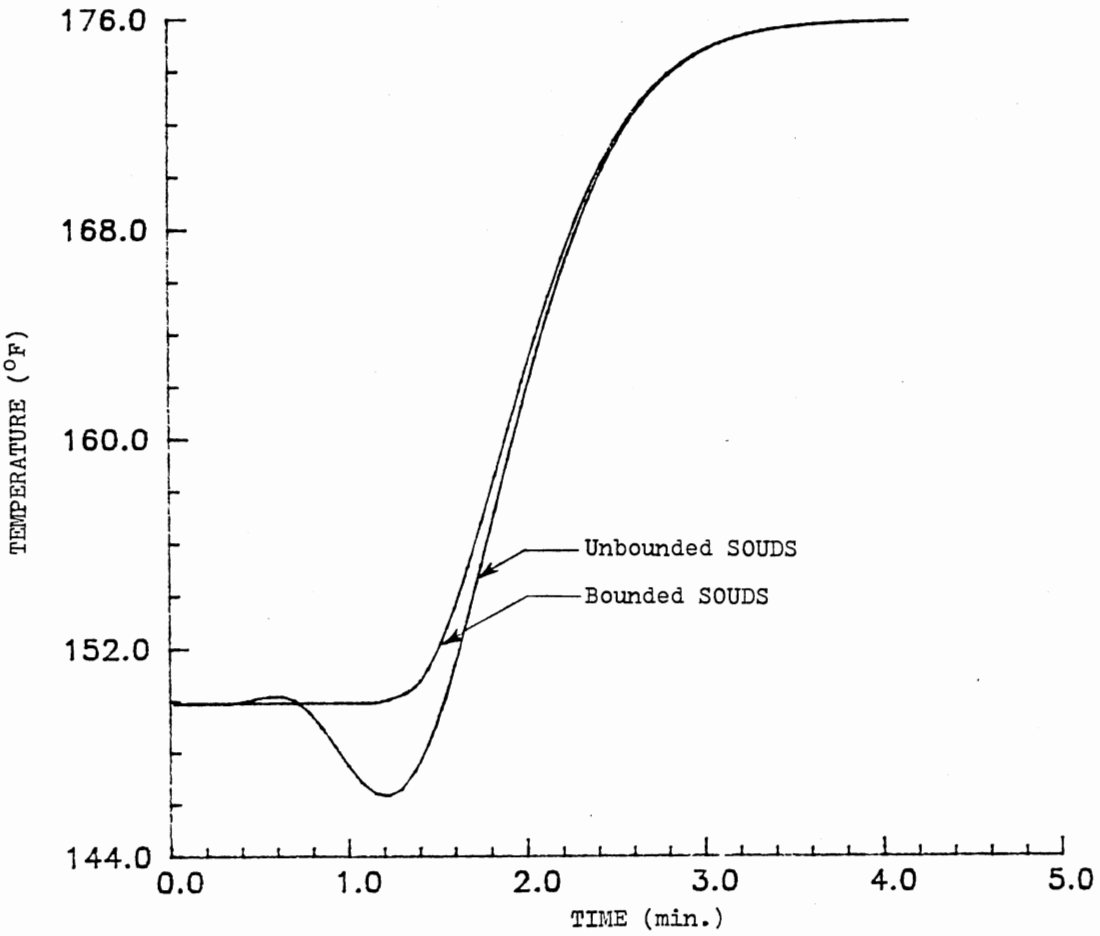

Figure 6.2 Transient Response to a Step Change in Temperature Using SOUDS Without and With Bounding

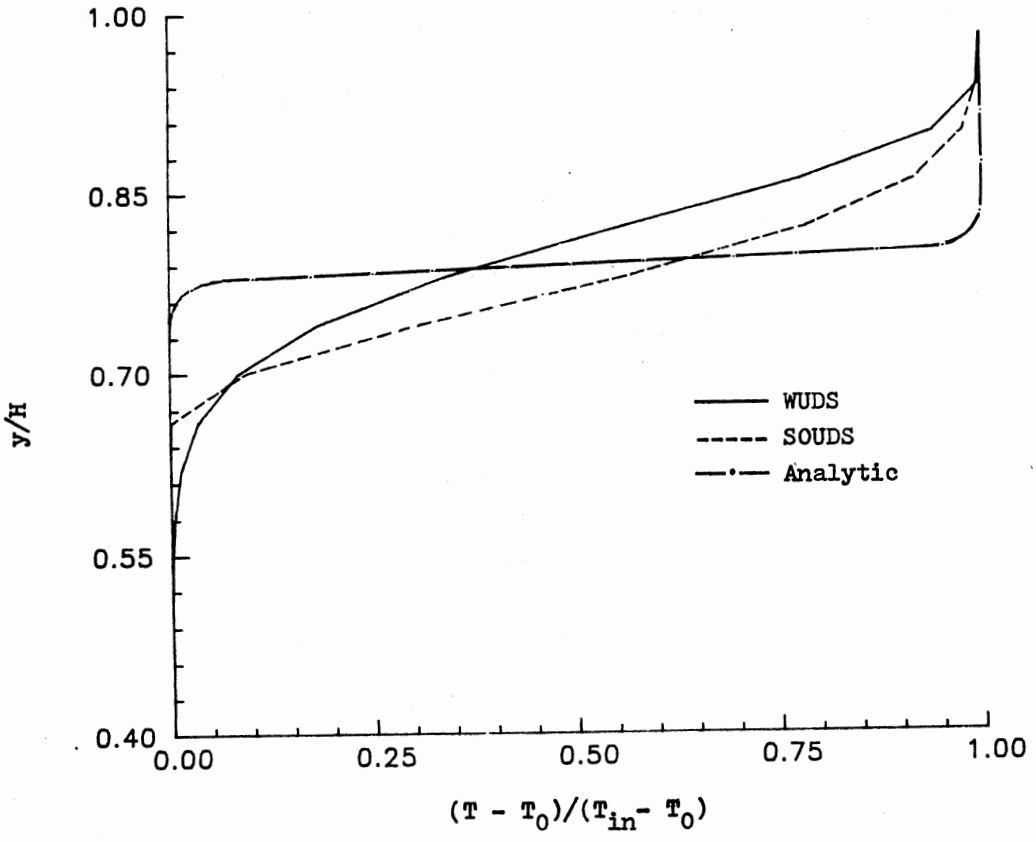

Figure 6.3 Transient Response to a Step Change in Temperature Using WUDS and Bounded SOUDS

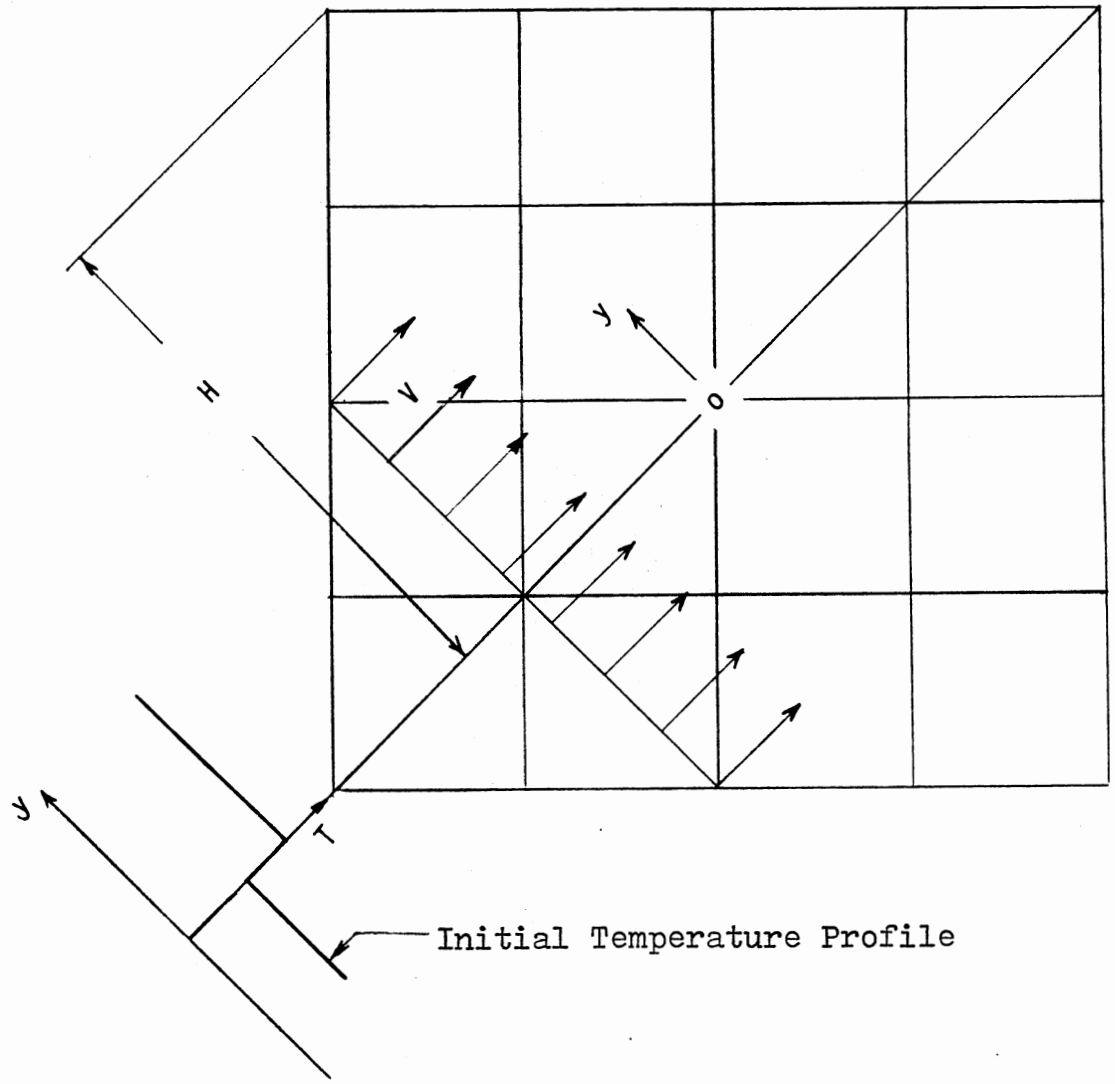

Figure 6.4 Uniform Flow at 45° to the Grid Lines with a Step Change in Temperature

uniform, identical velocities, but different temperatures, cut through the computational domain at 45°. This is another test problem widely used in computational fluid dynamics since both the truncation and crossflow diffusion are present.

Figure 6.5 shows the temperature profile monitored at the diagonal of the flow domain (see Figure 6.4). It can be seen that the SOUDS, while again exhibiting over- and under-shoots, substantially reduces the numerical diffusion as compared with WUDS.

The temperature profile shown in Figure 6.5 becomes biased as the velocity of the lower stream is increased to twice that of the upper stream (see Figure 6.6). Notice that the solution shown in Figures 6.5 and 6.6 are purely forced-convection-solutions. Figure 6.7 shows that the buoyancy effects dramatically distort the temperature profile shown in Figure 6.5 (SOUDS solution).

6.1.3 Application of Boundary Conditions on Baffles

Certain boundary conditions discussed in the previous chapter may be applied to obstructions placed in the flow field. For example, free-slip or no-slip boundary conditions may be imposed on solid baffles. The program developed in this study incorporates the option of applying these conditions in addition to the option of no-boundary condition-imposition. Figure 6.8 shows the flow passing a solid baffle. This configuration was chosen since the forced convection flow velocity profiles should exhibit symmetry around the inlet axis when the baffle extends equally above and below the inlet axis.

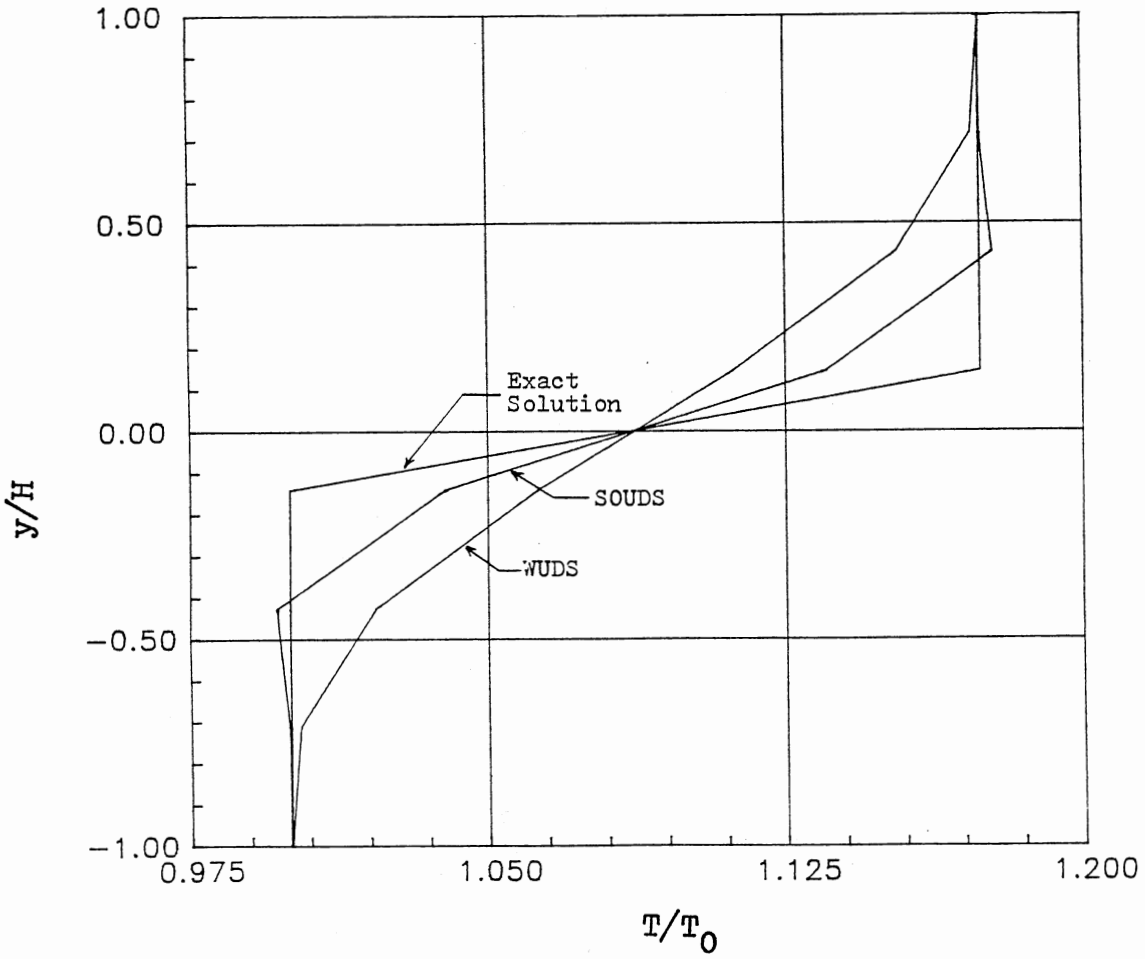

Figure 6.5 Temperature Profiles of Two Interacting Parallel Streams Shown in Figure 6.4 as Calculated with WUDS and SOUDS

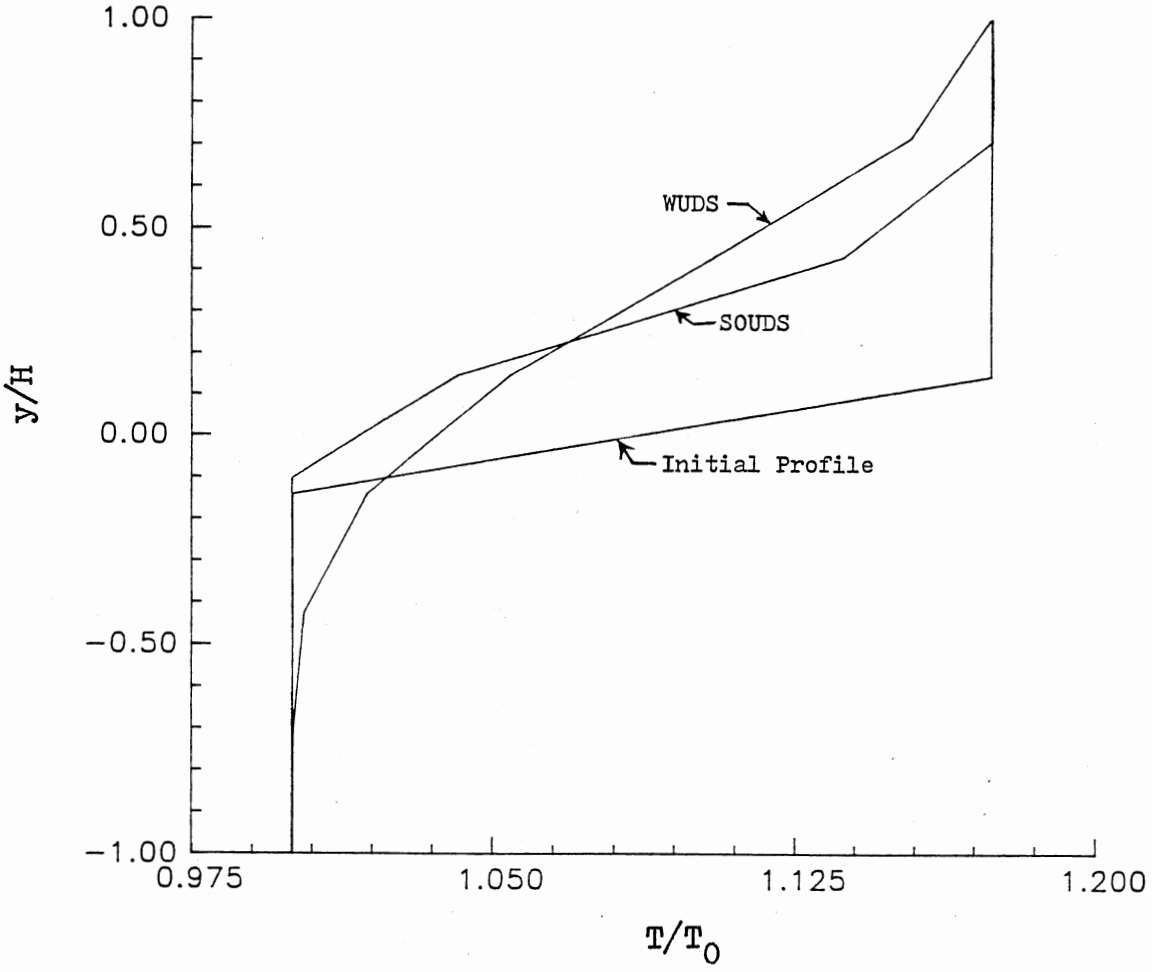

Figure 6.6 Temperature Profile of the Flow Shown in Figure 6.4 with the Velocity of the Lower Stream Being Twice That of the Upper Stream (SOUDS Solution)

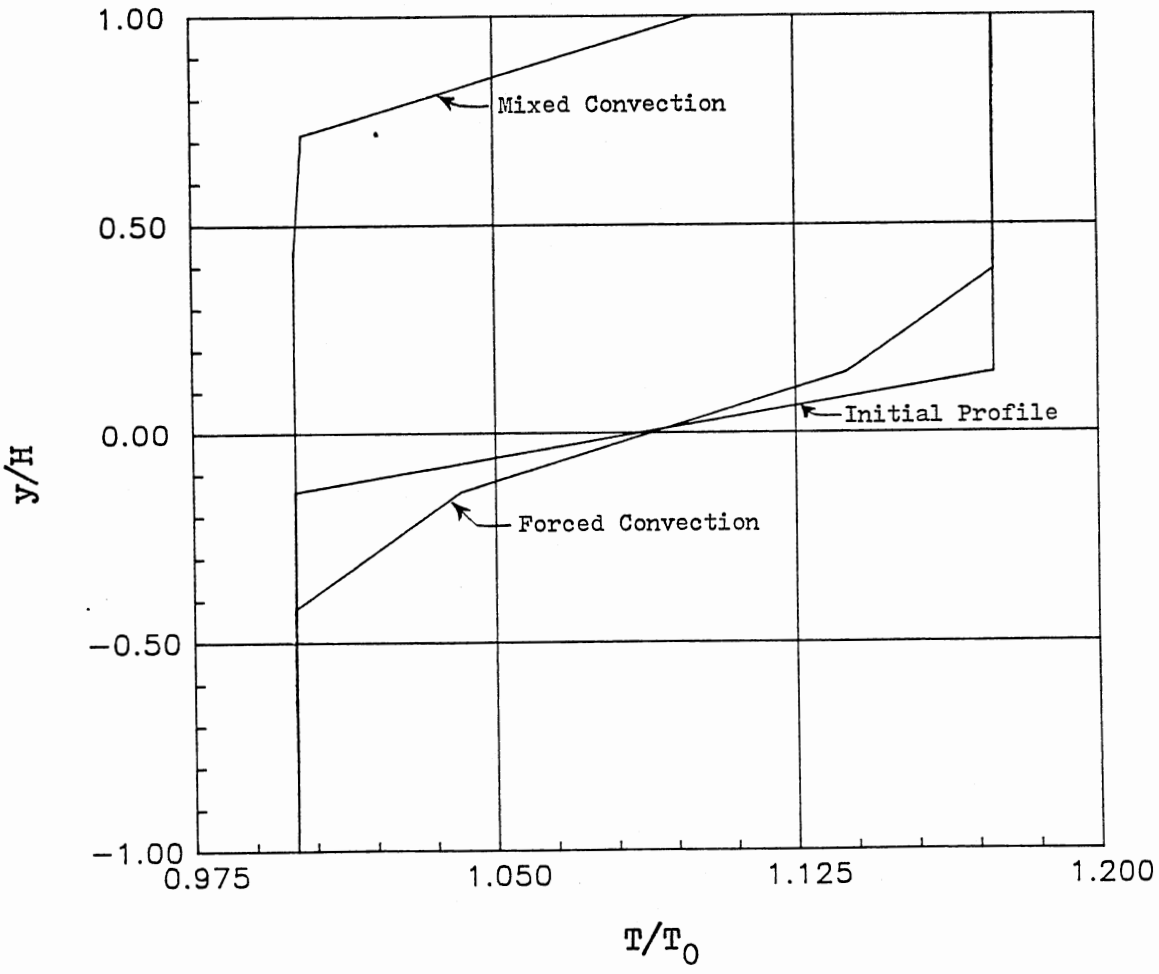

Figure 6.7 Comparison of Forced and Mixed Convection Flow Solutions of the Flow Configuration Shown in Figure 6.4

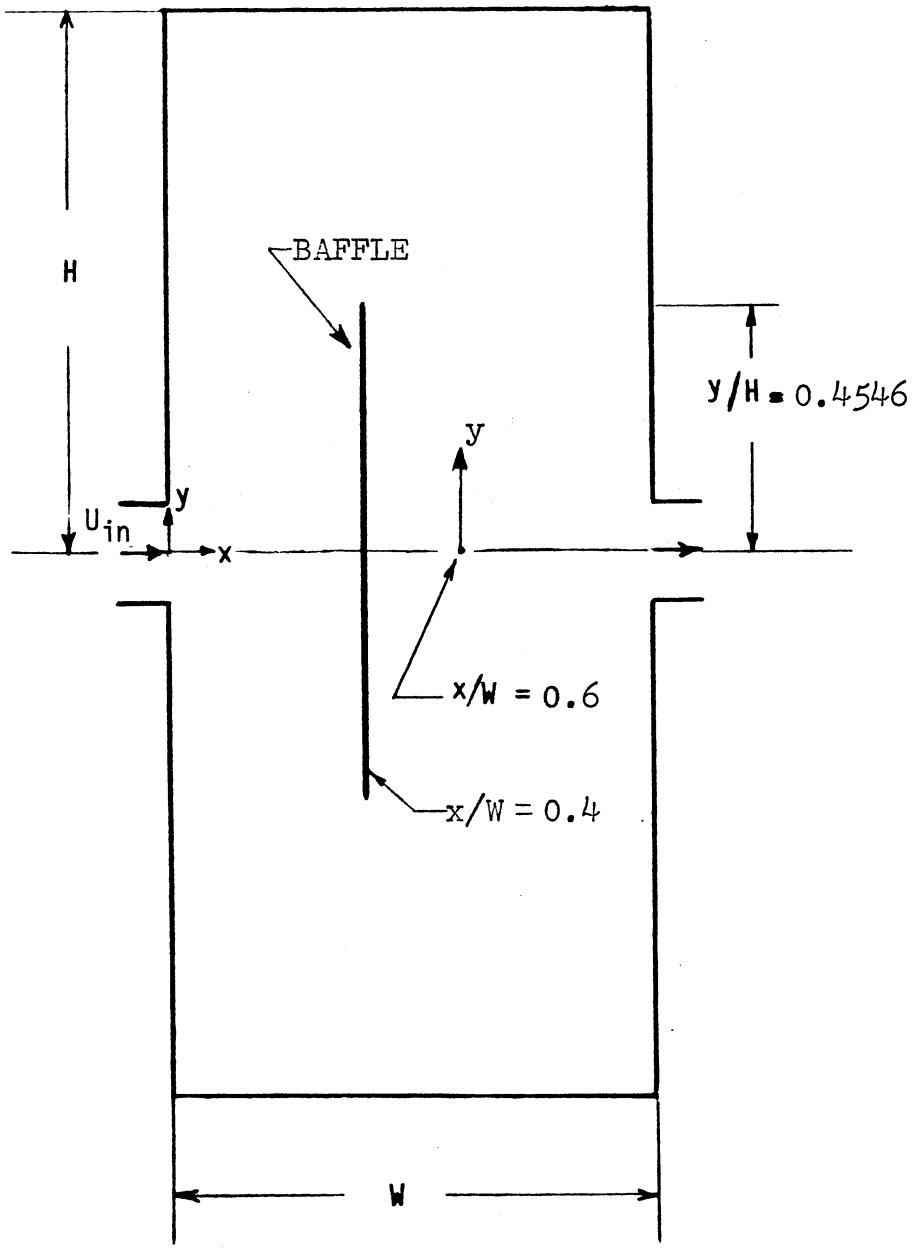

Figure 6.8 Flow Passing a Vertical Non-perforated Baffle in Enclosure
(W = H = 2.953 ft.; U_{in} = 0.03281 ft/sec)

To investigate the effect of different boundary conditions on the velocity field, the u-velocity was monitored at a vertical cross-section behind the baffle (x/W = 0.6; see Figure 6.8). The baffle was displaced 0.4W from the inlet. Figure 6.9 shows the velocity profiles for the conditions indicated. For free-slip boundary condition the velocity in the wake of the baffle is higher (9 percent) than for that of no-slip condition. Small difference between the velocities with no-slip condition and with no-boundary condition-imposition cases is observed (see Figure 6.9). When doubling the inlet velocity, the velocity in the wake of the baffle with free-slip boundary condition is 22.4 percent higher than that with no-slip (see Figure 6.10). The computer code also incorporates the option of insulated and conducting baffles. In the case of conducting baffles, however, the conductivity of the baffles assumes that of the fluid. This is justified for thin baffles as that employed in this study.

The purpose of this section was to demonstrate the influence of baffle boundary condition imposition on the flow field predictions. However, this influence is insignificant for short baffles, the case investigated in this study.

6.1.4 Validation With Data from Literature

Consider the problem of transient mixed convection flow in a thermal storage tank shown in Figure 6.11 (Chan et al. 1983). The transient temperature profiles along the height of the tank were monitored at x/W = 0.5. The solution generated using WUDS and SOUDS is compared to that obtained by Chan et al., (1983) (see Figure 6.12). A close agreement with the published results is seen to exist. Moreover,

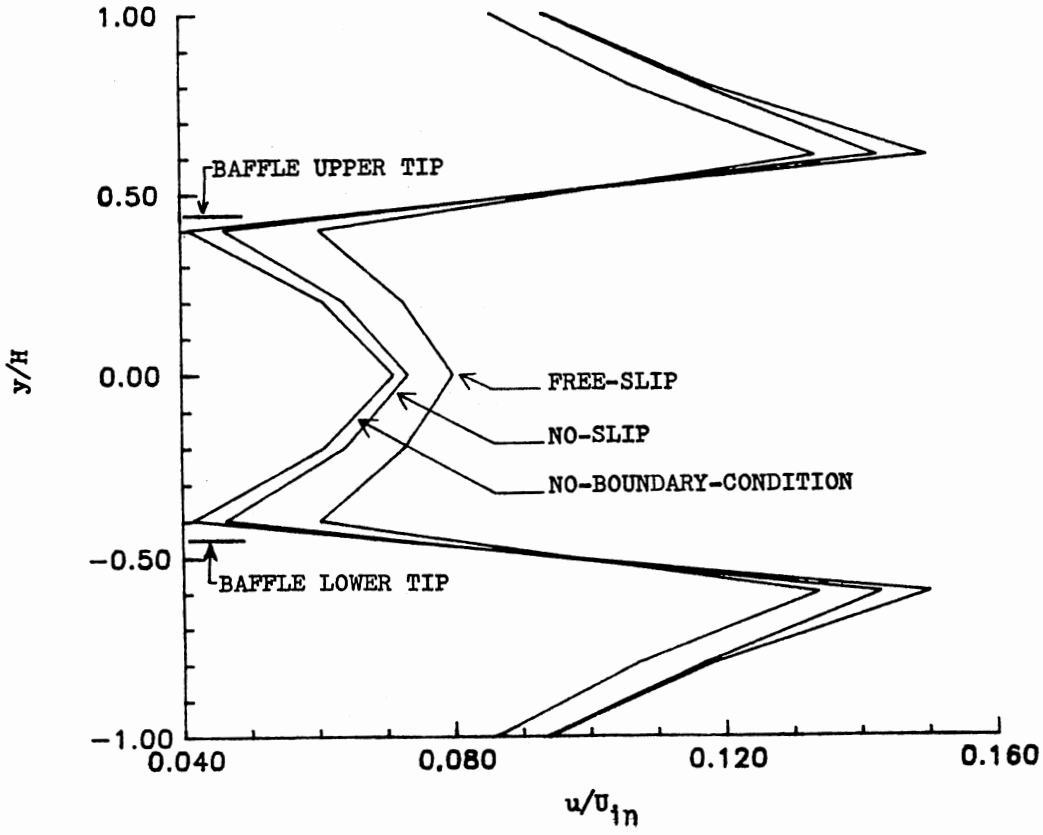

Figure 6.9 Dimensionless Velocity Profiles at x/W = 0.6 of Flow Passing a Vertical Non-perforated Baffle Placed at x/W = 0.4

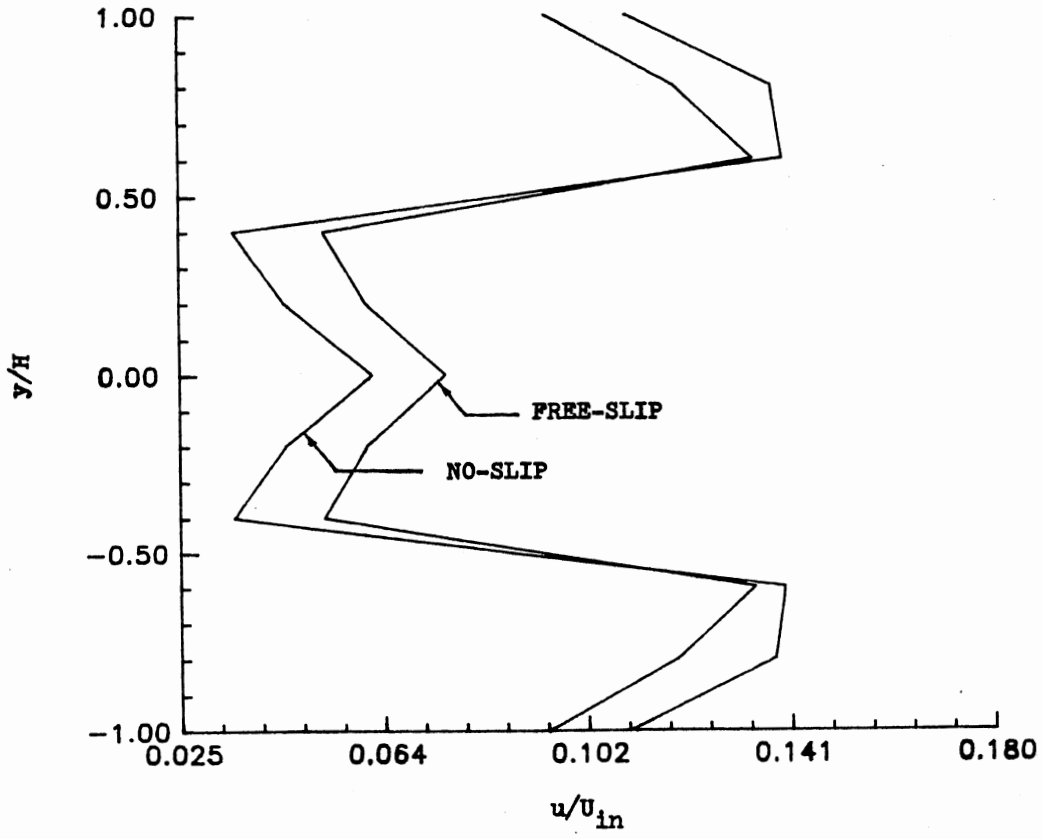

Figure 6.10 Configuration of Fig. 6.8 With Double the Inlet Velocity

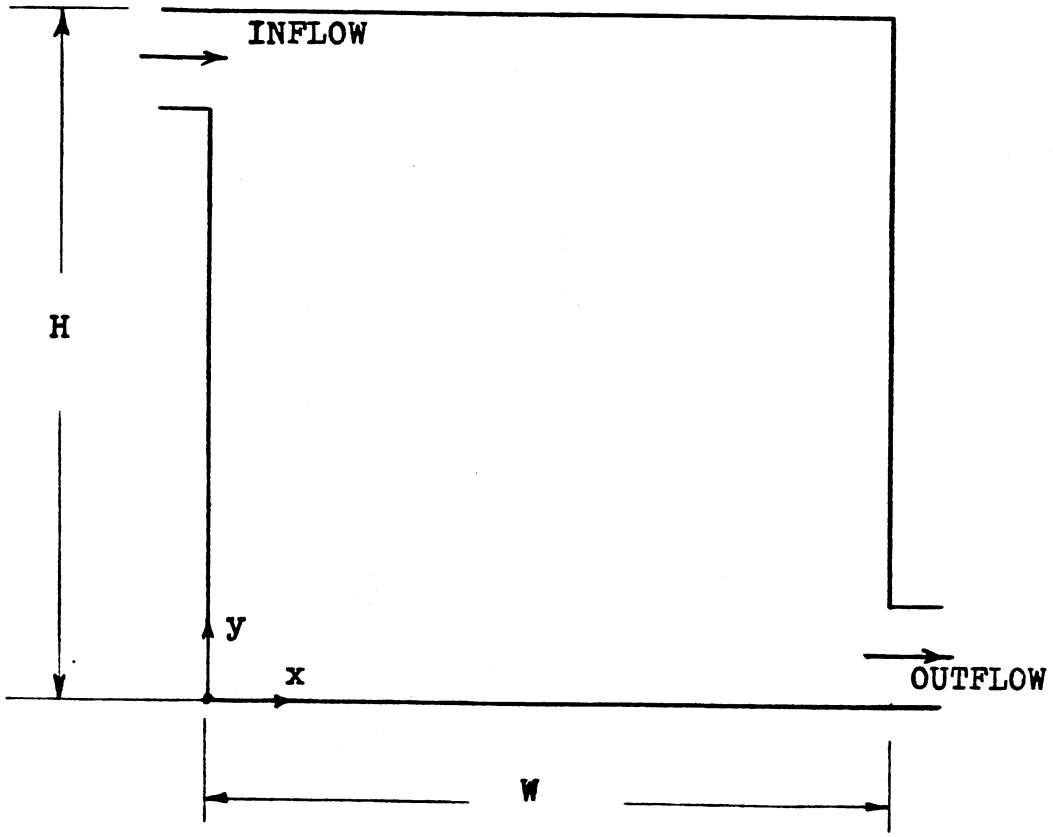

Figure 6.11 System Geometry for Transient Mixed Convection Flow Problem (Chan et al. 1983)

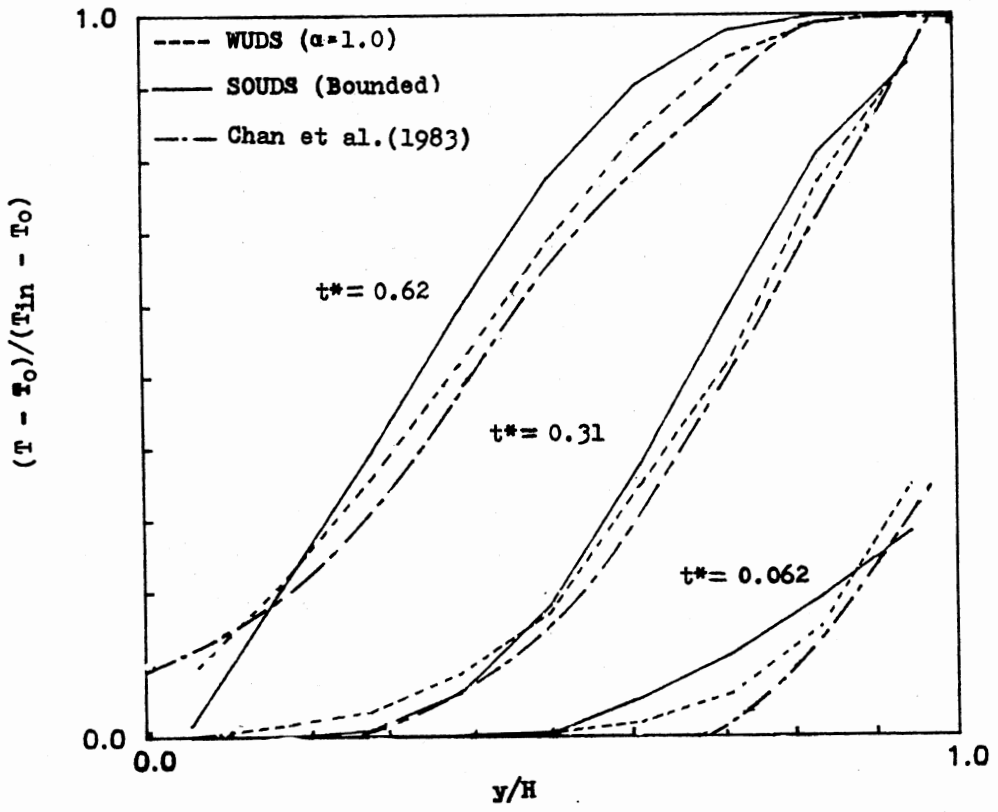

Figure 6.12 Predicted Transient Temperature Profiles in Thermal Storage Tank Using WUDS (α = 1.0) and SOUDS Compared With Results of Chan et al. (1983)

the predictions of the SOUDS seem, in general, to exhibit less numerical diffusion. The computer time for both methods is comparable (2 min. 4.33 sec CPU time for SOUDS and 2 min. 10 sec. for WUDS). It is seen that the SOUDS consumes less CPU time. This is partially due to faster convergence with SOUDS as compared with WUDS (see Figure 6.13).

It should be noted that the results of Chan et al. (1983) were obtained using WUDS. The slight disagreement between the present and published results could be due to a combination of reasons, for example, the choice of donor cell parameter, α, the time step, the initialization of the velocity field, and the convergence tolerance employed. All these factors affect the solution obtained with WUDS. Figure 6.14 shows that a closer agreement was achieved with $\alpha = 0.5$. It also shows the decrease in numerical diffusion as α is reduced. When using a time step similar to that used in the published results (2 sec), a better agreement is obtained (see Figure 6.15).

The bounding of SOUDS does not seem to affect the solution greatly. Figure 6.16 shows the solutions with and without bounding. The under-shoot, although small, is quite clear. The symbols represent the solution shown in Figure 6.12 with the scale being slightly altered. The difference, excluding the undershoots, is barely noticeable.

6.2 Application to SST Under Constant Inlet Temperature Conditions

Application of the computer code to thermocline thermal storage (constant inlet temperature) shows that the performance of SOUDS is much better than WUDS. Figure 6.17 shows the predictions compared with the

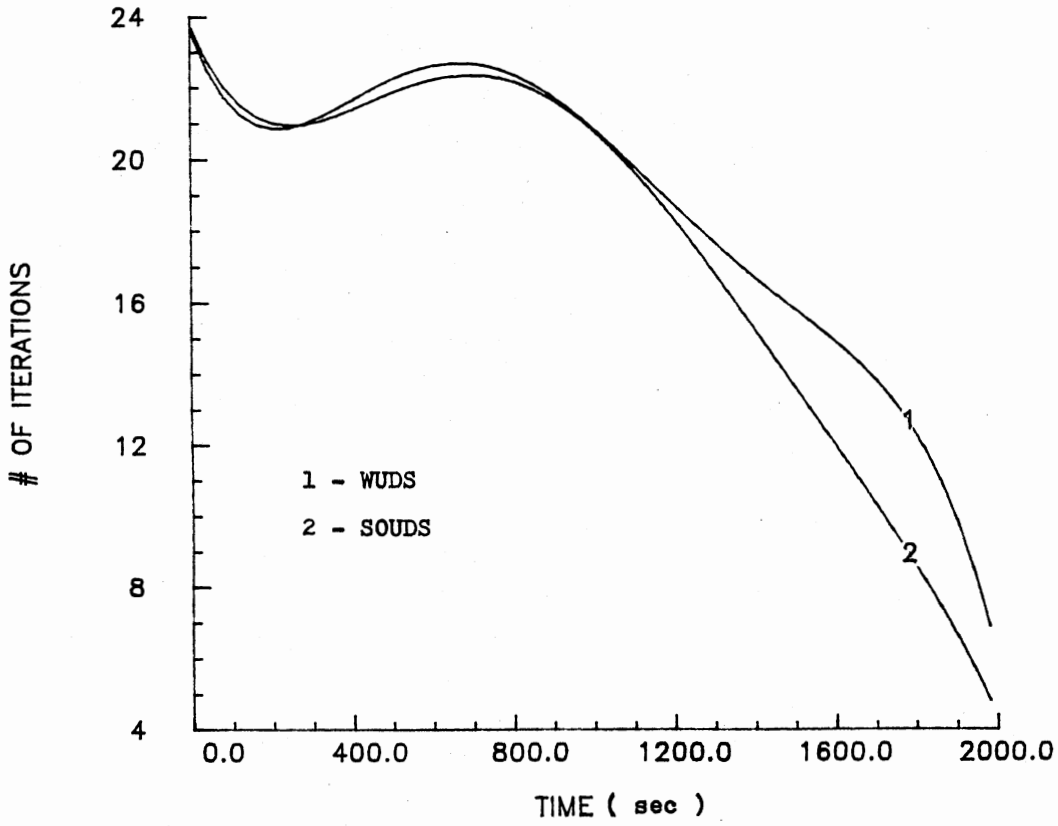

Figure 6.13 Number of Pressure-Velocity Adjustment Iterations Required by SOUDS and WUDS

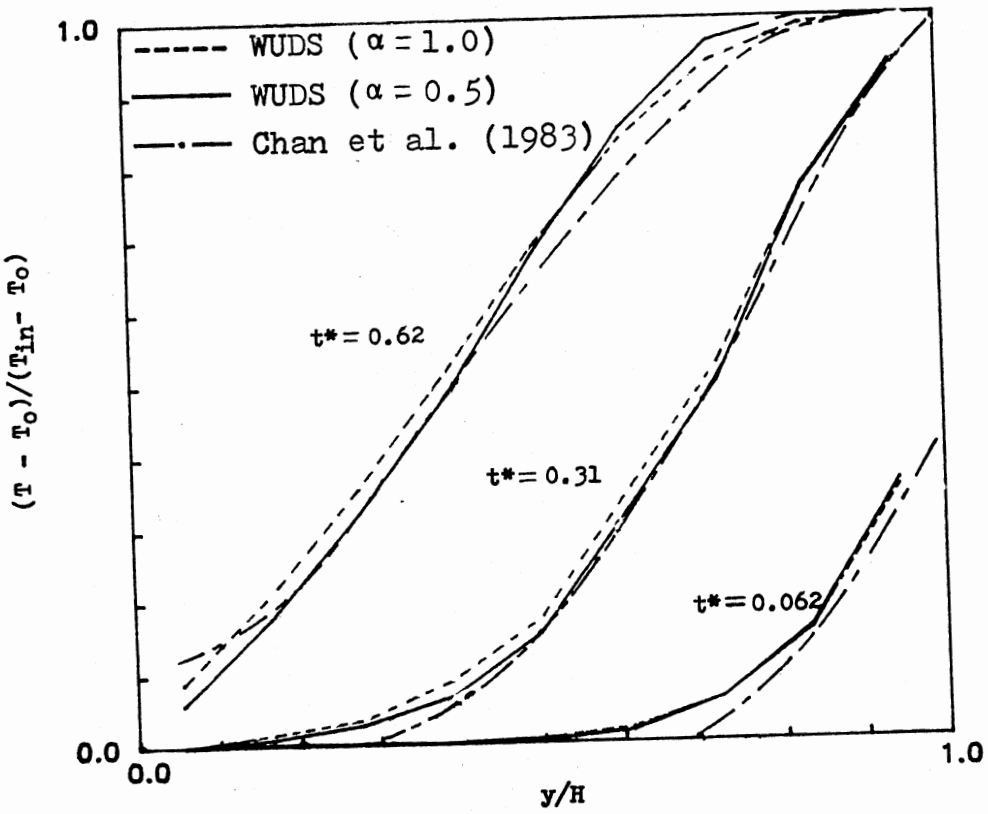

Figure 6.14 Predicted Transient Temperature Profiles in Thermal Storage Tank Using WUDS (α = 1.0 and 0.5) Compared With Results of Chan et al. (1983)

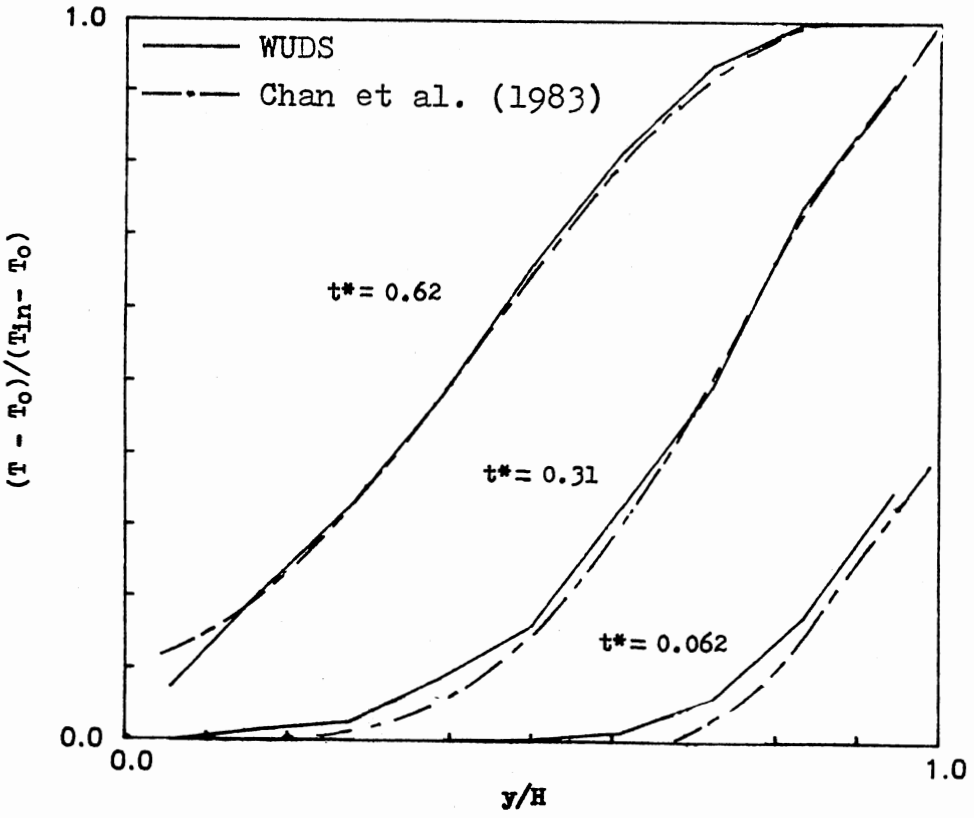

Figure 6.15 Predicted Transient Temperature Profiles in Thermal Storage Tank Using WUDS (α = 0.5, Δt = 2 sec) Compared With Results of Chan et al. (1983)

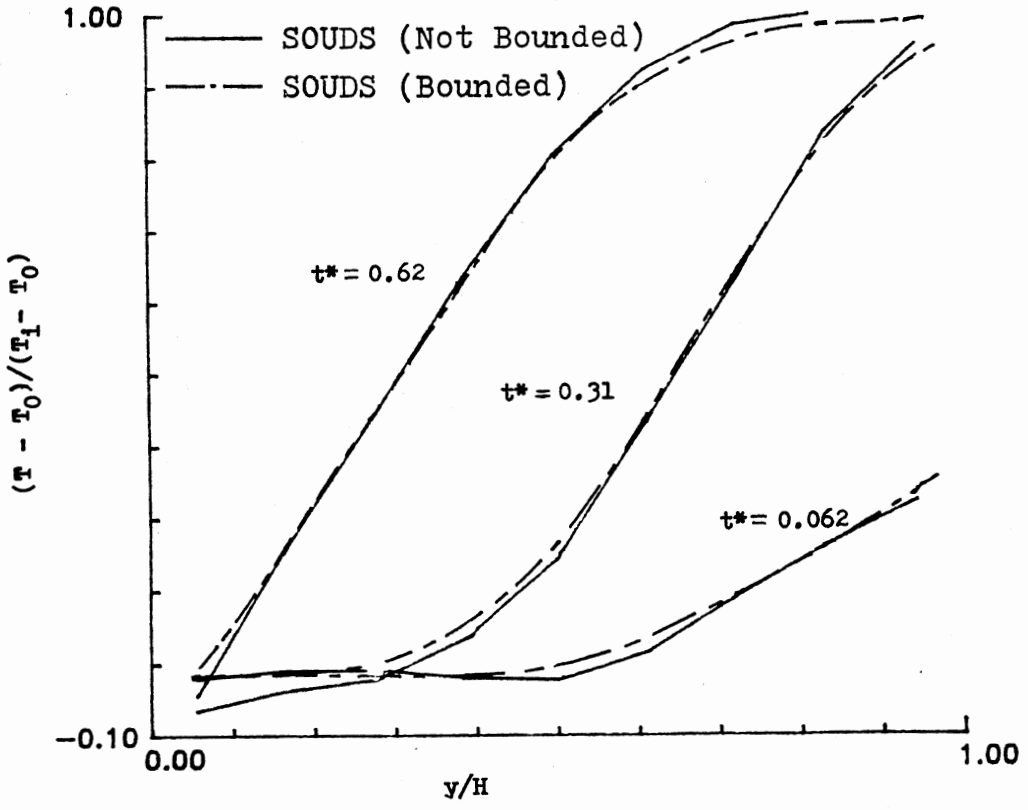

Figure 6.16 Comparison of Bounded and Unbounded SOUDS Predictions of Transient Temperature Profiles of Mixed Convection Flow Problem

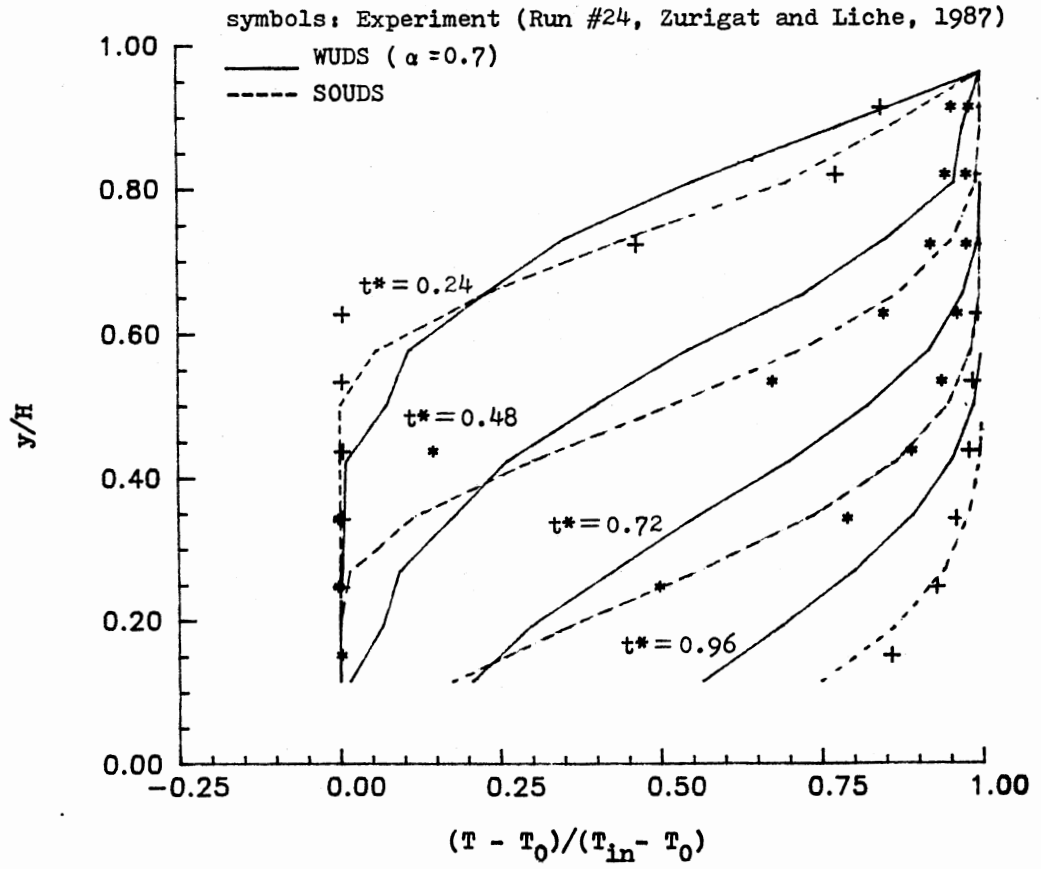

Figure 6.17 Predictions of Temperature Profiles in Thermocline Thermal Storage Tank Using SOUDS and WUDS Compared With Experiment

experiment. The agreement between the predictions using SOUDS and the experiments is satisfactory. A high level of numerical diffusion is seen to result when using WUDS. Figure 6.18 shows the same trend. It should be noted that the agreement between the predictions and the experiment is not complete throughout the tank at all times (see Figures 6.17 and 6.18). This is due to the fact that duplication of the physical dimensions and the inlet size and geometry is difficult to achieve because of computer time limitations. This is especially true for the case of the impingement inlet used in the experiments of Figures 6.17 and 6.18.

The results obtained so far point to the fact that realistic predictions of the flow field in thermal storage tank are possible. However, the choice of the solution scheme is an important factor in achieving these predictions. Interpretation of the results based on these predictions may become a solution method-dependent process. Therefore, a decision about which method to use has to be made. Based on the results discussed in the foregoing and those in the preceding sections the SOUDS will be used throughout the rest of this study.

The SOUDS is first applied to a more suitable geometry; the perforated inlet (Zurigat and Liche 1987). Figure 6.19 shows that a good agreement with the experiment is achieved. In this case, the conditions of the experiment were closely matched. However, laminar flow was assumed in the simulation. The predictions with turbulent flow assumption showed negligible difference indicating the flow being laminar under the conditions considered.

As mentioned earlier, the inlet geometry has a decisive effect on thermocline development in the storage tank. In the early phase of this

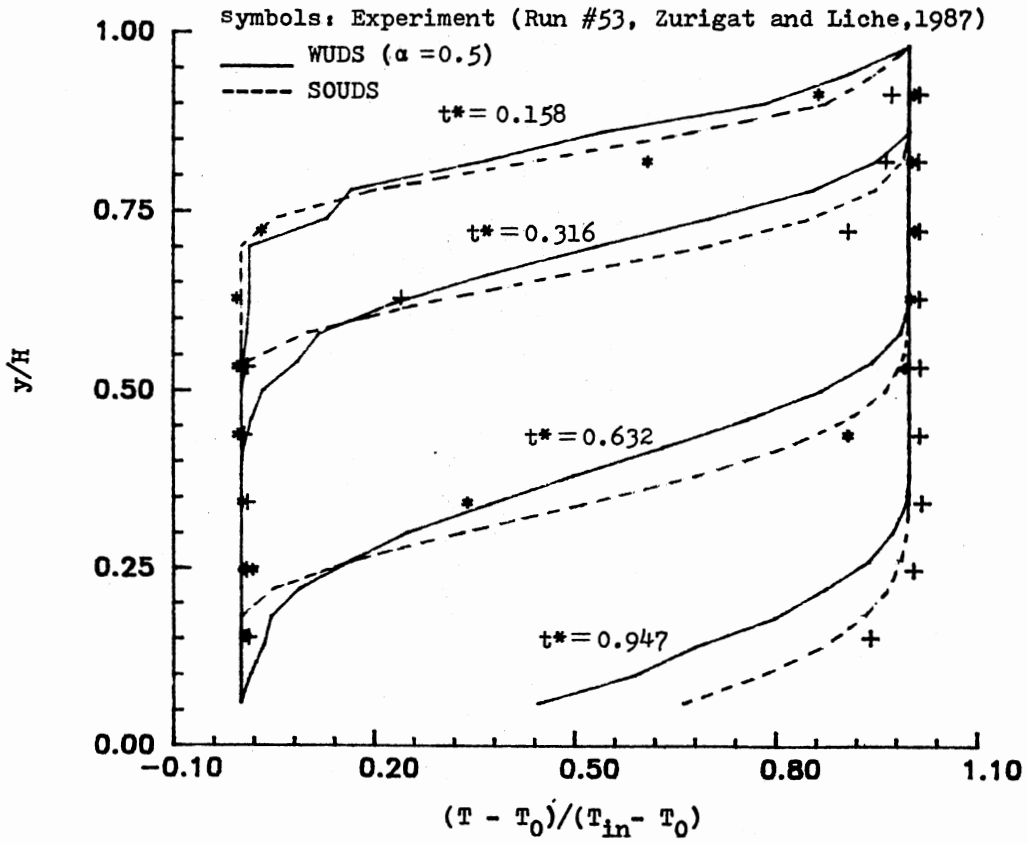

Figure 6.18 Predictions of Temperature Profiles in Thermocline Thermal Storage Tank Using SOUDS and WUDS Compared With Experiment

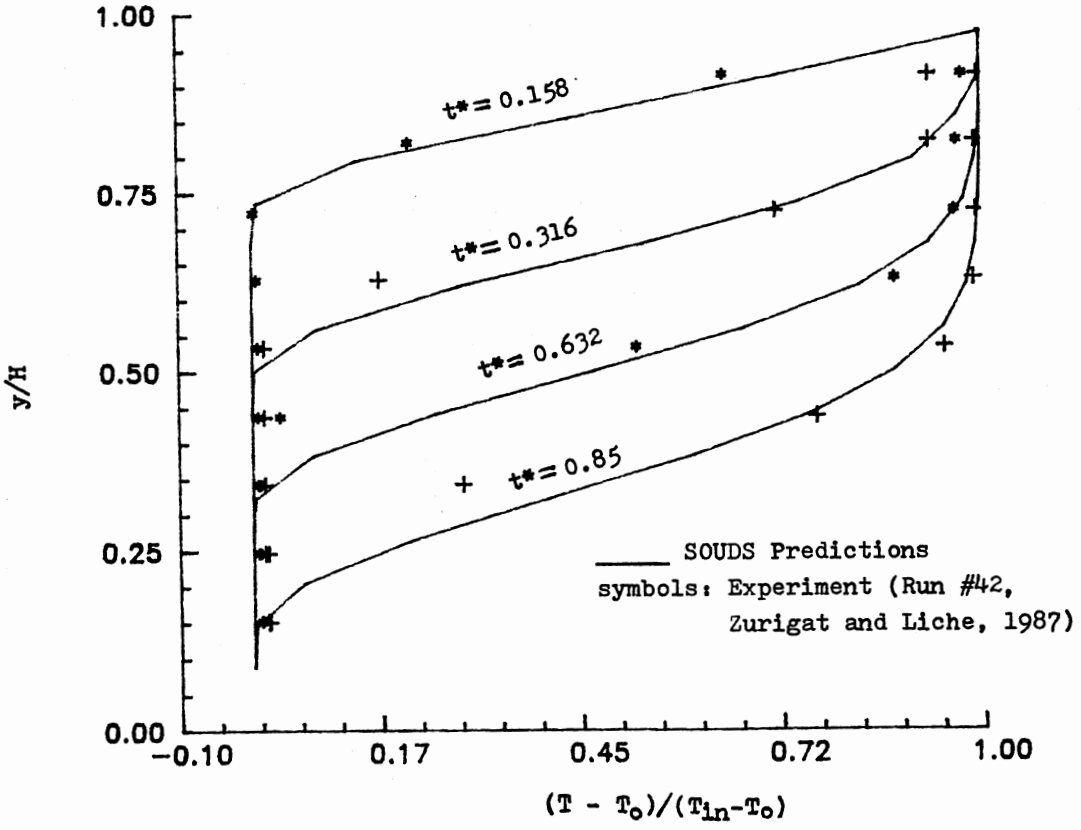

Figure 6.19 SOUDS Prediction Compared With Experiment

study (see Chapter III) it was found that there exists a limiting Richardson number above which the inlet geometry becomes less important to thermal stratification in thermal storage tank. Richardson number values of 5.0 (Zurigat et al. 1988a) and 3.6 (Zurigat et al. 1988b) were deduced. These findings were based on one-dimensional flow model in which a mixing index was introduced to account for departures from one-dimensional flow behavior. With the two-dimensional model developed in this study, it is of interest to verify the above mentioned findings.

Two inlet geometries were used in the simulations. The first was a circular disk of diameter 1.0 inch displaced 0.5 inch from the inlet pipe which was located at the center of the top of the tank (tank dimensions are those used in Zurigat et al. 1988b). For reference purposes this inlet geometry will be referred to as solid disk diffuser. The second geometry was formed by adding to the solid disk diffuser a perforated extension which spanned the rest of the tank cross-sectional area. This geometry will be referred to as perforated diffuser.

Simulations for the charge mode of operation (hot water pumped through the top and cold water discharged through the bottom) were conducted with the above mentioned inlet geometries for several values of Richardson number. The Richardson number was varied by varying the temperature difference between the inlet and the initial water temperatures while maintaining the same flow rate. Figures 6.20 to 6.24 show the predictions of thermocline in the storage tank as it passes through different elevations close to the inlet region for Richardson numbers of 5.0, 9.0, 14.0, 28.0 and 46.0 correspondingly. It can be seen that the addition of perforated extension (perforated inlet with

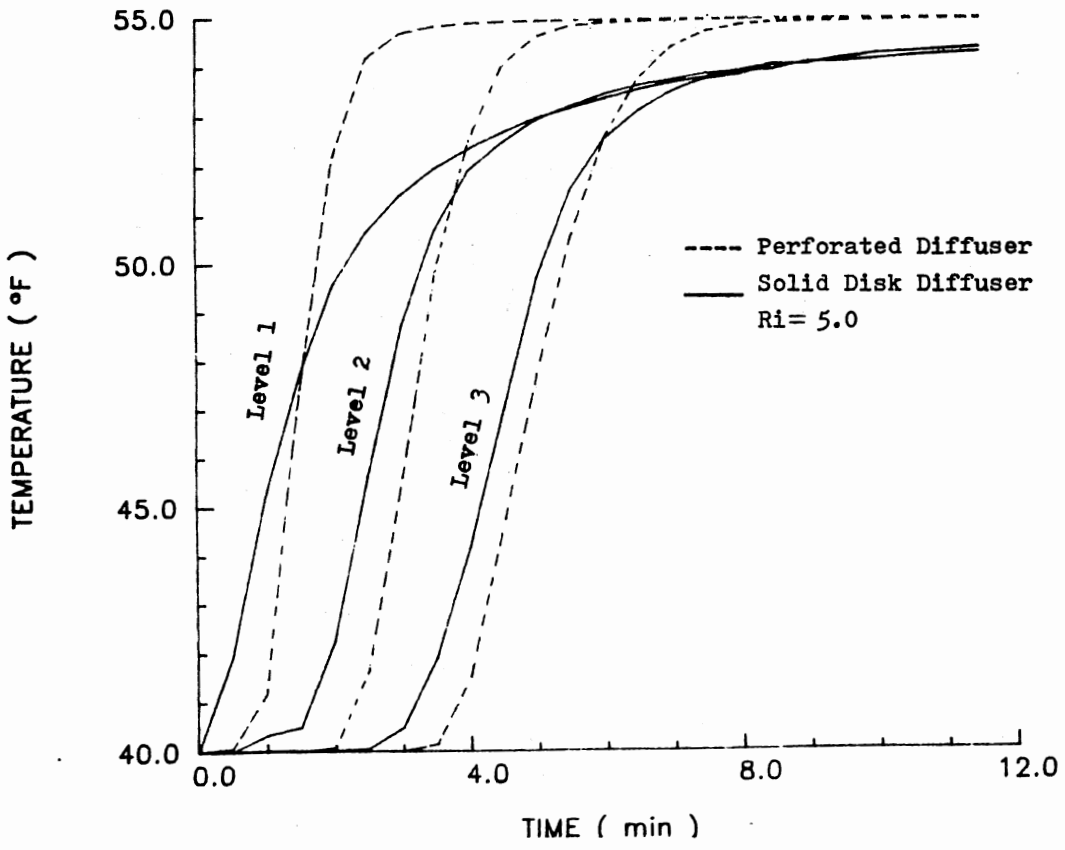

Figure 6.20 Comparison of the Predicted Thermocline Using SOUDS for Two Different Inlet Configurations (Ri = 5.0) (see Figure 3.1)

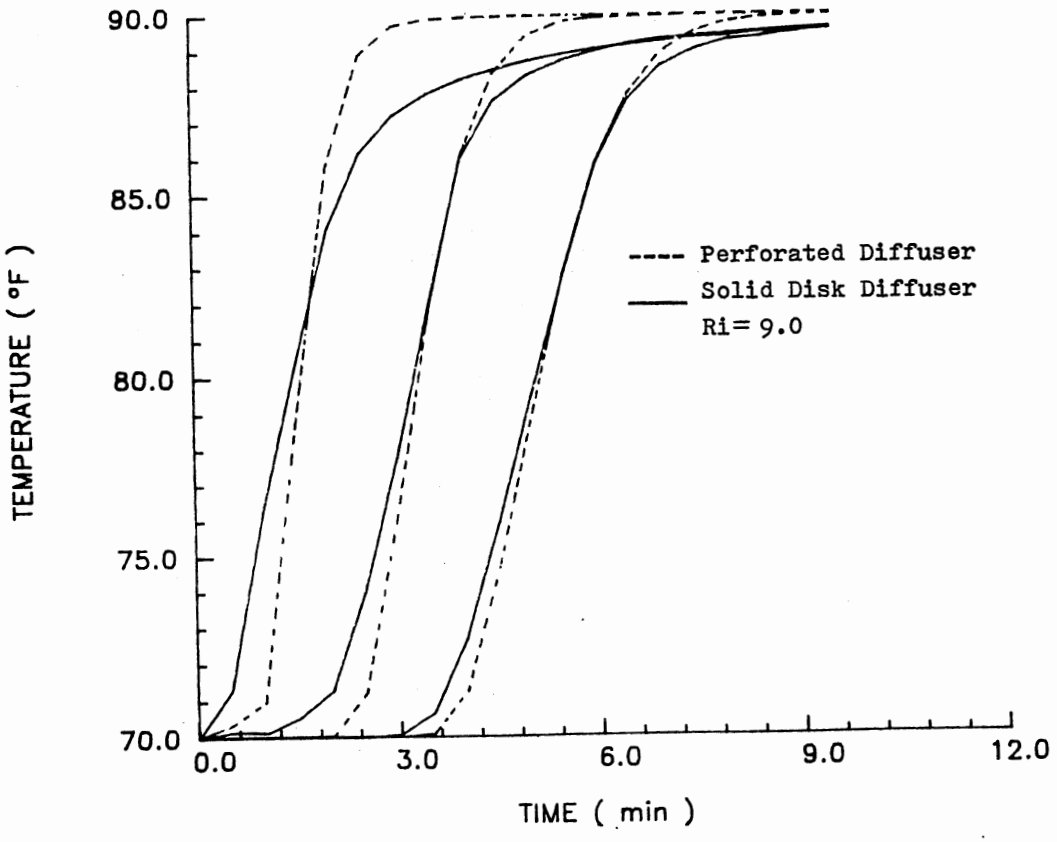

Figure 6.21 Comparison of the Predicted Thermocline Using SOUDS for Two Different Inlet Configurations (Ri = 9.0)

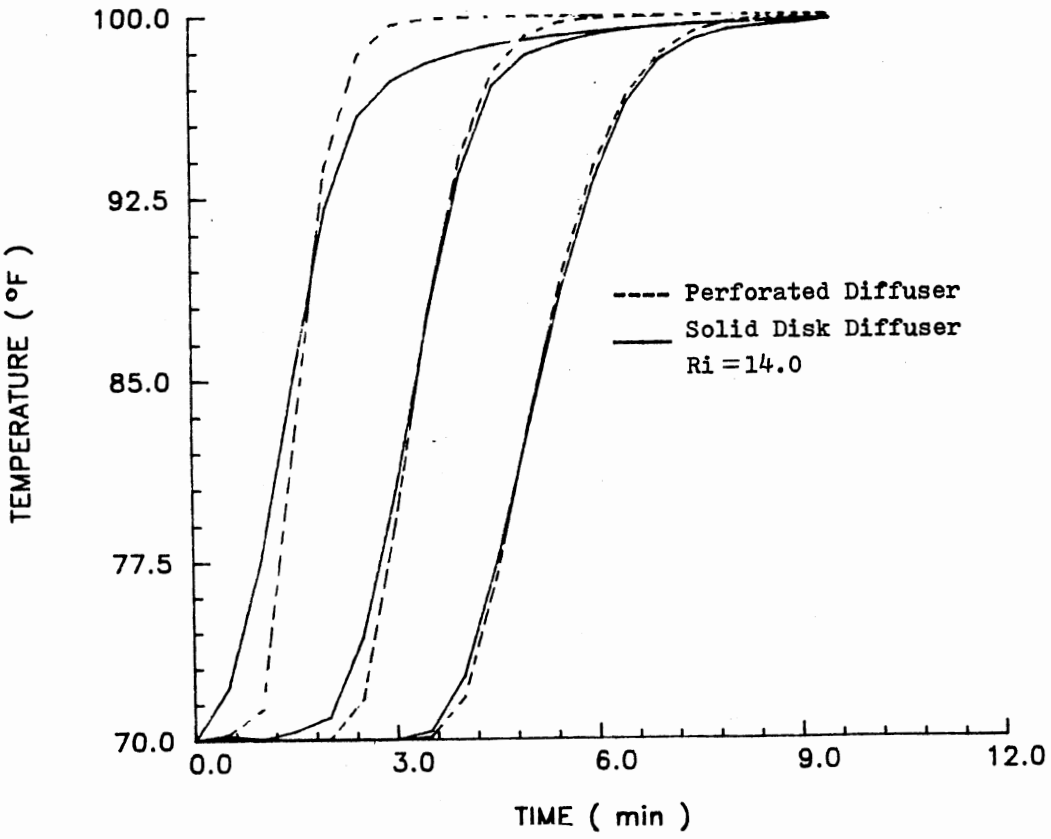

Figure 6.22 Comparison of the Predicted Thermocline Using SOUDS for Two Different Inlet Configurations (Ri = 14.0)

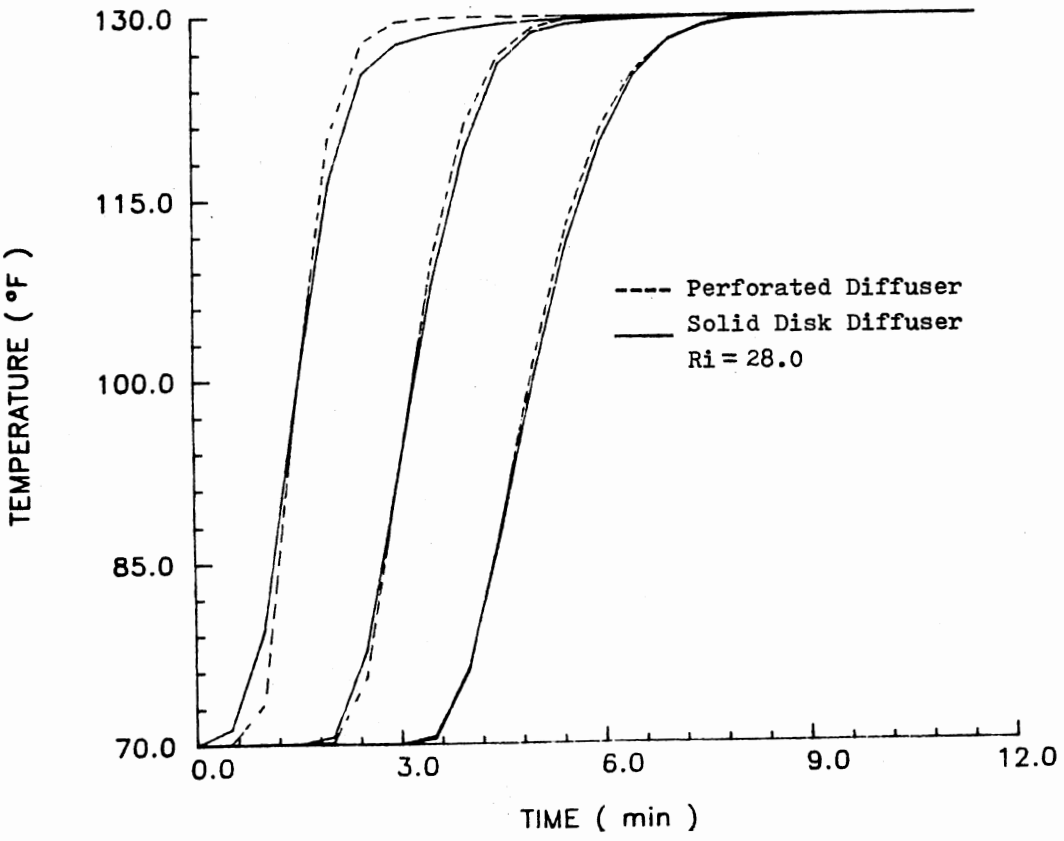

Figure 6.23 Comparison of the Predicted Thermocline Using SOUDS for Two Different Inlet Configurations (Ri = 28.0)

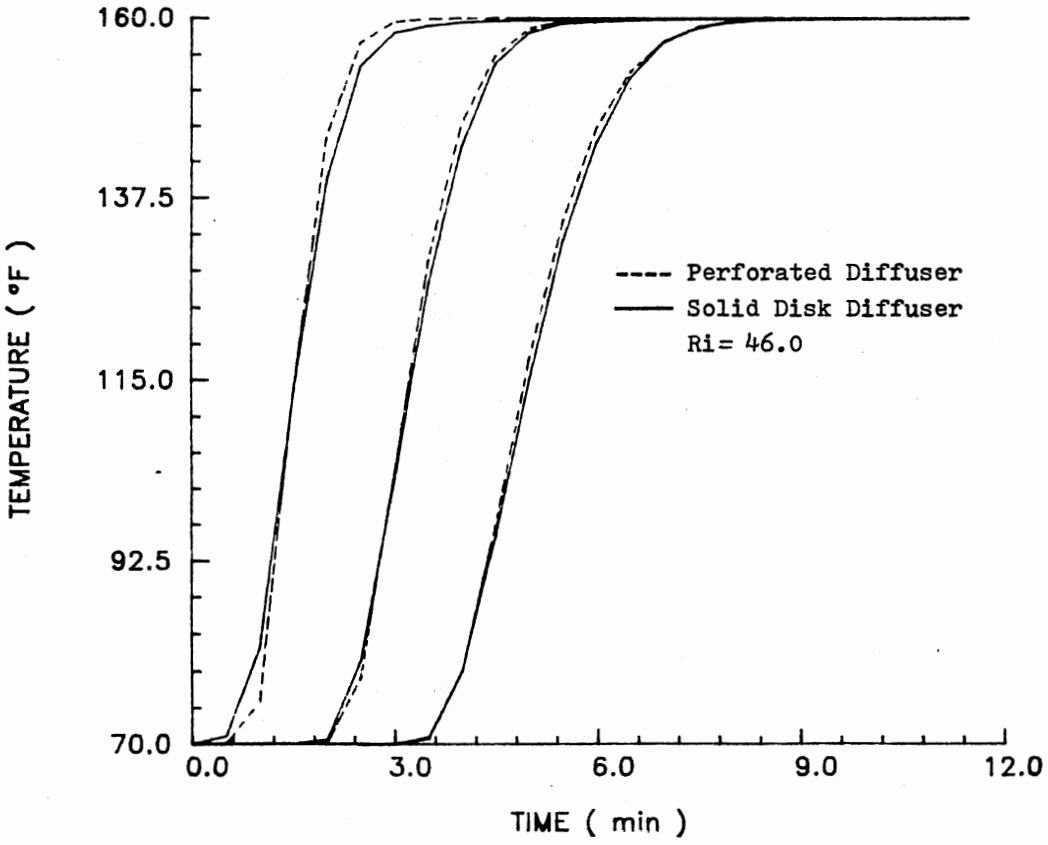

Figure 6.24 Comparison of the Predicted Thermocline Using SOUDS for Two Different Inlet Configurations (Ri = 46.0)

solid center) results in a varying degree of improvement in stratification level in the tank depending on the Richardson number. Significant improvement is observed at Richardson number of 5.0 (see Figure 6.20). As Richardson number increases beyond 9.0 (see Figures 6.21 to 6.24) the difference in performance of the two inlets becomes insignificant especially at elevations passed 1.3 ft from the inlet (third elevation from the inlet). Based on these results a limiting value of Richardson number of 9.0 may be deduced.

The results described in the foregoing agree well with the previous results of Zurigat et al. (1988a) and (1988b) concerning the existence of a limiting Richardson number above which the effect of the inlet geometry on stratification in thermal storage tank vanishes. However, the number deduced from the results presented in this section differs from those previously obtained (see Chapter III). This should be expected for the following reasons:

1. The result of Zurigat el al. (1988a) was based on one-point concentration measurements far from the inlet in fresh-saline water system. Figures 6.21 to 6.24 indicate that the difference in performance of the two inlet geometries used gets smaller at locations removed from the inlet region especially for Richardson numbers greater than 5.0.
2. The result of Zurigat el al. (1988b) was based on mixing correlations obtained based on temperature measurements with hot-cold water system. The measurements away from the inlet (last 5 to 6 thermocouples levels see Figure 3.1) were used in obtaining the correlations. Although, it was possible to detect differences in performance of different inlets at Richardson

numbers of up to 8.0 (Zurigat and Liche, 1987) only those below 3.6 were considered significant.

Based on the results described in this section it may be stated that the inlet geometry has a significant effect on stratification for $R_i \leq 5.0$, a moderate effect for $5.0 < Ri \leq Ri$ and a negligible effect for $Ri > 10.0$. These results while confirming the previous results show the predictive capability of the computer code developed in this study. Further application to single stratified tank under variable inlet temperature conditions has been conducted. The results are presented in the next section.

6.3 Application to SST Under Variable Inlet Temperature Conditions

The performance of single stratified tank (SST) under variable inlet temperature conditions is the least studied aspect of thermal energy storage in SST. The recent experimental study of Abu-Hamdan (1988) has dealt with this problem. The primary objective of that study was to furnish the data base needed for validation of the computer code developed in this study. Before discussing the validation results, an overview of the experimental results is presented.

6.3.1 Overview and Further Analysis of the Experimental Results

The experiments were conducted with four different inlet configurations (see Abu-Hamdan 1988):

1. Top inlet: a 0.75 inch diameter port located at the center of the top side of the test tank with a solid circular diffuser of

14 inch diameter placed 1.0 inch from the top. This leaves a one inch gap from the sides of the 16.0-inch inside diameter test tank used.

2. Side inlet: a 0.75 inch diameter port flush with the inside surface of the test tank and located at 1.5 in. distance from the top of the tank to the centerline of the port.
3. Solid distributor: a 6.0 in. high solid circular steel baffle of 0.1 in. thickness and 13.75 in. diameter was located symmetrically around the mid-height of the test tank. The function of the baffle was to divert the incoming flow which was supplied through 32 inlet ports located at equally spaced intervals around the test tank at mid-height.
4. Perforated distributor: a 0.0625 in. thick, 14.0 in. diameter, 58 in. high black iron baffle having a 6.0 in. high solid portion while the rest is perforated. The solid portion is located symmetrically around the mid-height of the baffle. The perforated portions have a porosity (ratio of the total area of the perforations to the total area) of 15 percent. The function of the baffle is similar to that of the solid distributor. However, the perforated portions were employed to reduce the entrainment of the fluid in the tank with the incoming fluid flowing in the annulus between the baffle and the tank wall and allow leakage of the incoming fluid into the neutral buoyancy level in the tank.

Tests with different flow conditions, i.e., flow rates and transient inlet temperature profiles were carried out. Figures 6.25 to 6.27 show the transient temperature profiles monitored at 9 elevations in the test

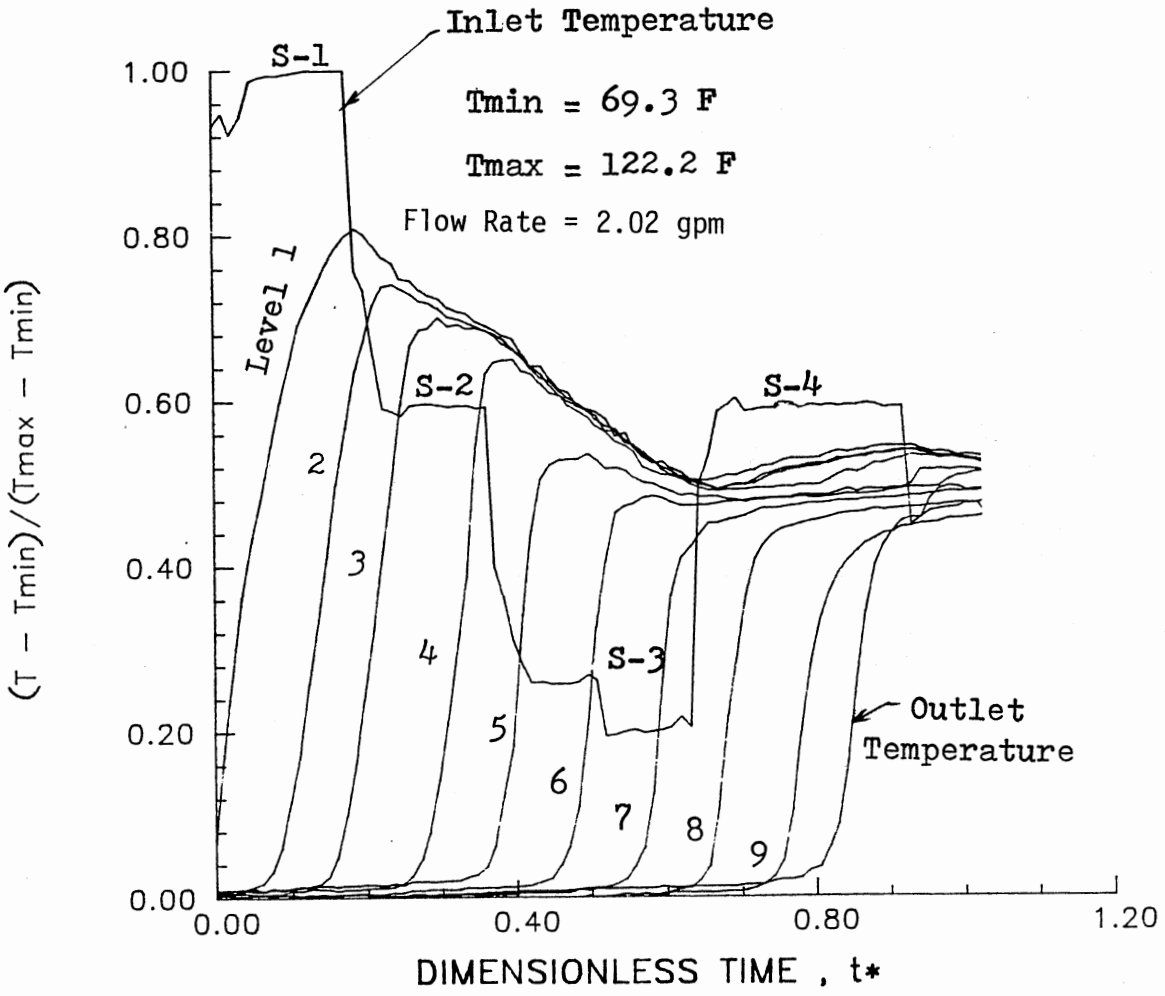

Figure 6.25 Transient Temperature Profiles Under Variable Inlet Temperature Condition (Side Inlet; Run No. 30 of Abu-Hamdan (1988)).Levels ordered as of Figure 3.1

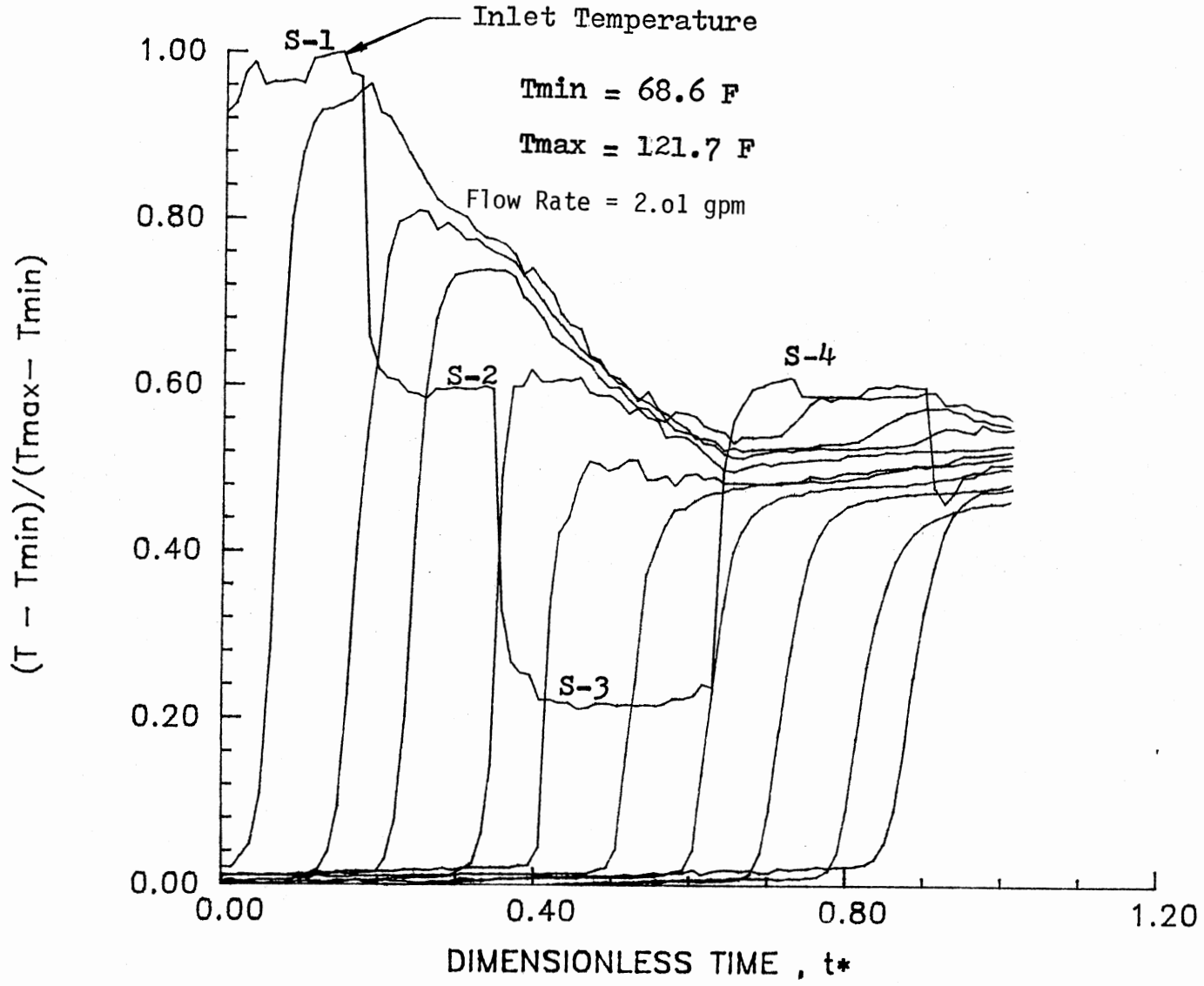

Figure 6.26 Transient Temperature Profiles Under Variable Inlet Temperature Condition (Top Inlet; Run No. 33 of Abu-Hamdan (1988))

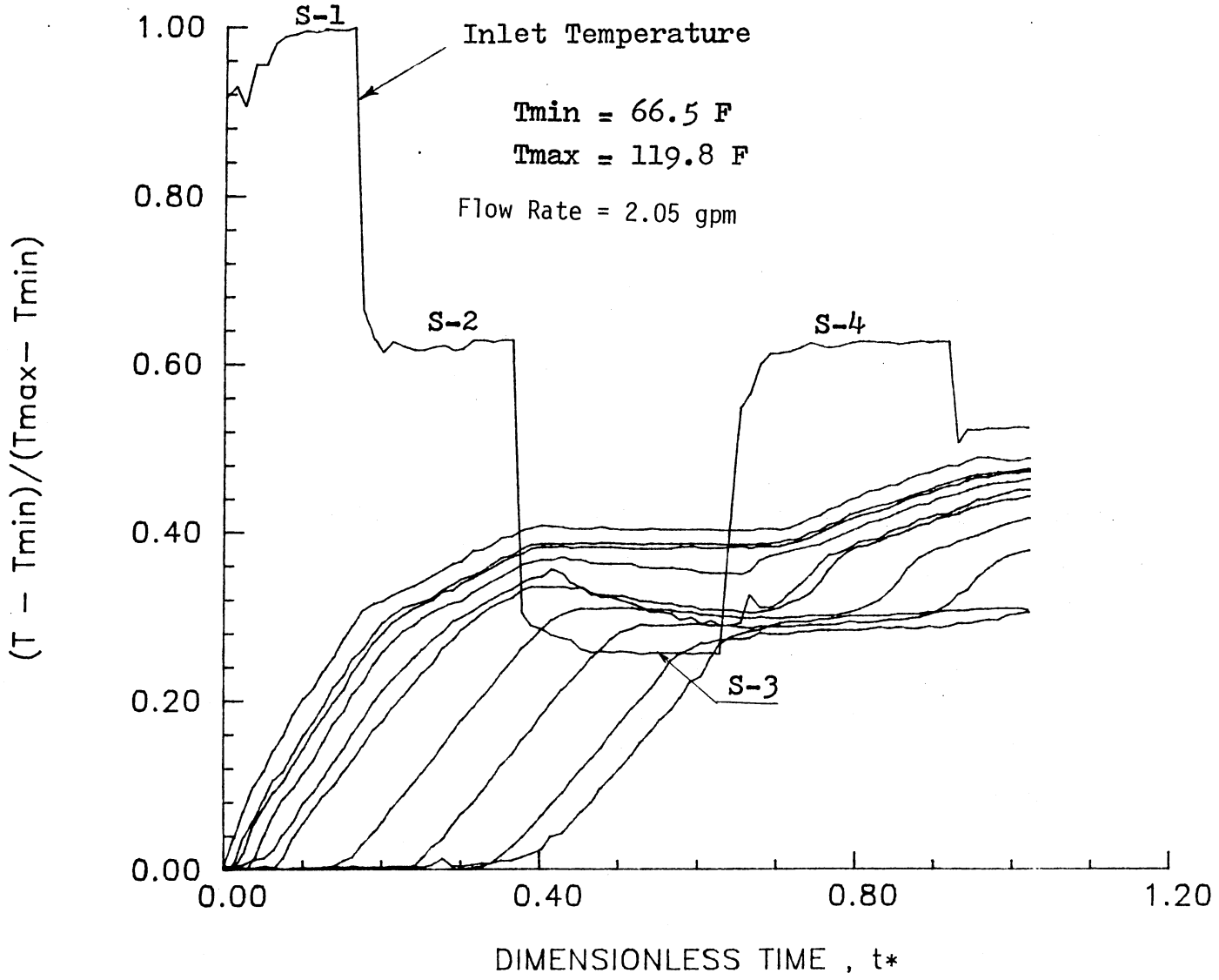

Figure 6.27 Transient Temperature Profiles Under Variable Inlet Temperature Condition (Perforated Distributor; Run No. 22 of Abu-Hamdan (1988))

tank for the side and top inlets and the perforated distributor, respectively. The transient inlet and outlet temperature profiles are also shown. While these figures are crowded, it will be seen below that they tell the whole story of the flow behavior inside the test tank. In the following discussion, reference will be made to the regions of step change (minor step changes are ignored) in the inlet temperature as S-1 for the first step, S-2 for the second step and so on.

The transient temperature response to the first step in the inlet temperature (S-1) is seen to be a function of the inlet configuration used. While the responses for the side and top inlets are similar in character (see Figures 6.25 and 6.26), there is a quantitative difference among them, and also they both differ from that of the perforated distributor (see Figure 6.27). Observing the temperature response to S-1, it can be seen that the side inlet causes more mixing than the top inlet. This is evident, since the maximum temperature reached at the first level is less for the side inlet than for the top inlet. In fact, the first three levels for the side inlet have responded to S-1 while only the first two levels have responded in the case of the top inlet. This is indicative of the extent of mixing caused by the two inlets considered. Before leaving S-1 region, observation of the response for the case of perforated distributor gives a rather different picture. The first five levels responded to S-1 almost simultaneously. The sixth level, although later in time, has also responded to S-1. This indicates that severe mixing is taking place in a large portion of the tank. While flow visualization tests could not be performed in the test tank, the computer simulations have provided the explanation for this behavior. That is, the hot fluid

flowing in the annulus between the perforated baffle and the tank wall entrains cold fluid from the upper half of the tank. This leads to setting up localized recirculation zones which in turn enhance mixing greatly.

The second step change in temperature (S-2 in Figures 6.25 to 6.27) is seen to produce severe mixing, extending through the first 4 levels in the tank for both cases of side and top inlets. Again it is observed that the mixing is more severe in the case of the side inlet compared with the top inlet. At the end of S-2, the first four levels, in the case of side inlet, have essentially the same temperature (see Figure 6.25) while for the top inlet, only the first three are fully mixed (see Figure 6.26). A further decrease in the inlet temperature, (step S-3), causes the tank to be essentially fully mixed. It should be noted that in S-3 step, while the inlet temperature has dropped below that of the first 4 levels (see Figure 6.26), the temperature in these levels did not drop at the same rate. This indicates that the incoming fluid, possessing a negatively buoyant force, slips down to the level where neutral buoyancy is encountered and displaces the fluid layer there. This is evident from the temperature history of the different elevations in the tank (note the leveled parts of the temperature profiles).

Turning to Figure 6.27 for the perforated distributor, it is demonstrated that the step change in temperature (S-2) was immediately felt by the bottom half of the tank, particularly by level 7 and later by level 8. It should be noted that this warming up of the lower part of the tank is not justified on the basis of buoyancy force arguments since the inlet temperature (S-2) is still much higher than that of the bottom of the tank. The only justification is that advanced earlier in

this section regarding the entrainment and the subsequent development of recirculation zones which have a catastrophic effect on stratification. Slight warming of the upper half of the tank is observed (see Figure 6.27). As the inlet temperature dropped, as in step S-3, the temperature of both level 9 and the outlet responded without any time lag. This indicates that the flow is short-circuiting to the outlet, causing a single large recirculating zone in the bottom half of the tank which results in the bottom half of the tank becoming fully mixed while the upper half maintains the same prestep temperature distribution. It is, therefore, not surprising that this inlet has performed better than any other inlet in the special case where the upper half of the tank was filled initially with hot water and the cold water from the bottom half was circulated back to the tank through different types of inlets (see Figure 2.3 and the duplicate experiment of Abu-Hamdan (1988)). These types of runs were rather impressive at the first look. However, engineering designs cannot be judged based on a single performance test.

In view of the above results, a question arises regarding the performance of different inlets under the conditions considered. In thermocline thermal storage case, the mixing index was introduced (see Chapter III) as a measure of performance. In the case of variable inlet temperature, a measure of performance had to be devised. Observing that the final outcome of stratification enhancement is to improve solar collector efficiency, the latter parameter was chosen as an index of performance. This is done by using the transient tank outlet temperature profile as an input to a solar collector model and calculating the solar collector efficiency. Comparison of the efficiencies obtained for different inlets gives the relative performance. However, this

procedure may be perfectly justified when the conditions of the experiments are identical from one experiment to the next. The results shown in Figures 6.25 to 6.27 show that this is difficult to achieve. Some variations in the inlet temperature profiles or in the flow rates will undoubtedly occur. Therefore it was decided to devise a reference measure in addition to the one described above. That is, the tank outlet temperature profiles calculated based on the fully mixed model were also fed into the solar collector model and the efficiency is calculated. This represents the lower limit since the fully mixed case is the worst condition possible. On the other hand, the other extreme condition of interest is that of a fully stratified case. That is, the flow seeks its temperature level without mixing throughout the path. However, mixing with the adjacent layers is allowed. This happened to be the conditions modeled by Sharp (1978). The computer code based on this model (Maloney 1987) was modified for the variable inlet temperature condition and the tank outlet temperature profile calculated is used in a similar manner to that for fully mixed model. The solar collector model is described in Abu-Hamdan (1988).

Figure 6.28 shows the tank outlet temperature profiles calculated by the fully mixed and the fully stratified models compared with the experimental profile which corresponds to the experimental data of Figure 6.26 for the top inlet. The inlet temperature profile is also shown. The corresponding instantaneous efficiency profiles are shown in Figure 6.29. It is seen that the efficiency based on the experimental results falls between the two profiles corresponding to the fully mixed and the fully stratified cases. However, it is closer to the fully stratified behavior. Figures 6.30 and 6.31 are analogous to

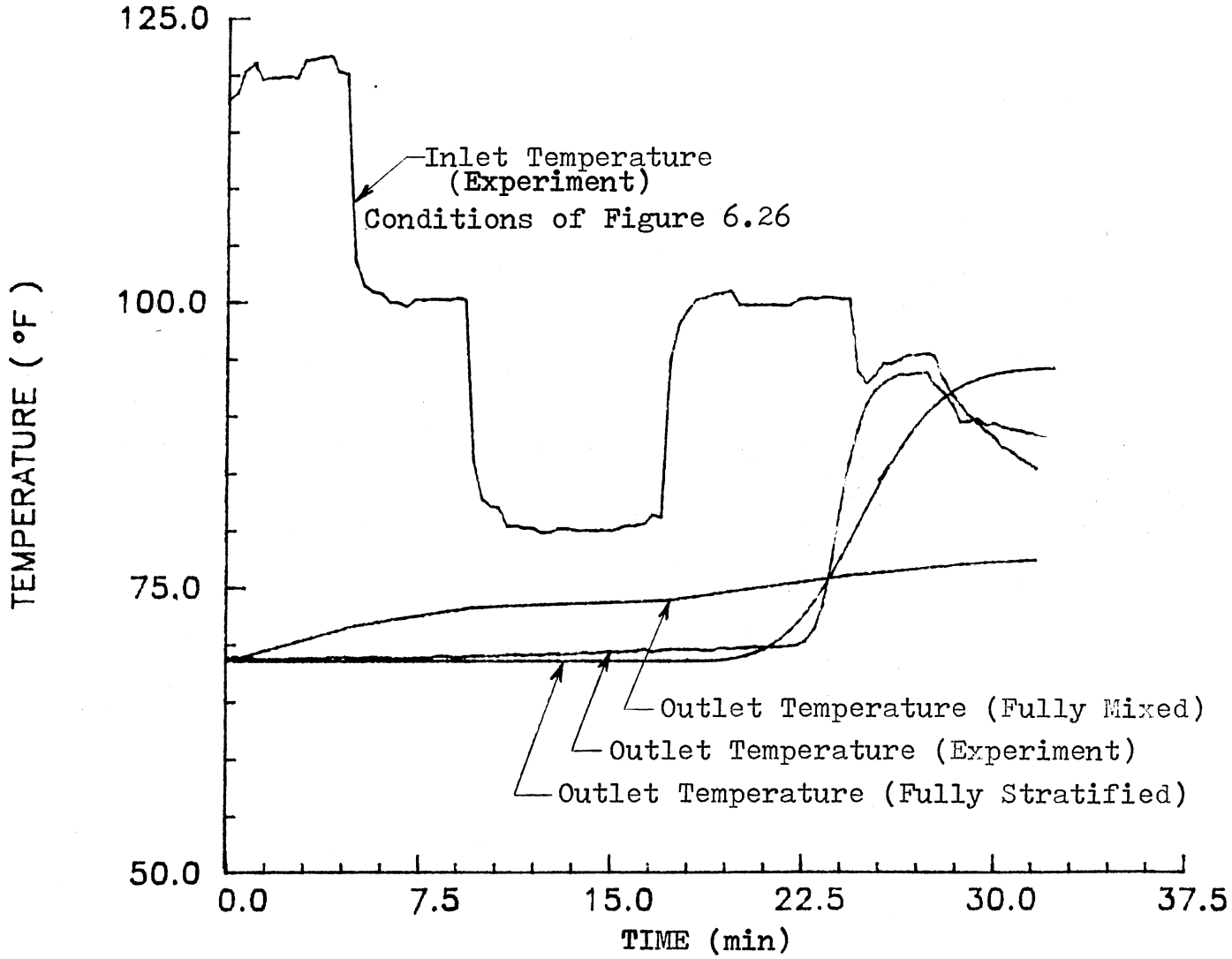

Figure 6.28 Thermal Storage Tank Transient Inlet and Outlet Temperature Profiles

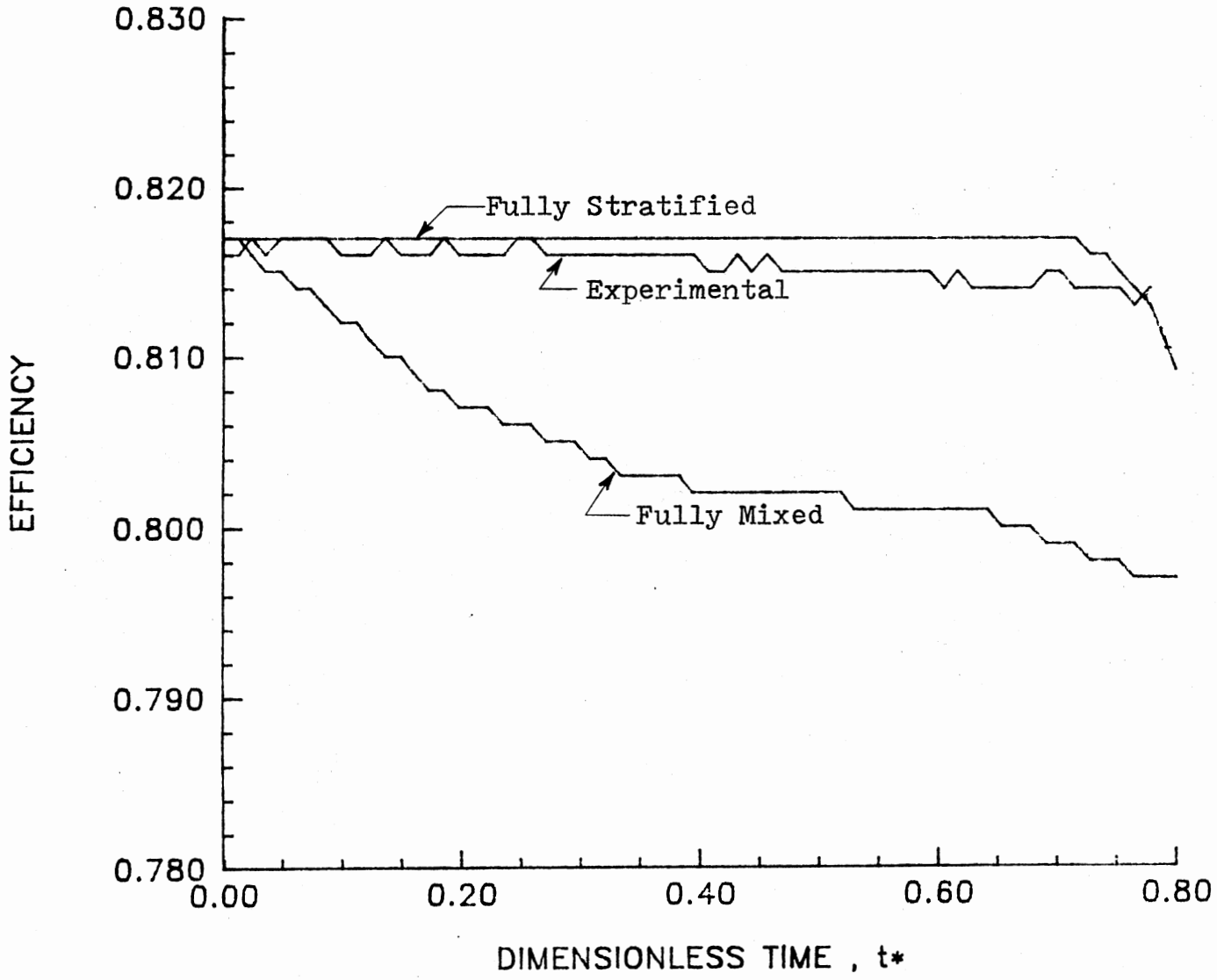

Figure 6.29 Solar Collector Instantaneous Efficiency Calculated Based on Outlet Temperature Profiles of Figure 6.28

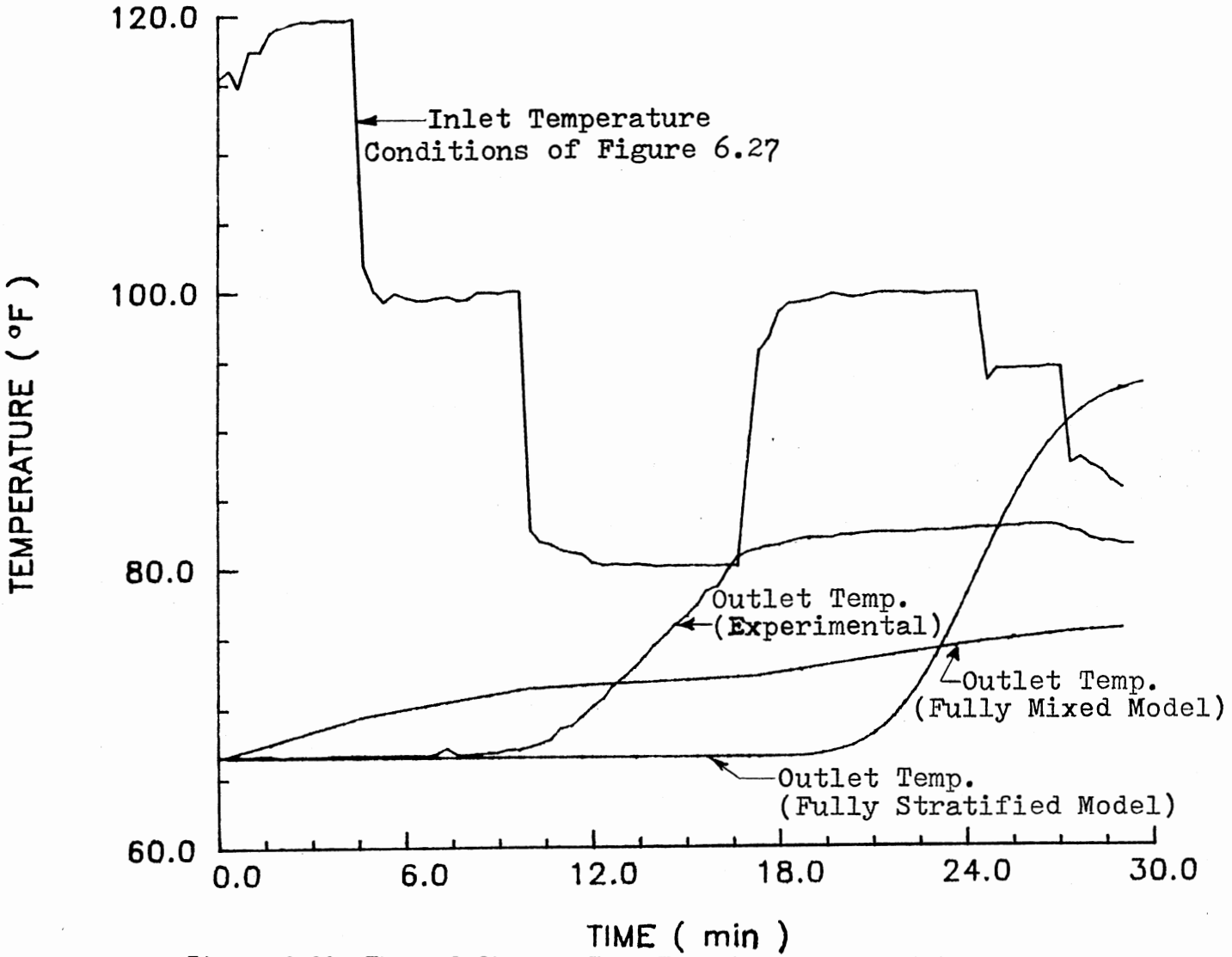

Figure 6.30 Thermal Storage Tank Transient Inlet and Outlet Temperature Profiles

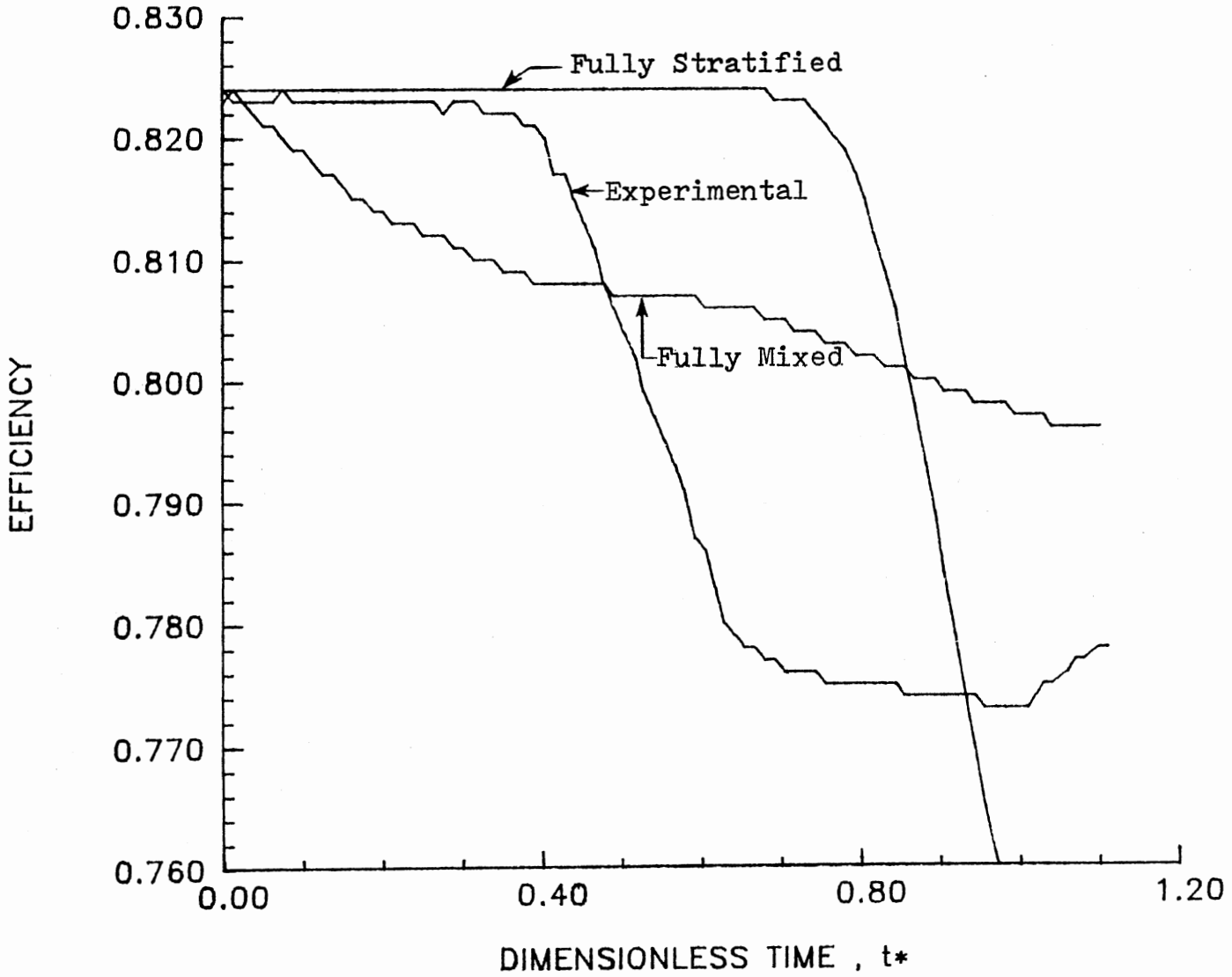

Figure 6.31 Solar Collector Instantaneous Efficiency Calculated Based on Outlet Temperature Profiles of Figure 6.30

Figures 6.28 and 6.29 respectively and correspond to the experimental conditions of Figure 6.27 for the perforated distributor. The experimental and fully mixed tank outlet temperature profiles cross at t = 13 minutes (see Figure 6.30) which corresponds to t* = 0.5 in Figure 6.31. The increase in experimental temperature profile over the predicted by the fully mixed model proves the suggestions made earlier in this section about the short circuiting phenomenon observed when examining Figure 6.27. Integration over the time of the collector efficiencies shown in Figures 6.29 and 6.31 (based on experimental data) shows that the perforated distributor offers no advantage over the conventional top inlet (0.80 for the distributor versus 0.815 for the top inlet).

Based on the results discussed above is should be noted that the flow behavior is a strong function of many variables. Therefore prediction of the flow behavior under the influence of individual variables is fundamental to any design developments. The primary objective of this phase of the study was to develop the simulation tool. The next subsection deals with the simulation effort under the conditions of variable inlet temperature.

6.3.2 Code Validation and Application to SST Under Variable Inlet Temperature Conditions.

The computer code developed in this study has been applied to stratified thermal storage under variable inlet temperature conditions. Simulations were carried out for the top inlet and the perforated distributor. Figure 6.32 shows the predicted thermal storage tank temperature response to the inlet temperature profile shown in

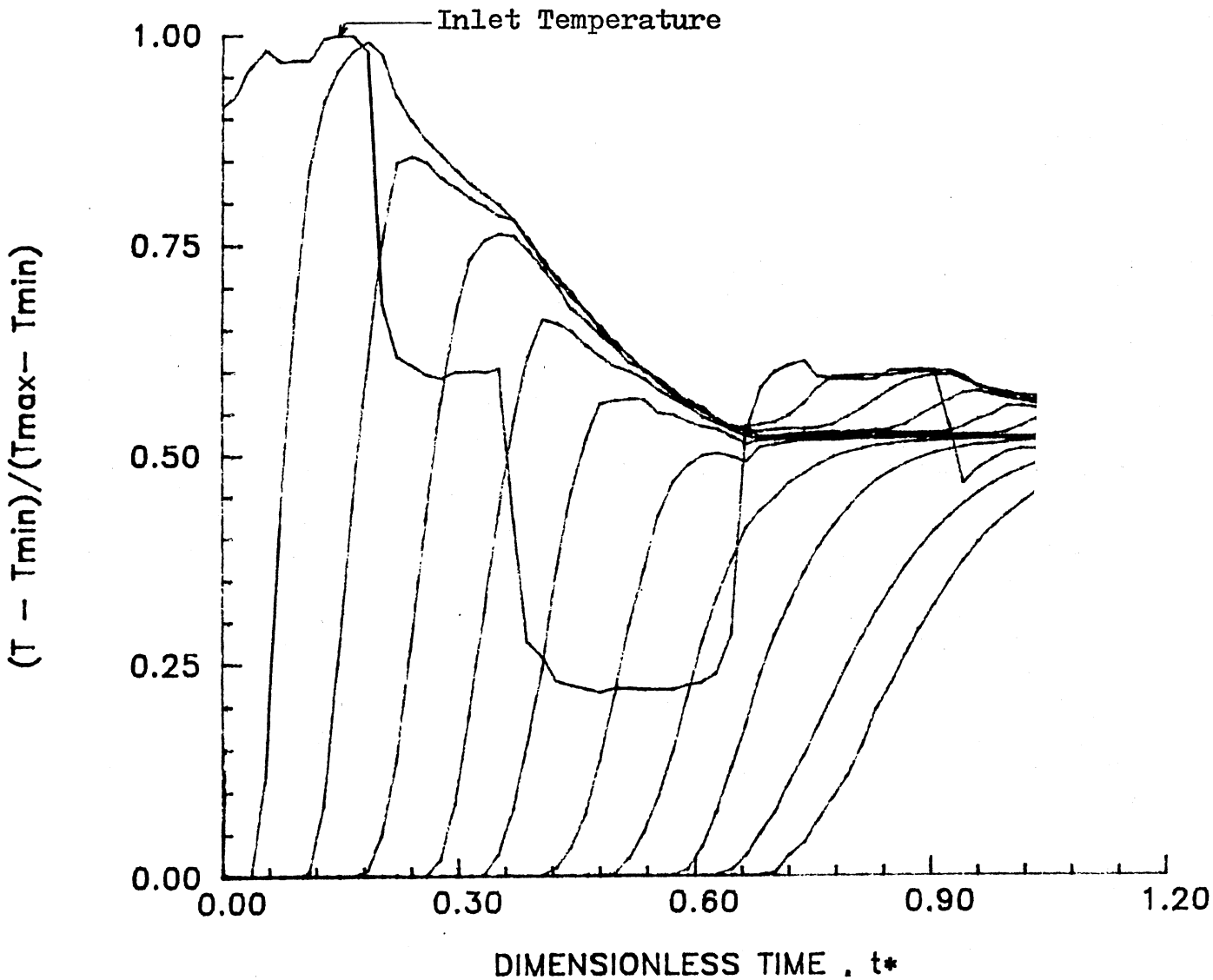

Figure 6.32 Predicted Temperature Profiles in Stratified Thermal Storage Tank Under Variable Inlet Temperature Conditions (Conditions of Figure 6.26)

Figure 6.26 (top inlet). Comparison of Figures 6.32 and 6.26 reveals that the overall behavior obtained experimentally is well predicted. However, the model predicts greater mixing at the bottom of the tank than observed experimentally. It should be noted that duplication of the exact experimental conditions is difficult to achieve. Therefore, it is natural to expect slight disagreements with the experiments. Despite this the model is seen to be capable of duplicating the flow behavior accurately.

Predictions using the perforated distributor show similar results. Figure 6.33 shows the predictions for the conditions of the experiment illustrated in Figure 6.27. In this case the agreement with the experiment is poor. However, the main features of the thermal response were captured satisfactorily. Reducing the spacing between the baffle and the tank wall to 0.5 in. produces slightly better results (see Figure 6.34). Figure 6.35 shows the predicted temperature response to a step change in inlet temperature for the perforated baffle. The corresponding experimental data are shown in Figure 6.36. Again, the predictions are good and represent the flow behavior very well.

Based on the above results, a stage has been reached where the computer code is used to produce information that is not available or not obtainable experimentally due to the cost and time involved. For example, information about the influences of the porosity of the baffle, the spacing between the baffle and the wall, the absence of a baffle and the influence of any additional perforated or nonperforated obstructions in the flow field is of interest for selection of optimal designs. Figure 6.37 shows the predictions of the temperature variation along the tank centerline after 10.0 minutes ($t^* = 0.376$) for different

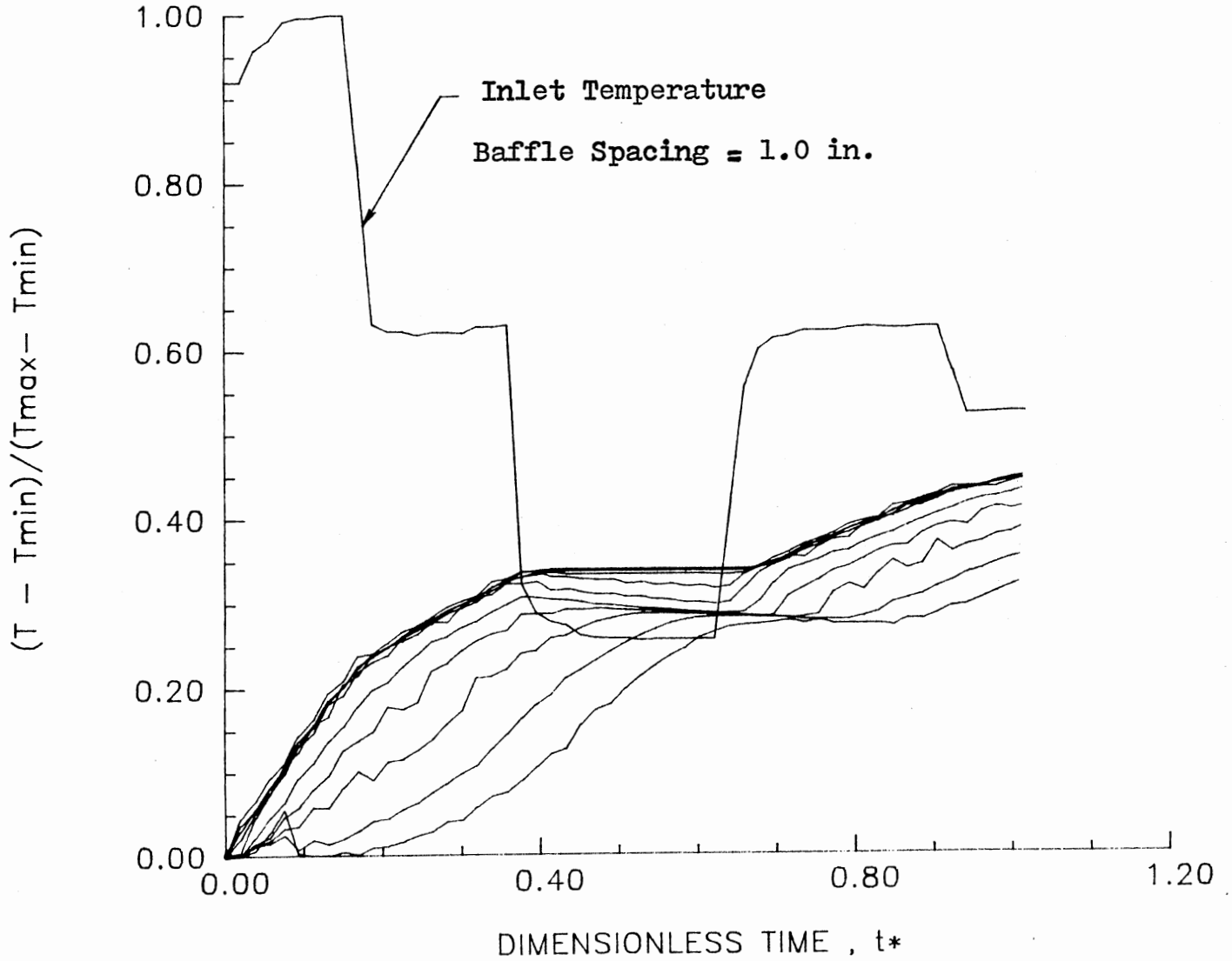

Figure 6.33 Predicted Temperature Profiles in Stratified Thermal Storage Tank Under Variable Inlet Temperature Conditions (Conditions of Figure 6.27)

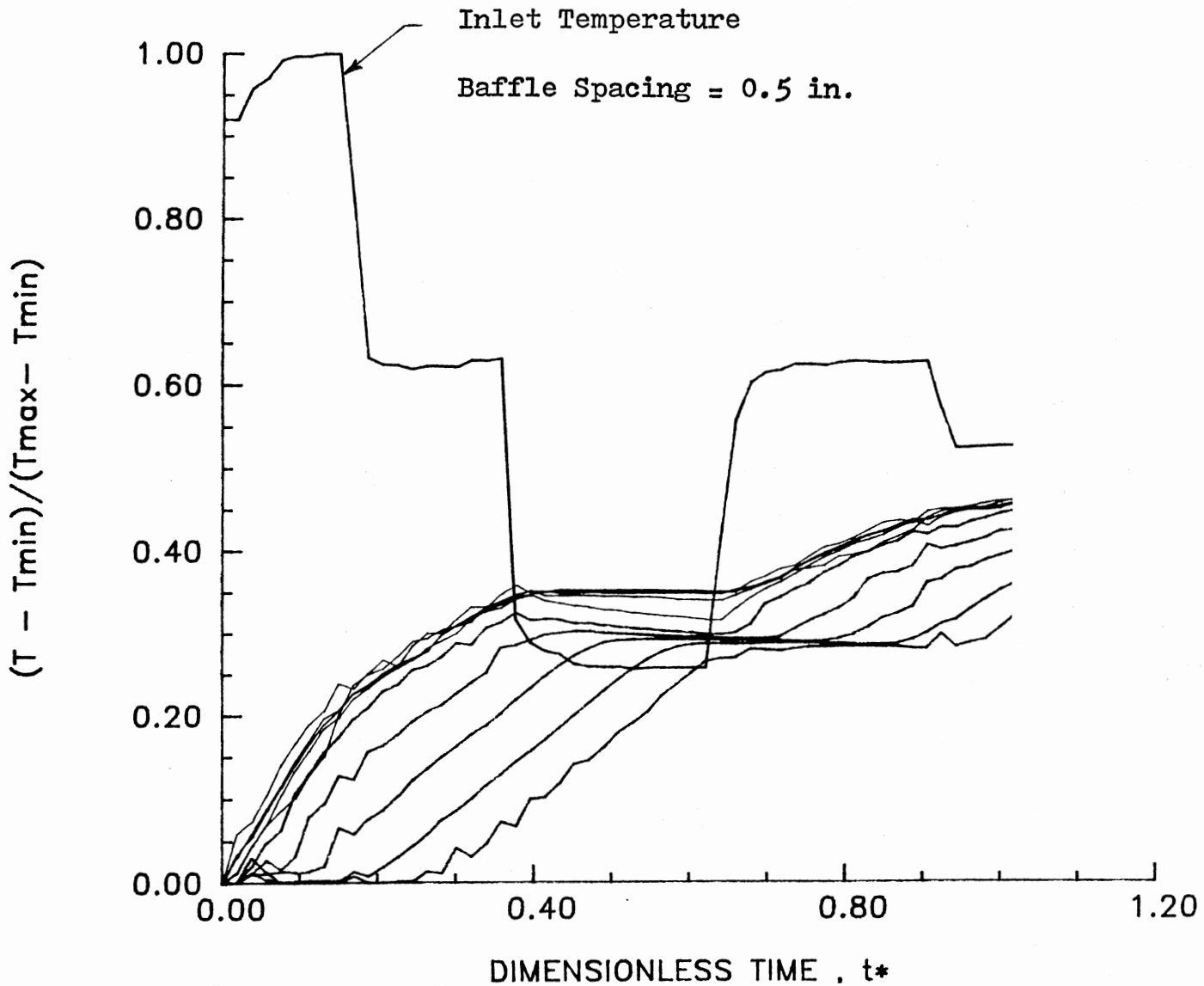

Figure 6.34 Predicted Temperature Profiles in Stratified Thermal Storage Tank Under Variable Inlet Temperature Conditions (Conditions of Figure 6.27)

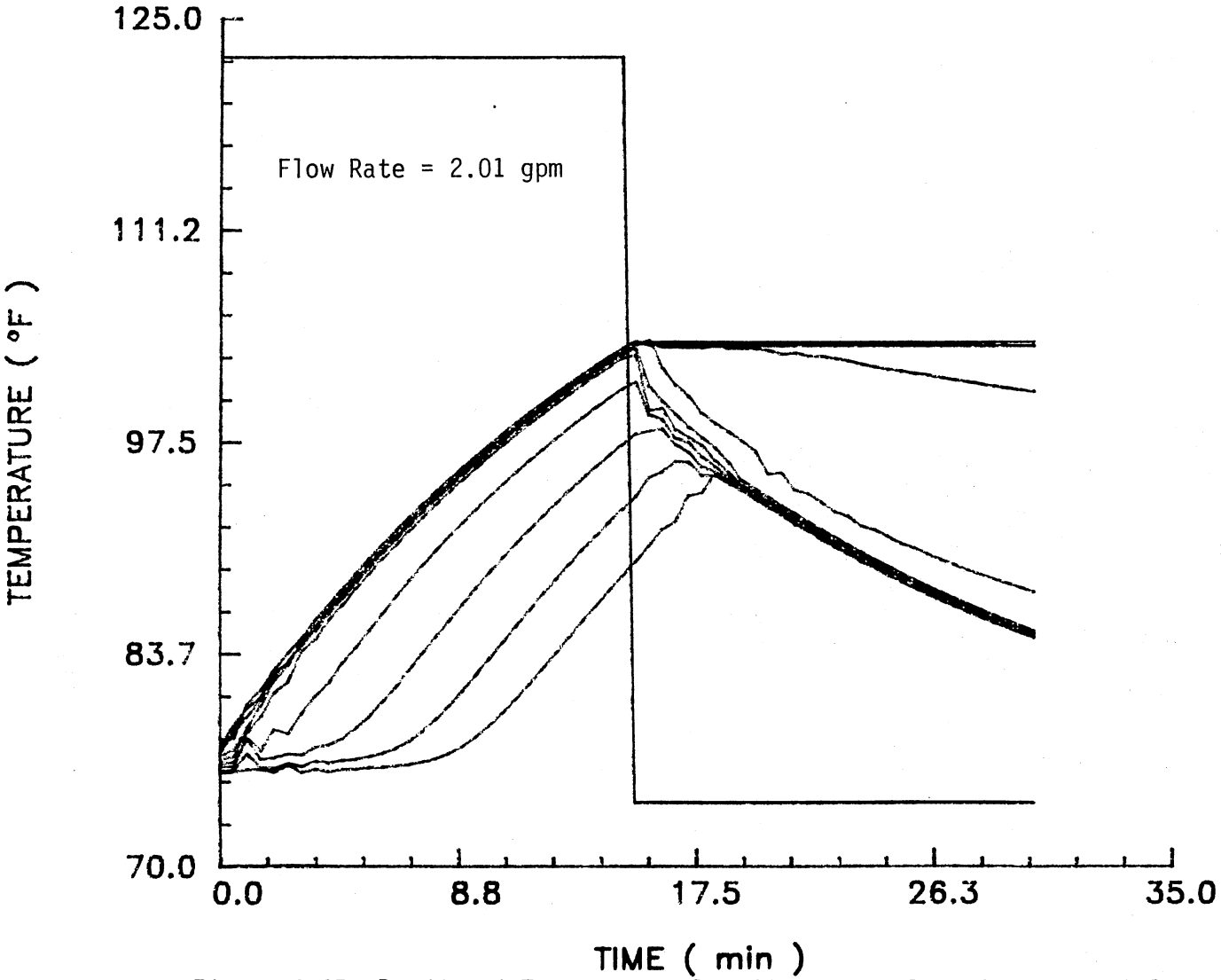

Figure 6.35 Predicted Temperature Profiles for a Step Change in Inlet Temperature (Perforated Distributor)

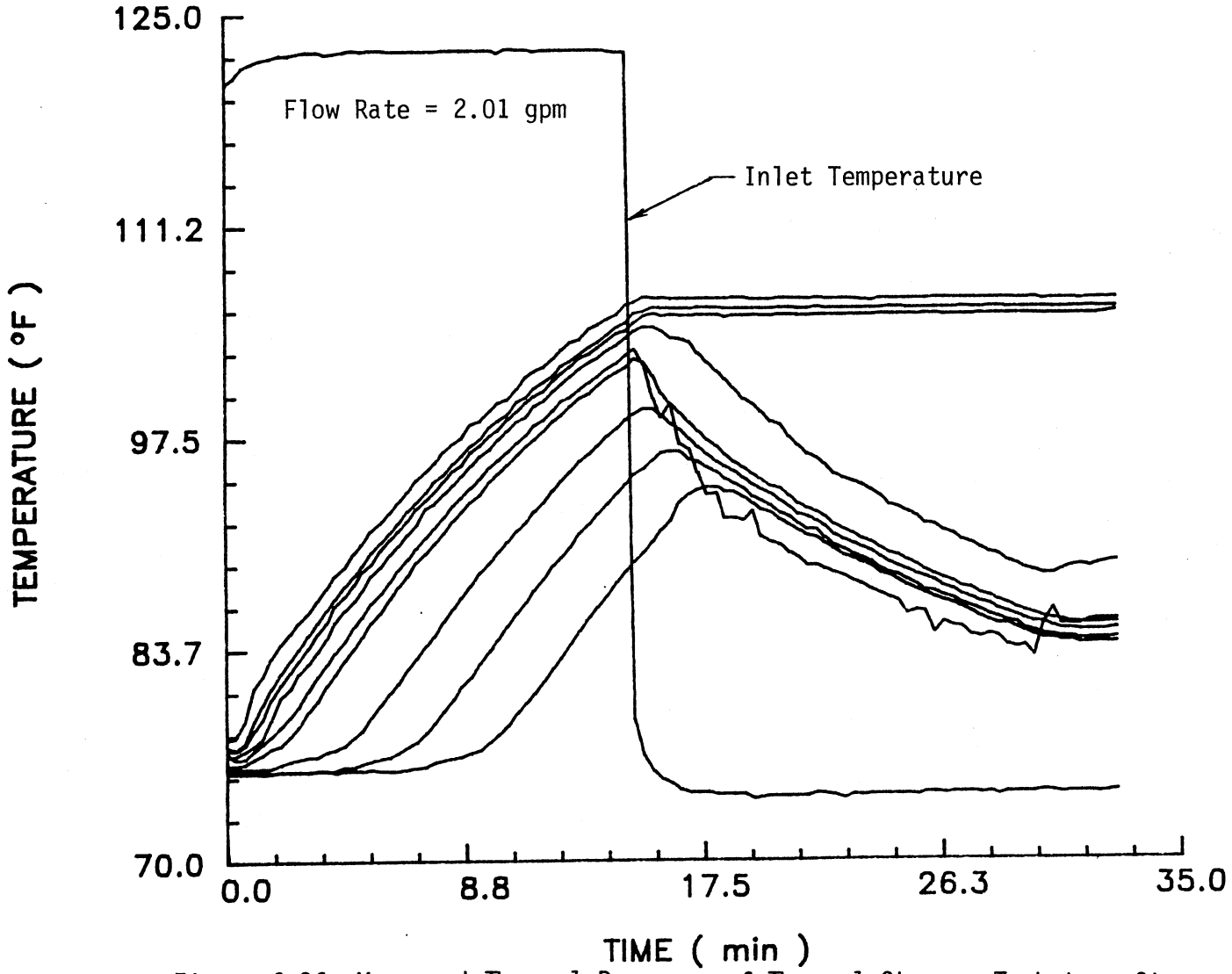

Figure 6.36 Measured Thermal Response of Thermal Storage Tank to a Step Change in Inlet Temperature (Perforated Distributor)

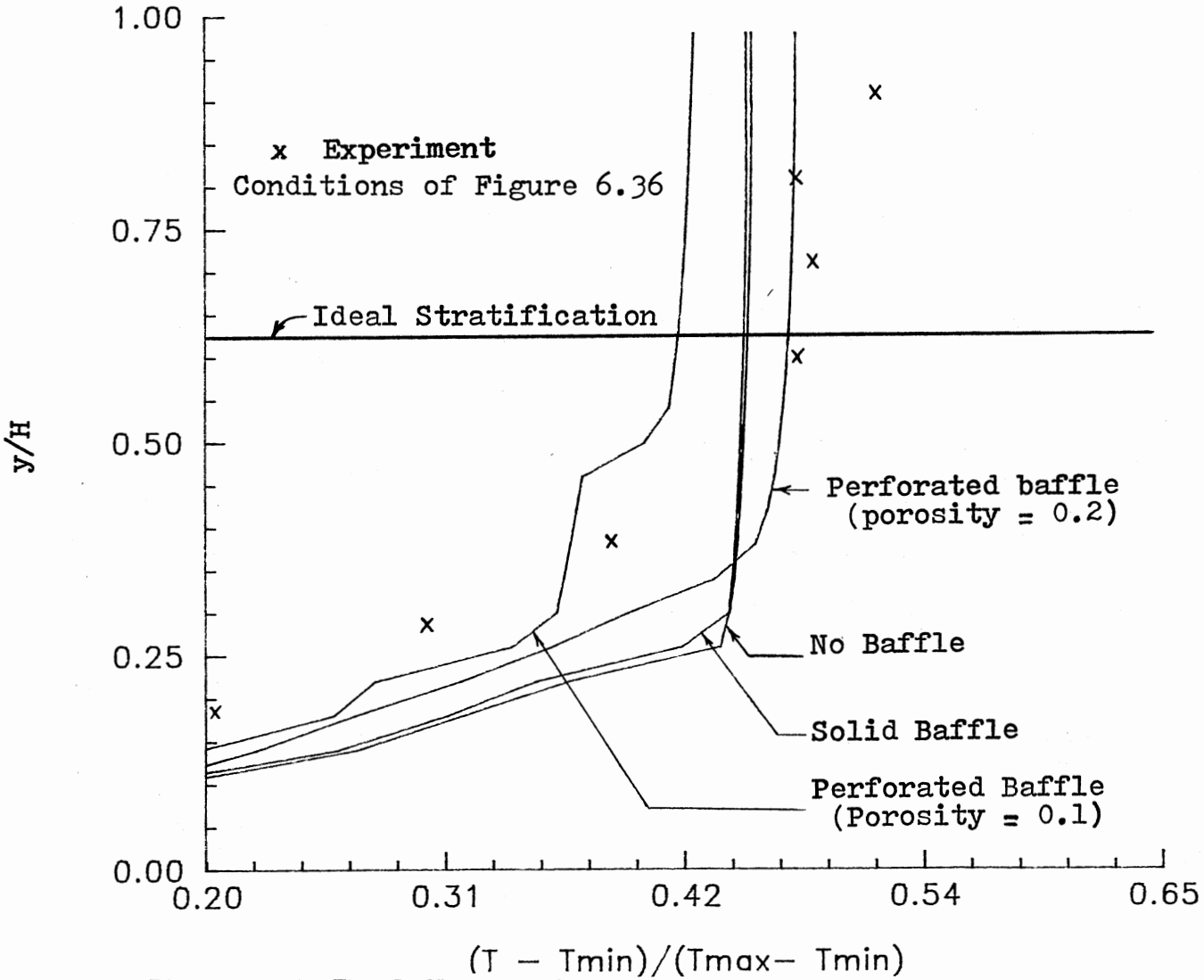

Figure 6.37 The Influence of Geometric Configuration on Predicted Thermal Response in Thermal Storage Tank (t* = 0.376)

baffle configurations. The inlet temperature profile of Figure 6.36 was used. The experimental data of Figure 6.36 are plotted for comparison. Notice that the inlet temperature profile is constant over the duration considered in Figure 6.37. In this case the ideal stratification would be represented by the horizontal line which indicates that 0.376 of the tank volume is filled with water at temperature equal to the inlet temperature. Evidently a high degree of mixing is present. The model predicts higher mixing than observed experimentally for all the conditions simulated. The effect of different geometric parameters is clearly distinguished. For example, the solid baffle produces results similar to those with no baffle present. The porosity is seen to have the greater influence. The results favor higher porosity. However, in the limit of no baffle present (porosity of unity) the results favor lower porosity. This indicates the existence of a critical porosity for better performance. Figure 6.38 represents the same conditons of Figure 6.37 but at a different time frame (t = 20.0 min.; t^* = 0.75). Similar conclusions to those stated above can be drawn. Thus, it is seen that the computer code produces consistent results. Hence, a simulation tool is now available.

Based on the results discussed in Section 6.3, it is concluded that under the conditions investigated the use of distributor offers no advantage over conventional inlets except for the special case mentioned earlier. Therefore, other geometries should be investigated. The computer code developed in this study has been shown to be capable of performing this task. The next chapter summarizes the findings and recommendations for further work are presented therein.

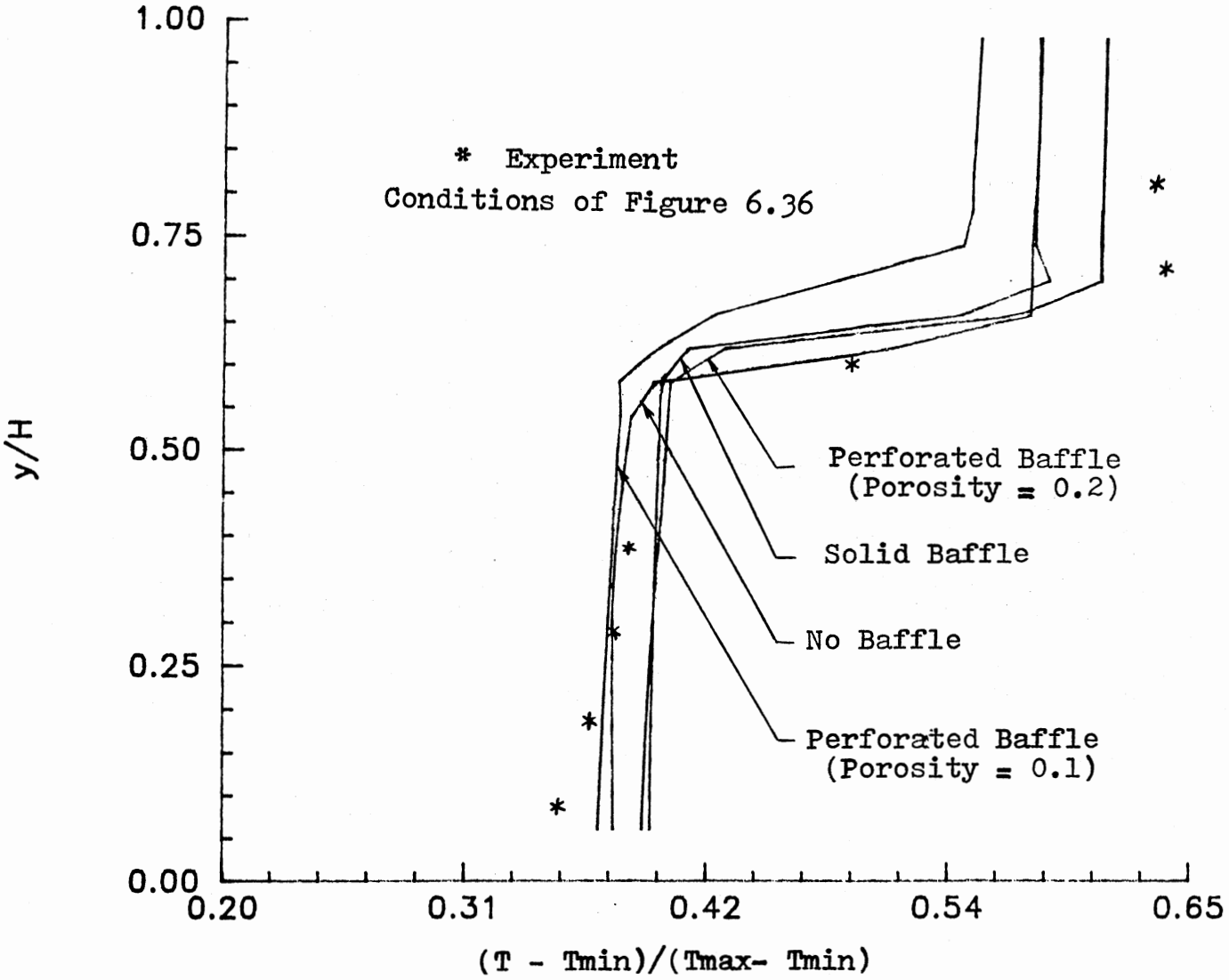

Figure 6.38 The Influence of Geometric Configuration on Predicted Thermal Response in Thermal Storage Tank (t* = 0.75)

CHAPTER VII

SUMMARY, CONCLUSIONS AND RECOMMENDATIONS

Thermal storage has a number of potential benefits in both heating and cooling applications. It is a key technology in successful exploitation of solar energy and cutting down the demand on conventional energy sources. Most recently, thermal storage has been increasingly used in load management applications, that is, shifting all or part of the energy demand to off-peak hours of the day, leading to improved utilities' load factors and reduced cooling capacity in air conditioning systems.

Among the many thermal storage concepts developed in the last two decades, sensible thermal storage in water has found a wide acceptance for its abundance, low cost, high specific heat and benign character. Chilled or hot water is stored in tanks which vary in design.

One of the most promising designs is the single stratified tank in which both hot and cold water are stored without any physical barriers. In these tanks, natural stratification is the separating mechanism. However, the degree to which stored thermal energy can be extracted without loss of thermodynamic availability depends on several design and operating factors:

-- on the one hand, in chilled water systems, the density differences are normally small and the stratification very weak, leading to low Richardson numbers and a tendency for

the chilled water to mix excessively with warmer water in the tank if disturbed by uncontrolled inlet flows;

-- on the other hand, water heated by solar panels varies continuously in temperature, and must be inserted into the stratified thermal storage tank at the proper level, which also varies, to avoid excessive mixing.

In addition to the above problems, the integration of thermal storage into a large energy system requires knowledge of the tank performance under wide range of operating and control modes. The availability of efficient and accurate analytical modeling is the key factor in making overall energy system simulations possible. This is a major step in promoting the use of thermal storage in both residential and commercial sectors so that the ensuing benefits from thermal storage can become a reality.

This study was undertaken to investigate the design improvements of single stratified tanks to achieve high performance under wide range of flow conditions. The study required a number of steps that were carried out in the course of this study:

1. Experimentation with a fresh-saline water system to obtain wide range of densities and isolate parasitic effects, i.e., heat loss to the ambient, conduction along the wall and the associated buoyancy driven motions and to assist in developing a one-dimensional analytical model incorporating inlet mixing characterization (see Chapter III and Zurigat et al. 1988a).
2. Experimentation with hot-cold water system to investigate the performance of single stratified tank (SST) under actual

conditions. Upgrading the one-dimensional analytical model developed in Step 1 above to include heat loss to the ambient (Ghajar et al. 1987) and developing mixing correlations for different inlet designs (see Chapter III and Zurigat et al. 1988b).

3. Development of microcomputer-based data acquisition system and data reduction software to increase the capacity, speed and reliability of data collection and analysis (see Rao et al. 1988).
4. Conducting a comparative study of one-dimensional single stratified tank models available in the literature by validation with our experimental data (Zurigat et al. 1987) and with those of other investigators (Maloney 1987).

The results established the relationship between mixing effects and inlet design conditions as well as flow parameters. The introduction of the mixing index which served as a quantifying measure of mixing casued by different inlet designs was successfully used to characterize inlet configurations and identify the best configuration for enhancement of stratification in a single stratified tank. Two inlet configurations were shown to enhance stratification, i.e., perforated and impingement inlets.

Mixing correlations were developed based on the experimental data. These, when incorporated in a one-dimensional model developed in this study resulted in an efficient and accurate model suitable for large energy systems simulations. This was shown to be true by the comparative study of different one-dimensional models available in the literature (see Zurigat et al. 1987).

A by-product of this study was the development of a data acquisition system and data reduction software that is versatile and capable of collecting data from a large number of channels for both temperature and mass concentration measurements with high accuracy (Rao et al. 1988). In this manner, the data collected in the course of this study has contributed in enlarging the data base for future analytical studies.

While the aforementioned work was restricted to the thermocline thermal storage (constant inlet temperature), the more general case of variable inlet temperature is equally important. As the literature review shows (see Chapter II), very little has been done to investigate the performance of a single stratified tank under these conditions. A further study was carried out to develop the simulation tool for assessments of design improvements that make use of the hydrostatic and hydrodynamic effects to guide the incoming flow to its proper stratification level with minimal mixing (see Chapter IV). Both laboratory model tests and numerical simulation was used. Discussion of these approaches was presented along with the specific methodology used (see Chapters IV and V).

The computer code developed in this study, based on the theory and formulation of Chapters IV and V respectively, incorporates the following features:

1. Equations Solved: the conservation equations of mass, momentum and energy in either plane cartesian or axisymmetric cylindrical coordinates are solved. The bidirectional coupling between momentum and energy equations through the

buoyancy term in the former and through the velocity terms in the latter was also treated. The resistance to flow through perforated and nonperforated obstructions was modeled with no limitation on the number or arrangement of these obstructions.

2. Numerical Formulation: explicit finite difference method was used and two different schemes of discretization of the advection terms were employed, that is, the Weighted Upwind Difference Scheme (WUDS) and the Second Order Upwind Difference Scheme (SOUDS). Discretization over uniform and non-uniform grid spacing was implemented.

3. Flow Regime: both laminar and turbulent flow regimes were treated under either forced or mixed (buoyant) convection flow conditions.

4. Other Features: both constant and variable flow rates and inlet temperatures are permitted.

The computer code was applied to several fluid flow problems with known solutions. Thus, the functional status of the code was established. The numerical tests showed that the SOUDS is superior to WUDS. Therefore, the former was applied in predictions of thermal storage tank performance under both constant and variable inlet temperature conditions. Comparison between the predictions and the experimental data obtained in this study and in a companion study (Abu-

Hamdan 1988) was also conducted.

The results of the simulations of thermocline thermal storage (constant inlet temperature conditions) confirmed the previously obtained results regarding the existence of a limiting Richardson number above which the influence of the inlet geometry on stratification in thermal storage tank vanishes. A Richardson number value of 9.0 was deduced. Further analysis of the experimental data of Abu-Hamdan (1988) showed that in general the perforated distributor used offered no advantage over the conventional inlets in promoting stratification. However, the versatile two-dimensional model developed in this study offers the tool for investigating a wide variety of inlet geometries under both constant and variable inlet temperature conditions. The predictions of thermal response in single stratified tank were shown to be good and compare well with the experiments. Thus, a simulation tool is now available.

Based on the results obtained in this study the following recommendations may be stated:

1. The simulation tools developed so far including the one- and two- dimensional models proved the viability of obtaining reliable information and design guidelines for stratified thermal storage. However, to expand the applicability of the aforementioned two-dimensional model to wider variety of geometries and orientations of stratified thermal storage devices, it is necessary to expand the model to non-axisymmetric geometries. Moreover, improvements on the efficiency of the computational technique used in this study

to reduce the computer CPU time, which is often restrictive, is recommended. This may be done by adopting implicit formulation instead of the explicit one used.

2. The present effort was aimed at stratified thermal storage devices with thin walls which is the type tested in our experimental facilities. However, thick walls are frequently used in practice. Therefore, modeling of the interaction between the wall and the fluid stored in the storage device is recommended.

3. While the simulations produce results comparable with experiments, limited flow visualization experiments may shed light onto the practicality of certain geometries and/or orientations.

BIBLIOGRAPHY

Abdoly, M.A. (1981), Thermal Stratification in Storage Tanks, Ph.D. dissertation, University of Texas at Dallas, July, 1981.

Abdoly, M. A. and Rapp, D. (1982), Theoretical and Experimental Studies of Stratified Thermocline Storage of Hot Water, Energy Convers. Mgmt, v. 22, pp. 275-285.

Abu-Hamdan, M. G. (1988), An Experimental Study of Stratified Thermal Energy Storage Under Variable Inlet Temperature Conditions, M.S. thesis, Oklahoma State University, Stillwater, Oklahoma, July, 1988.

Baines, W.D., Martin, W.W. and Sinclair, L.A. (1982), On the Design of Stratified Thermal Storage Tanks, ASHRAE Transactions, v. 88, part 2, pp. 426-439.

Bradshaw, P., Cebeci, T. and Whitelaw, J.H. (1981), Engineering Calculation Methods for Turbulent Flow, Academic Press.

Brumleve, T.D. (1974), Sensible Heat Storage in Liquids, Sandia Labs Report, SLL-73-0263.

Busnaina, A. A. (1979), Numberical Simulation of Local Destratification of Lakes, M.S. thesis, Oklahoma State University, Stillwater, Oklahoma.

Busnaina, A. A. (1983), Transient Three-Dimensional Predictions of Turbulent Flows in cylindrical and Cartesian Coordinate Systems, Ph.D. dissertation, Oklahoma State University, Stillwater, Oklahoma.

Cabelli, A. (1977), Storage Tanks-A Numerical Experiment, Solar Energy, v. 19, pp. 45-54.

Carnahan, B., Luther, H. A. and Wilkes, J. O. (1969), Applied Numerical Methods, John Wiley & Sons.

Chan, A.M.C., Smereka, P.S. and Giusti, D. (1983), A Numerical Study of Transient Mixed Convection Flows in a Thermal Storage Tank, ASME Trans., J. Heat Transfer, v. 105, August 1983, pp. 246-253.

Chang, S.H. (1981), Comparative Analysis of Numerical Methods for the solution of Navier-Stokes Equations, Ph.D. dissertation, Massachusetts Institute of Technology (MIT), May, 1981.

Chen, C.J. and Rodi, W. (1979), Vertical Turbulent Buoyant Jets, A Review of Experimental Data, Pergamon Press.

Claus, R.W., Neely, G.M., Syed, S.A. (1984), Reducing Numerical Diffusion for Incompressible Flow Calculations, NASA-TM-83621.

Close, D.J. (1967), A Design Approach for Solar Processes, Solar Energy, v. 11, no. 2, pp. 112-122.

Cole, R.L. and Bellinger, F.O. (1982), Thermally Stratified Tanks, ASHRAE Transactions, v. 88, part 2, TO-82-9, No. 1, pp. 1005-1017.

Crapper, P.F. and Baines, W.D. (1977), Non Boussinesq Forced Plumes, Atmospheric Environment, v. 11, pp. 415-420.

Davis, E.S. and Bartera, R. (1975), Stratification in Solar Water Heater Storage Tanks, Proc. of the Workshop on Solar Energy Storage Subsystems for the Heating and Cooling of Buildings, Charlottesville, Virginia, pp. 38-42.

Duffie, J.A. and Beckman, W.A. (1974), Solar Energy Thermal Processes, John Wiley & Sons, N.Y., pp. 215-239.

Engineering Sciences Data Item No. 72010 (1972), Pressure Losses Across Perforated Plates, Orifice Plates and Cylindrical Tube Orifices in Ducts, Engineering Sciences Data Unit Ltd., U.K.

Ferziger, J. H. (1987), Review: Simulation of Incompressible Turbulent Flows, J. Comp. Physics, v. 69, pp. 1-48.

Gari, H.N., Loehrke, R.I. and Holzer, J.C. (1979), Performance of an Inlet Manifold for a Stratified Storage Tank, ASME Paper 79-HT-67, Joint ASME/AIChE 18th National Heat Transfer Conference, San Diego, California, August 1979.

Ghajar, A.J., Moretti, P.M. and Zurigat, Y.H. (1987), Eddy Diffusivity Model for a Stratified Thermal Storage Tank, AIAA Paper No. 87-1593, AIAA 22nd Thermophysics Conference, Honolulu, Hawaii, June 8-10, 1987.

Gross, R.J. (1982), An Experimental Study of Single Medium Thermocline Thermal Energy Storage, ASME Paper 82-HT-53.

Guo, K.L. and Wu, S.T. (1985), Numerical Study of Flow and Temperature Stratification in a Liquid Thermal Storage Tank, J. Solar Energy Eng., v. 107, February 1985, pp. 15-20.

Guyer, E.C. and Brownell, D.L. (1983), Review of Heat Storage Materials, EPRI Report, EPRI EM-3353, December 1983.

Han, S.M. and Wu, S.T. (1978), Computer Simulation of a Solar Energy System with a Viscous-Entrainment Liquid Storage Tank Model, Proc. of the Third Southeastern Conference on Application of Solar Energy, (eds.) Wu, S.T., Christensen, D.L. and Head, R.R., pp. 165-183.

Herrick, C.S., Jaster, H., Miller, R.S. and Williams, R. (1977), Cool Storage Assessment Study, EPRI Report, EPRI EM-468, May 1977, pp. 2-17-2-24.

Hirt, C. W., Nichols, B. D. and Romero, N. C. (1975), SOLA - A Numerical Solution Algorithm for Transient Fluid Flows, Report No. LA -5852, Los Alamos Scientific Laboratory, Los Alamos, New Mexico, April 1975.

Huang, P.G., Launder, B.E. and Leschziner, M.A. (1985), Discretization of Nonlinear Convection Processes - A Broad-Range Comparison of Four Schemes, Comp. Methods in Appl. Mech. and Eng., v. 48, no. 1, pp. 1-24.

Huh, K.Y., Golay, M.W. and Manno, V.P. (1986), A Method for Reduction of Numerical Diffusion in the Donor Cell Treatment of Convection, J. Comp. Physics, v. 63, pp. 201-221.

Issa, R.I. (1983), Numerical Methods in Two- and Three-Dimensional Recirculating Flows, Computational Methods for Turbulent, Transonic and Viscous Flows, Springer Verlag, (ed.) Essers, J.A., pp. 183-211.

Jones, W.P. and Launder, B.E. (1973), The Calculation of Low-Reynolds-Number Phenomena with a Two-Equation Model of Turbulence, Int. J. Heat Mass Tran., v. 16, pp. 1119-1130.

Kuhn, J.K., von Fuchs, G.F. and Zob, A.P. (1980), Developing and Upgrading of Solar-System Thermal-Energy-Storage Simulation Models, Final Report, prepared by Boeing Computer Services Company for the Department of Energy, Contract DE-AC02-77CS 34482, August, 1980.

Krenz, J.H. (1984), Energy Conversion and Utilization, Allyn and Bacon, Inc., Newton, Massachusetts, pp. 5-11.

Launder, B.E. and Spalding, D.B. (1972), Lectures in Mathematical Models of Turbulence, Academic Press.

Lavan, Z. and Thompson, J. (1977), Experimental Study of Thermally Stratified Hot Water Storage Tanks, Solar Energy, v. 19, pp. 519-524.

Leonard, B.P. (1979), A Stable and Accurate Convective Modeling Procedure Based on Quadratic Upstream Interpolation, Computer Methods in Applied Mech. and Engng., v. 19, pp. 59-98.

Leonard, B.P. (1981), A Survey of Finite Differences with Upwinding for Numerical Modeling of the Incompressible Convective Diffusion Equation, Recent Advances in Numerical Methods, v. 2, (ed.) Taylor, C., Pineridge Press, Swansea, U.K.

Lilley, D.G. and Rhode, D.L. (1982), A Computer Code for Swirling Turbulent Axisymmetric Recirculating Flows in Practical Isothermal Combustor Geometries, NASA Contractor Report 3442.

Lilley, D. G. (1986), Expanding Grid Specification, CFD Class Notes, Spring, 1986.

Lilley, D. G. (1988), Three-Dimensional Flow Prediction for Industrial Mixing, 1988 ASME International Computers in Engineering Conference, San Francisco, California, July 31 to August 3, 1988.

Loehrke, R.I., Holzer, J.C., Gari, H.M. and Sharp, M.K. (1979), Stratification Enhancement in Liquid Thermal Storage Tanks, J. Energy, v. 3, no. 3, pp. 129-130.

Maloney, K.J. (1987), A Comparison Study of One-Dimensional Stratified Thermal Storage Tank Models, M.S. report, School of Mechanical and Aerospace Engineering, Oklahoma State University, Stillwater, Oklahoma.

Markatos, N.C. (1986), The Mathematical Modeling of Turbulent Flows, Appl. Math. Modeling, v. 10, pp. 190-220.

McGuirk, J.J., Taylor, A.M.K.P. and Whitelaw, J.H. (1982), The Assessment of Numerical Diffusion in Upwind Difference Calculations of Turbulent Recirculating Flows, Turbulent Shear Flows 3, Springer-Verlag, pp. 206-224, (eds.) Bradbury, L.J.S. et al.

Miller, C.W. (1977), Effect of a Conducting Wall on a Stratified Fluid in a Cylinder, AIAA Paper No. 77-792, AIAA 12th Thermophysics Conference, Albuquerque, New Mexico.

Nallasamy, M. (1985), A Critical Evaluation of Various Turbulence Models as Applied to Internal Fluid Flows, NASA Technical Paper 2474.

Oppel, F.J., Ghajar, A.J. and Moretti, P.M. (1986), A Numerical and Experimental Study of Stratified Thermal Storage, ASHRAE Trans., v. 92, pt. 2, pp. 293-309.

Parker, J.D. and Moretti, P.M. (1985), A Study of Chilled Water Expansion for the Oklahoma State University (OSU) Campus, Final Report, OSU Funded Resarch No. EN-85-R-16, September 1985.

Patankar, S.V. (1980), Numerical Heat Transfer and Fluid Flow, McGraw-Hill, New York.

Patankar, S.V., Karki, K.C. and Mongia, M.C. (1987), Development and Evaluation of Improved Numerical Schemes for Recirculating Flows, AIAA Paper No. AIAA-87-0061.

Pera, L. and Gebhart, B. (1975), Laminar Plume Interaction, J. Fluid Mech., v. 68, pp. 259-271.

Raithby, G.D. (1976), Skew-Upstream Differencing Schemes for Problems Involving Fluid Flow, Computer Methods in Applied Mechanics and Engineering, v. 9, pp. 153-164.

Rapp, D. (1981), Solar Energy, Prentice-Hall, Inc., Englewood Cliffs, N.J., pp. 1-10.

Rao, K. S. S., Zurigat, Y. H. and Ghajar, A. J. (1988), "A Microcomputer-Based Data Acquisition System and Software for Thermal Studies," Heat Transfer Engineering, v. 9, no. 2, pp. 58-66.

Runchal, A. K. (1972), Convergence and Accuracy of Three Finite Difference Schemes for a Two-Dimensional Conduction and Convection Problem, Int. J. Numerical Methods in Engineering, v. 4, pp. 541-550.

Runchal, A.K. (1986), CONDIF: A Modified Central-Difference Scheme with Undonditional Stability and Very Low Numerical Diffusion, Proc. of the Eighth International Heat Transfer Conference, San Francisco, Ca, Aug. 1986, (eds.) Tien, C.L., Carey, V.P. and Ferrell, J.K.

Runchal, A.K., Anand, M.S. and Mongia, C. (1987), An Unconditionally-Stable Central Differencing Scheme for High Reynolds Number Flows, AIAA paper No. AIAA-87-0060.

Schlichting, H. (1979), Boundary Layer Theory, McGraw Hill Book Co., p. 183.

Seth, D.S. and Leduc, R.G. (1983), Daily Thermal Energy Storage: Canadian Experience, EPRI EM-3159-SR, Special Report on Opportunities in Thermal Storage R&D, July 1983, pp. P7-1 - P7-9.

Sha, W.T. and Lin, E.I.H. (1978), Three Dimensional Mathematical Model of Flow Stratification in Thermocline Storage Tanks, Application of Solar Energy, (eds) Wu, S.T., et. al., pp. 185-202.

Sha, W.T., Lin, E.I.H., Schmitt, R.C., Lin, K.V., Hull, J.R., Oras Jr., J.J. and Domanus, H.M. (1980), COMMIX-SA-1: A Three-Dimensional Thermohydrodynamic Computer Program for Solar Applications, Argonne National Laboratory Report, ANL-80-8.

Sharif, A.R. and Busnaina, A.A. (1987), Assessment of Finite Difference Approximations for the Advection Terms in the Simulation of Practical Flow Problems, Report No. MIE-148, Clarkson University, Potsdam, N.Y., June 1987.

Sharp, M.K. (1978), Thermal Stratification in Liquid Sensible Heat Storage, M.S. thesis, Colorado State University, Fort Collins, Colorado.

Sharp, M.K. and Loehrke, R.I. (1979), Stratified Thermal Storage in Residential Solar Energy Applications, J. Energy, v. 3, no. 2, pp. 106-113.

Sherman, C., Wood, B.D. and Mason, J. (1979), Effect of Wall Conductance on Temperature Relaxation in Thermally Stratified Liquid Thermal Storage Tanks, Proc. of the 1979 Annual Meeting of the Am. Section of ISES, Atlanta, Georgia, vo. 1, Pergamon Press, pp. 591-595, (eds.) Böer, K.W. and Glenn, B.H.

Shyy, W. (1985), A Study of Finite Difference Approximations to Steady State Convection Dominated Flow Problems," J. Comp. Physics, v. 57, pp. 415-438.

Sliwinski, B.J., Mech, A.R. and Shih, T.S. (1978), Stratification in Thermal Storage During Charging, Proc. of 6th International Heat Transfer Conference, Toronto, Ontario, v. 4, pp. 149-154.

Smith, R.M. and Hutton, A.G. (1982), The Numerical Treatment of Advection: A Performance Comparison of Current Methods, Numerical Heat Transfer, v. 5, pp. 439-461.

Spalding, D.B. (1972), A Novel Finite Difference Formulation for Differential Expressions Involving Both First and Second Derivatives, Int. J. Num. Methods Engng., v. 4, pp. 551-559.

Syed, S. and Chiappetta L. (1985), Finite Difference Methods for Reducing Numerical Diffusion in TEACH-Type Calculations, AIAA paper No. AIAA-85-0057.

Syed, S., Gosman, A. and Peric, M. (1985), Assessment of Discretization Schemes to Reduce Numerical Diffusion in the Calculation of Complex Flows, AIAA paper No. AIAA-85-0441.

Tamblyn, R.T. (1980), Thermal Storage Resisting Temperature Blending, ASHRAE Journal, vo. 22, no. 1, January 1980, pp. 65-70.

Welch, J.E., Harlow, F.H., Shannon, J.P. and Daly, B.J. (1966), The MAC METHOD: A Computing Technique for Solving Viscous, Incompressible, Transient Fluid-Flow Problems Involving Free Surfaces, Los Alamos Scientific Laboratory report LA-3425, March 1966.

Wildin, M.W., and Truman, C.R. (1985), "Evaluation of Stratified Chilled Water Storage Technique," EPRI Report, EPRI EM-4352, December 1985.

Wong, H.H. and Raithby, G.D. (1979), Improved Finite-Difference Methods Based on a Critical Evaluation of the Approximating Errors, Numerical Heat Transfer, v. 2, p. 131.

Zurigat, Y.H., Ghajar, A.J. and Moretti, P.M. (1988a), Stratified Thermal Storage Tank Inlet Mixing Characterization, Applied Energy, v. 30, pp. 99-111.

Zurigat, Y.H., Maloney, K.J., Ghajar, A.J. and Moretti, P.M. (1987), A Comparative Study of Various Models of Stratified Thermal Storage Tanks, Computers in Engineering 1987, (eds.) Raghavan, R. and Cokonis, T.J., ASME, v. 3, pp. 101-109.

Zurigat, Y. H., and Liche, P. R. (1987), Turbulent Mixing Correlations for Thermocline Thermal Storage Tank, Internal Report, Research Project No. EN 87-R-103, Mechanical and Aerospace Engineering Department, Oklahoma State University, Stillwater, Oklahoma, December 1987.

Zurigat, Y. H., Liche, P. R. and Ghajar, A. J. (1988b), Turbulent Mixing Correlations for a Thermocline Thermal Storage Tank, Proceedings of the 1988 ASME/AIChE National Heat Transfer Conference, Houston, Texas, July 24-27, 1988, AIChE Symposium Series; no. 263, v. 84, pp. 160-168.

APPENDIX A

WEIGHTED UPWIND AND SECOND ORDER UPWIND DIFFERENCING OF ADVECTION TERMS

WEIGHTED UPWIND AND SECOND ORDER UPWIND DIFFERENCING OF ADVECTION TERMS

In this Appendix, the discretization of the advection terms appearing in the mathematical model using the WUDS and SOUDS is presented. A sample derivation of the two methods is given to illustrate the differences between the two approaches. This is demonstrated by application to the advection term $(\frac{\partial uu}{\partial x})_{i,j}$. Other terms are derived similarly and only the final results are given.

A.1 Weighted Upwind Difference Scheme (WUDS)

Consider the u-cell control volume shown in Figure A.1. The discretization of the advected u-velocity can be written as:

$$(\frac{\partial uu}{\partial x})i,j = [u_{E,u}\ \tilde{u}_E - u_{W,u}\ \tilde{u}_W]/\Delta x_i^u \qquad (A.1.1)$$

where $u_{E,u}$ and $u_{W,u}$ are the velocities at the east and west faces of the u-cell correspondingly. These are given by:

$$u_{E,u} = 0.5\ (u_{i+1,j} + u_{i,j}) \qquad (A.1.2a)$$

$$u_{W,u} = 0.5\ (u_{i,j} + u_{i-1,j}) \qquad (A.1.2b)$$

and $\tilde{u}_E$ and $\tilde{u}_W$ take different forms depending on the type of discretization considered. For example, in central difference form they are given by:

$$\tilde{u}_E = u_{E,u} \qquad (A.1.3a)$$

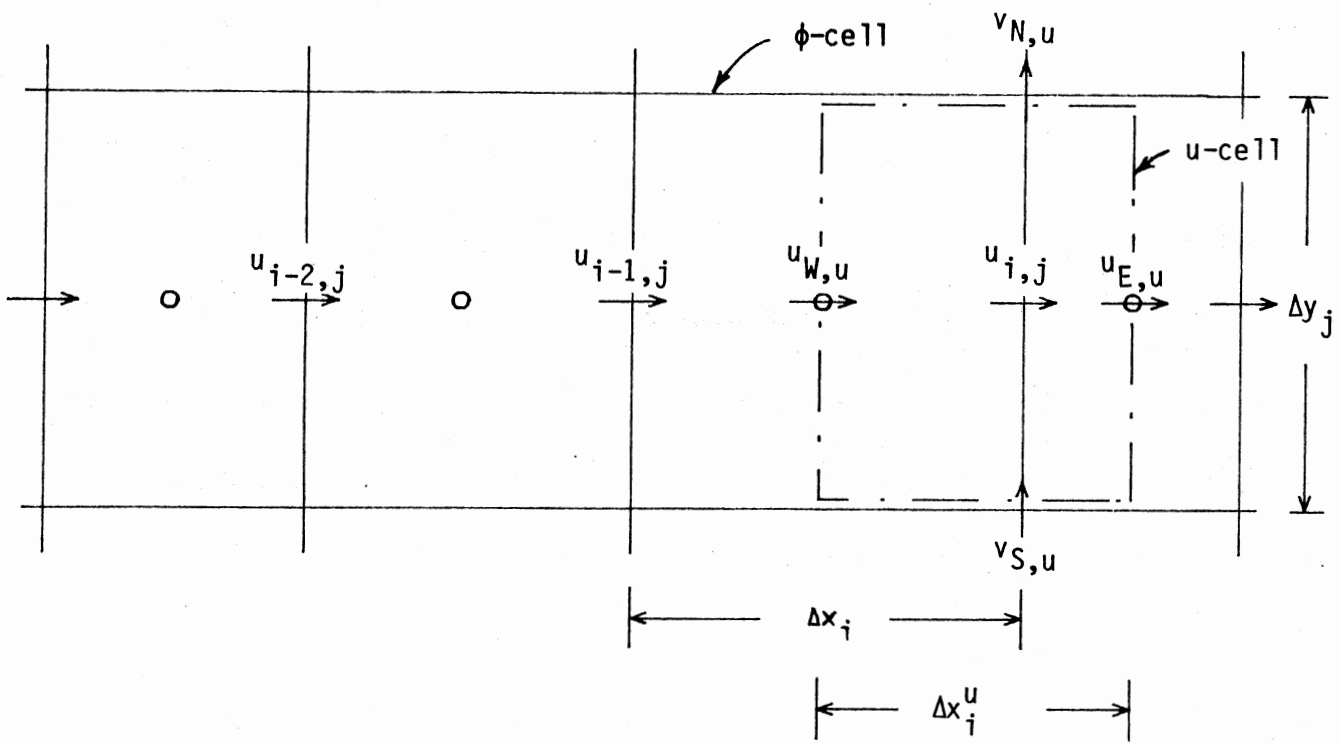

Figure A.1 Grid System Showing the u-cell and the Location of Related u-velocities

$$\tilde{u}_W = u_{W,u} \tag{A.1.3b}$$

which when substituted in Equation (A.1.1) gives the central difference form:

$$\left(\frac{\partial uu}{\partial x}\right)_{i,j} = \left[(u_{i+1,j} + u_{i,j})^2 - (u_{i,j} + u_{i-1,j})^2\right]/4\Delta x_i^u \tag{A.1.4}$$

The fully upwind form of Equation (A.1.4) is derived by rewriting the terms $\tilde{u}_E$ and $\tilde{u}_W$ taking into account the flow direction. This is done by analogy with the tank-and-tube model (Patankar, 1980). Thus for $u > 0$ we have:

$$\tilde{u}_E = u_{i,j} \tag{A.1.5a}$$

$$\tilde{u}_W = u_{i-1,j} \tag{A.1.5b}$$

and for $u < 0$

$$\tilde{u}_E = u_{i+1,j} \tag{A.1.5c}$$

$$\tilde{u}_W = u_{i,j} \tag{A.1.5d}$$

Substitution of Equations (A.1.5) in Equation (A.1.1) gives the upwind difference form. Thus for $u > 0$ we get:

$$\left(\frac{\partial uu}{\partial x}\right)_{i,j} = \left[(u_{i+1,j} + u_{i,j})\, u_{i,j} - (u_{i,j} + u_{i-1,j})u_{i-1,j}\right]/2\Delta x_i^u \tag{A.1.6}$$

and for $u < 0$ we have:

$$\left(\frac{\partial uu}{\partial x}\right)_{i,j} = \left[\left(u_{i+1,j} + u_{i,j}\right) u_{i+1,j} - \left(u_{i,j} + u_{i-1,j}\right) u_{i,j}\right]/2\Delta x_i^u \quad \text{(A.1.7)}$$

The Weighted Upwind Difference Scheme is obtained by combining Equations (A.1.4), (A.1.6) and (A.1.7) using a donor cell parameter, α, which takes values between zero and unity (Hirt et al., 1975):

$$\left(\frac{\partial uu}{\partial x}\right)_{i,j} = \left[\left(u_{i,j} + u_{i+1,j}\right)^2 + \alpha\left|u_{i,j} + u_{i+1,j}\right|\cdot\left(u_{i,j} - u_{i+1,j}\right)\right.$$

$$\left. - \left(u_{i-1,j} + u_{i,j}\right)^2 - \alpha\left|u_{i-1,j} + u_{i,j}\right|\cdot\left(u_{i-1,j} - u_{i,j}\right)\right]/4\Delta x_i^u \quad \text{(A.1.8)}$$

Equation (A.1.8) reduces to Equation (A.1.4) for $\alpha = 0.0$, to Equation (A.1.6) for $\alpha = 1.0$ and $u > 0$, and to Equation (A.1.7) for $\alpha = 1.0$ and $u < 0$. Sharif and Busnaina (1987) have put the terms $\tilde{u}_E$ and $\tilde{u}_W$ in a form more suitable for implementation in a computer code. That is:

$$\tilde{u}_E = 0.5\left[u_{i,j} + u_{i+1,j} + (is)\,\alpha\left(u_{i,j} - u_{i+1,j}\right)\right] \quad \text{(A.1.9)}$$

where

$$is = u_{E,u}/\left|u_{E,u}\right|$$

and $u_{E,u}$ is given by Equation (A.1.2a).

$$\tilde{u}_W = 0.5\left[u_{i-1,j} + u_{i,j} + (is)\,\alpha\left(u_{i-1,j} - u_{i,j}\right)\right] \quad \text{(A.1.10)}$$

where

$$is = u_{W,u}/\left|u_{W,u}\right|$$

and $u_{W,u}$ is given by Equation (A.1.2b)

It can be shown that substitution of Equations (A.1.9) and (A.1.10) in Equation (A.1.1) gives the result given by Equation (A.1.8).

The rest of the terms appearing in Sections 5.2.2 to 5.2.4 are derived similarly and the results are given below using the convention developed by Sharif and Busnaina (1987).

A.1.1 u-Momentum Equation (Section 5.2.2)

$$\tilde{u}_N = [u_{i,j}\Delta yh_{j+1} + u_{i,j+1}\Delta yh_j + (js)\alpha(u_{i,j} - u_{i,j+1})\Delta yh_{j+ja}]/\Delta y^v_j \quad (A.1.11a)$$

where

$$js = v_{N,u}/|v_{N,u}|$$

$$ja = (1 - js)/2$$

$$\tilde{u}_S = [u_{i,j-1}\Delta yh_j + u_{i,j}\Delta yh_{j-1} + (js)\alpha(u_{i,j-1} - u_{i,j})\Delta yh_{j-1+ja}]/\Delta y^v_{j-1} \quad (A.1.11b)$$

where

$$js = v_{S,u}/|v_{S,u}|$$

$$ja = (1-js)/2$$

The velocities, $v_{N,u}$ and $v_{S,u}$ are given by:

$$v_{N,u} = (v_{i+1,j}\Delta xh_i + v_{i,j}\Delta xh_{i+1})/\Delta x^u_i \quad (A.1.11c)$$

$$v_{S,u} = (v_{i+1,j-1}\,\Delta xh_i + v_{i,j-1}\,\Delta xh_{i+1})/\Delta x^u_i \quad (A.1.11d)$$

A.1.2 v-Momentum Equation (Section 5.2.3)

The following velocities are defined and shown in Figure A.2 and defined as:

$$u_{E,v} = (u_{i,j+1}\ \Delta yh_j + u_{i,j}\ \Delta yh_{j+1})/\Delta y^v_j \qquad \text{(A.1.12a)}$$

$$u_{W,v} = (u_{i-1,j+1}\ \Delta yh_j + u_{i-1,j}\ \Delta yh_{j+1})/\Delta y^v_j \qquad \text{(A.1.12b)}$$

$$v_{N,v} = 0.5\ (v_{i,j} + v_{i,j+1}) \qquad \text{(A.1.12c)}$$

$$v_{S,v} = 0.5\ (v_{i,j-1} + v_{i,j}) \qquad \text{(A.1.12d)}$$

$$\tilde{v}_E = [v_{i,j}\Delta xh_{i+1} + v_{i+1,j}\Delta xh_i + (is)\alpha(v_{i,j} - v_{i+1,j})\Delta xh_{i+ia}]/\Delta x^u_i \qquad \text{(A.1.12e)}$$

where

$$is = u_{E,v}/|u_{E,v}|$$

$$ia = (1-is)/2$$

$$\tilde{v}_W = [v_{i-1,j}\Delta xh_i + v_{i,j}\Delta xh_{i-1} + (is)\alpha(v_{i-1,j} - v_{i,j})\Delta xh_{i-1+ia}]/\Delta x^u_{i-1} \qquad \text{(A.1.12f)}$$

where

$$is = u_{W,v}/|u_{W,v}|$$

$$ia = (1-is)/2$$

$$\tilde{v}_N = 0.5\ [v_{i,j} + v_{i,j+1} + (js)\ \alpha\ (v_{i,j} - v_{i,j+1})] \qquad \text{(A.1.12g)}$$

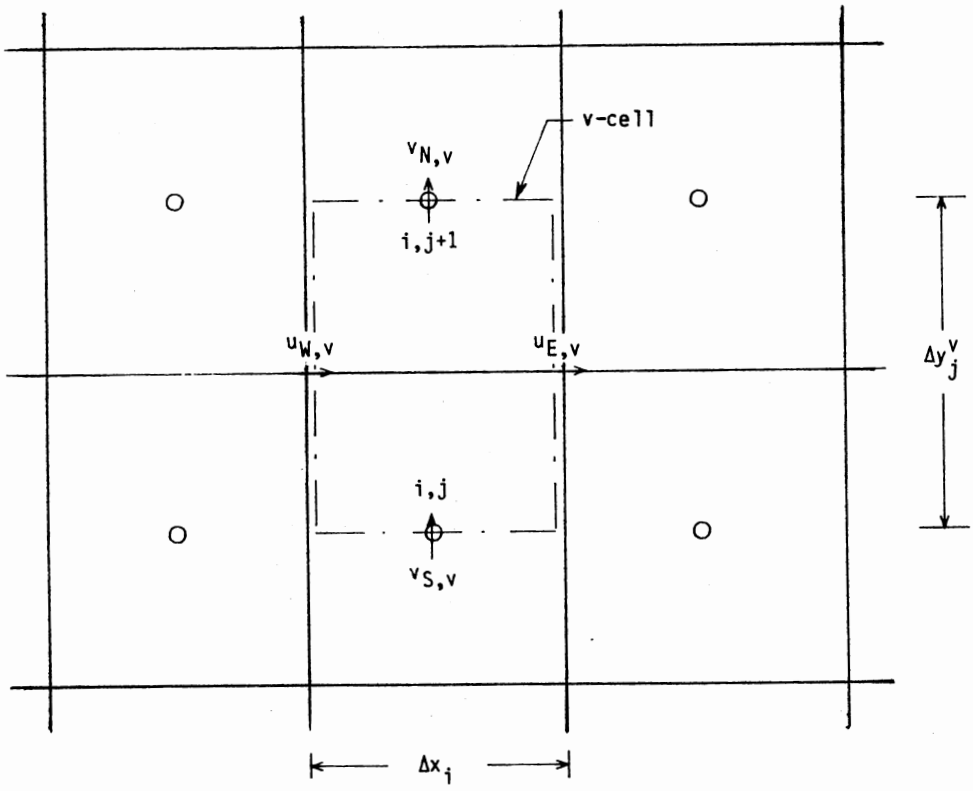

Figure A.2 Grid System Showing the v-cell and the Locations of Related u- and v-velocities

where

$$js = v_{N,v}/|v_{N,v}|$$

$$\tilde{v}_S = 0.5\,[v_{i,j-1} + v_{i,j} + (js)\,\alpha\,(v_{i,j-1} - v_{i,j})] \qquad \text{(A.1.12h)}$$

where

$$js = v_{S,v}/|v_{S,v}|$$

A.1.3 Energy Equation (Section 5.2.4)

The following velocities are defined and shown in Figure A.3.

$$u_{E,T} = u_{i,j} \qquad \text{(A.1.13a)}$$

$$u_{W,T} = u_{i-1,j} \qquad \text{(A.1.13b)}$$

$$v_{N,T} = v_{i,j} \qquad \text{(A.1.13c)}$$

$$v_{S,T} = v_{i,j-1} \qquad \text{(A.1.13d)}$$

$$\tilde{T}_E = [T_{i,j}\Delta xh_{i+1} + T_{i+1,j}\Delta xh_i + (is)\alpha(T_{i,j} - T_{i+1,j})\Delta xh_{i+ia}]/\Delta x_i^u \qquad \text{(A.1.13e)}$$

where

$$is = u_{E,T}/|u_{E,T}|$$

$$ia = (1-is)/2$$

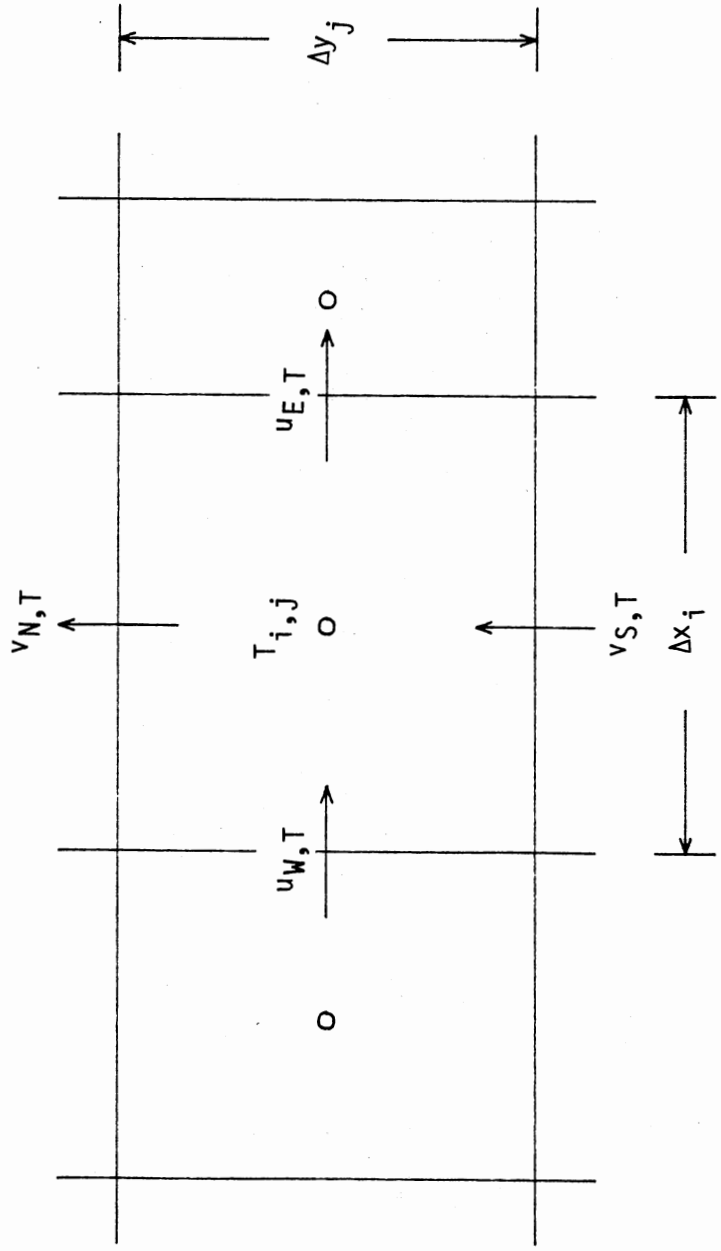

Figure A.3 Grid System Showing the ϕ-cell and the Locations of Related u- and v-velocities

$$\tilde{T}_W = [T_{i-1,j}\Delta xh_i + T_{i,j}\Delta xh_{i-1} + (is)\alpha(T_{i-1,j} - T_{i,j})\Delta xh_{i-1+ia}]/\Delta x^u_{i-1} \quad \text{(A.1.13f)}$$

where

$$is = u_{W,T}/|u_{W,T}|$$

$$ia = (1-is)/2$$

$$\tilde{T}_N = [T_{i,j}\Delta yh_{j+1} + T_{i,j+1}\Delta yh_j + (js)\alpha(T_{i,j} - T_{i,j+1})\Delta yh_{j+ja}]/\Delta y^v_j \quad \text{(A.1.13g)}$$

where

$$is = v_{N,T}/|v_{N,T}|$$

$$ja = (1-is)/2$$

$$\tilde{T}_S = [T_{i,j-1}\Delta yh_j + T_{i,j}\Delta yh_{j-1} + (js)\alpha(T_{i,j-1} - T_{i,j})\Delta yh_{j-1+ja}]/\Delta y^v_{j-1} \quad \text{(A.1.13h)}$$

where

$$js = v_{S,T}/|v_{S,T}|$$

$$ja = (1-js)/2$$

A.2 Second Order Upstream Difference Scheme (SOUDS)

As stated earlier in this Appendix, the SOUDS will be derived for the term $(\frac{\partial uu}{\partial x})_{i,j}$ only. Other quantities appearing in Sections (5.2.2) to (5.2.4) will be only listed in this section.

Consider the u-cell control volume shown in Figure A.1. The discretization of the advected u-velocity is given by Equation

(A.1.1). The velocities $\tilde{u}_E$ and $\tilde{u}_W$ appearing in the equation are derived as follows:

Depending on the flow direction, the velocities $\tilde{u}_E$ and $\tilde{u}_W$ are expressed in terms of velocities upstream of the location of interest. For example, for $u > 0$, $\tilde{u}_E$ is expressed in terms of $u_{i,j}$ and $u_{i-1,j}$ and similarly, $\tilde{u}_W$ is expressed in terms of $u_{i-1,j}$ and $u_{i-2,j}$. Thus, extrapolation for $\tilde{u}_E$ from $u_{i,j}$ and $u_{i-1,j}$ gives for $u > 0$:

$$\tilde{u}_E = [(2\Delta x_i + \Delta x_{i+1})u_{i,j} - \Delta x_{i+1}u_{i-1,j}]/2\Delta x_i \qquad (A.2.1)$$

and for $\tilde{u}_W$ from $u_{i-1,j}$ and $u_{i-2,j}$ gives:

$$\tilde{u}_W = [(2\Delta x_{i-1} + \Delta x_i)u_{i-1,j} - \Delta x_i u_{i-2,j}]/2\Delta x_{i-1} \qquad (A.2.2)$$

Equation (A.2.1) can be written as:

$$\tilde{u}_E = (1 + r_1)u_{i,j} - r_1 u_{i-1,j} \qquad (A.2.3)$$

where

$$r_1 = \Delta x_{i+1}/2\Delta x_i = \Delta xh_{i+1}/\Delta x_i$$

Similarly for $\tilde{u}_W$ we get:

$$\tilde{u}_W = (1 + r_2)u_{i-1,j} - r_2 u_{i-2,j} \qquad (A.2.4)$$

where

$$r_2 = \Delta x_i / 2\Delta x_{i-1} = \Delta x h_i / \Delta x_{i-1}$$

When $u < 0$, extrapolation for $\tilde{u}_E$ from $u_{i+1,j}$ and $u_{i+2,j}$ gives:

$$\tilde{u}_E = [(2\Delta x_{i+2} + \Delta x_{i+1})u_{i+1,j} - \Delta x_{i+1} u_{i+2,j}]/2\Delta x_{i+2} \qquad (A.2.5)$$

and for $\tilde{u}_W$ from $u_{i,j}$ and $u_{i+1,j}$ gives:

$$\tilde{u}_W = [(2\Delta x_{i+1} + \Delta x_i)u_{i,j} - \Delta x_i u_{i+1,j}]/2\Delta x_{i+1} \qquad (A.2.6)$$

These equations can be rewritten as:

$$\tilde{u}_E = (1 + r_3)u_{i+1,j} - r_3 u_{i+2,j} \qquad (A.2.7)$$

where

$$r_3 = \Delta x_{i+1} / 2\Delta x_{i+2} = \Delta x h_{i+1} / \Delta x_{i+2}$$

Similarly for $\tilde{u}_W$ we get:

$$\tilde{u}_W = (1 + r_4)u_{i,j} - r_4 u_{i+1,j} \qquad (A.2.8)$$

where

$$r_4 = \Delta x_i / 2\Delta x_{i+1} = \Delta x h_i / \Delta x_{i+1}$$

Equations (A.2.3) and (A.2.7) for $\tilde{u}_E$ can be combined in one recurrence relation (Sharif and Busnaina 1987) as:

$$\tilde{u}_E = (1 + r)u_{i+ia,j} - ru_{i-1+3ia,j} \qquad (A.2.9)$$

where

$$ia = (1 - is)/2$$

$$is = u_{E,u}/|u_{E,u}|$$

$$r = \Delta xh_{i+1}/\Delta x_{i+2ia}$$

Note that r reduces to r_1 or r_3 depending on the flow direction. Also Equation (A.2.9) reduces to Equation (A.2.3) for $u > 0$ and to Equation (A.2.7) for $u < 0$.

In a similar fashion, Equations (A.2.4) and (A.2.8) for $\tilde{u}_W$ are combined in the following relation:

$$\tilde{u}_W = (1 + r)u_{i-1+ia,j} - ru_{i-2+3ia,j} \qquad (A.2.10)$$

where

$$r = \Delta xh_i/\Delta x_{i-1+2ia}$$

$$ia = (1 - is)/2$$

$$is = u_{W,u}/|u_{W,u}|$$

This completes the derivation of SOUDS. The different terms appearing in Sections 5.2.2 to 5.2.4 are listed next.

A.2.1 u-Momentum Equation (Section 5.2.2)

$$\tilde{u}_N = (1 + r)u_{i,j+ja} - ru_{i,j-1+3ja} \qquad (A.2.11a)$$

where

$$r = \Delta yh_{j+ja} / \Delta y^{v}_{j-1+2ja}$$

$$ja = (1 - js)/2$$

$$js = v_{N,u}/|v_{N,u}|$$

$$\tilde{u}_S = (1 + r)u_{i,j-1+ja} - ru_{i,j-2+3ja} \qquad \text{(A.2.11b)}$$

where

$$r = \Delta yh_{j-1+ja} / \Delta y^{v}_{j-2+2ja}$$

$$ja = (1 - js)/2$$

$$js = v_{S,u}/|v_{S,u}|$$

A.2.2 v-Momentum Equation (Section 5.2.3)

$$\tilde{v}_E = (1 + r)v_{i+ia,j} - rv_{i-1+3ia,j} \qquad \text{(A.2.12a)}$$

where

$$r = \Delta xh_{i+ia} / \Delta x^{u}_{i-1+2ia}$$

$$ia = (1 - is)/2$$

$$is = u_{E,v}/|u_{E,v}|$$

$$\tilde{v}_W = (1 + r)v_{i-1+ia,j} - rv_{i-2+3ia,j} \qquad \text{(A.2.12b)}$$

where

$$r = \Delta xh_{i-1+ia} / \Delta x^{u}_{i-2+2ia}$$

$$ia = (1 - is)/2$$

$$is = u_{W,v}/|u_{W,v}|$$

$$\tilde{v}_N = (1 + r)v_{i,j+ja} - rv_{i,j-1+3ja} \qquad \text{(A.2.12c)}$$

where

$$r = \Delta yh_{j+1} / \Delta y_{j+2ja}$$

$$ja = (1 - js)/2$$

$$js = v_{N,v}/|v_{N,v}|$$

$$\tilde{v}_S = (1 + r)v_{i,j-1+ja} - rv_{i,j-2+3ja} \qquad \text{(A.2.12d)}$$

where

$$r = \Delta yh_{j} / \Delta y_{j-1+2ja}$$

$$ja = (1 - js)/2$$

$$js = v_{S,v}/|v_{S,v}|$$

A.2.3 Energy Equation (Section 5.2.4)

$$\tilde{T}_E = (1 + r)T_{i+ia,j} - rT_{i-1+3ia,j} \qquad \text{(A.2.13a)}$$

where

$$r = \Delta xh_{i+ia} / \Delta x^{u}_{i-1+2ia}$$

$$ia = (1 - is)/2$$

$$is = u_{E,T}/|u_{E,T}|$$

$$\tilde{T}_W = (1 + r)T_{i-1+ia,j} - rT_{i-2+3ia,j} \qquad \text{(A.2.13b)}$$

where

$$r = \Delta xh_{i-1+ia} / \Delta x^{u}_{i-2+2ia}$$

$$ia = u_{W,T}/|u_{W,T}|$$

$$is = (1 - ia)/2$$

$$\tilde{T}_N = (1 + r)T_{i,j+ja} - rT_{i,j-1+3ja} \qquad \text{(A.2.13c)}$$

where

$$r = \Delta yh_{j+ja} / \Delta y^{v}_{j-1+2ja}$$

$$ja = (1 - js)/2$$

$$js = v_{N,T}/|v_{N,T}|$$

$$\tilde{T}_S = (1 + r)T_{i,j-1+ja} - rT_{i,j-2+3ja} \qquad \text{(A.2.13d)}$$

where

$$r = \Delta yh_{j-1+ja} / \Delta y^{v}_{j-2+2ja}$$

$$ja = (1 - js)/2$$

$$js = v_{S,T}/|v_{S,T}|$$

The velocities $u_{E,T}$, $u_{W,T}$, $v_{N,T}$ and $v_{S,T}$ are given in Section A.1.3.

VITA

Yousef H. Zurigat

Candidate for the Degree of

Doctor of Philosophy

Thesis: AN EXPERIMENTAL AND ANALYTICAL EXAMINATION OF STRATIFIED THERMAL STORAGE

Major Field: Mechanical Engineering

Biographical:

Personal Data: Born in Soof, Jordan, the son of Mr. and Mrs. Hasan Zurigat.

Education: Graduated from Jerash Secondary School, Jerash, Jordan, in May 1969; received the Master of Science degree in Aeronautical Engineering from Kiev Institute of Civil Aviation Engineers, Kiev, USSR in February, 1976; received the Master of Science degree in Mechanical Engineering from Oklahoma State University in July, 1984; completed the requirements for the Doctor of Philosophy degree at Oklahoma State University in December, 1988.

Professional Experience: Mechanical and Aerospace Engineer, Royal Jordanian Air Force, Jordan, from September, 1976 to July, 1981; Teaching Assistant and Research Associate, School of Mechanical and Aerospace Engineering, Oklahoma State University, 1984-1988.

Professional Societies: American Society of Mechanical Engineers; American Society of Heating, Refrigerating, and Airconditioning Engineers.